Proprioceptive Equalization in Manual Control Cybernetics

MSc Thesis

Savneek Bhatia

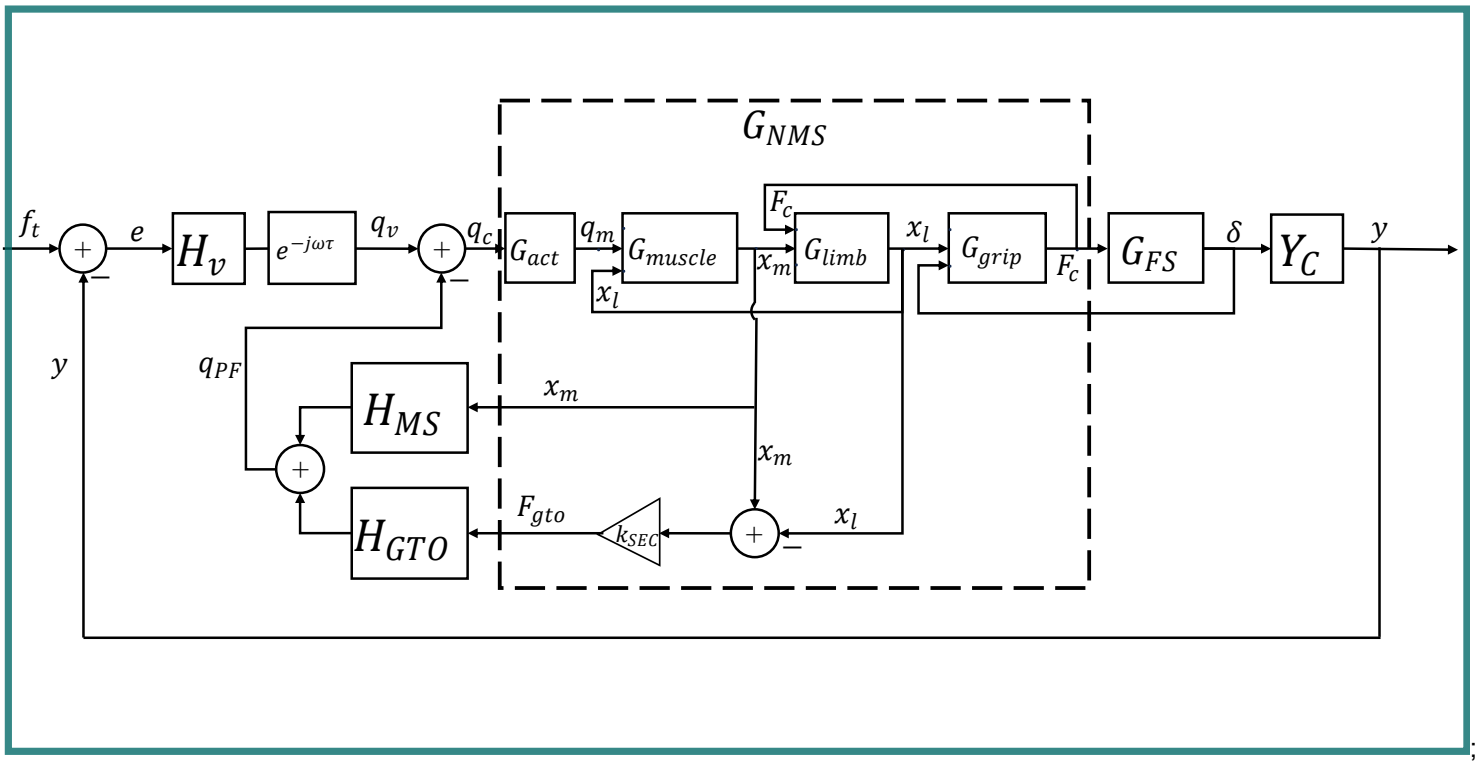

TU Delft

Proprioceptive Equalization in Manual Control Cybernetics

MSc Thesis

by

Savneek Bhatia

to obtain the degree of Master of Science
at the Delft University of Technology
to be defended publicly on May 28, 2025 at 09:00

Under the Supervision of:

Supervisors:	Dr. ir. Max Mulder
	Dr. ir. Rene van Passen
Course Duration:	September 2023 - May 2025
Student number:	5460638

Faculty of Aerospace Engineering · Delft University of Technology

Preface

This report is the culmination of a lot of hard work, through many ups and downs. Being able to present work that I can be proud of, and receive a Master's in Aerospace Engineering at TU Delft is a dream come true. I am truly grateful to my family, for not giving up on me through everything, and to my friends for all of their support.

I have learnt a lot while conducting this research, and can truly appreciate the value of academia and science. I would not have been able to complete this work without the unending guidance and patience of my supervisors, Professors Max and René.

I hope my research is helpful for any future academics working in this field!

Savneek Bhatia

May 2025

Contents

Nomenclature

Abbreviations

CL	Closed Loop
CM	Crossover Model
CNS	Central Nervous System
NMS	Neuromuscular system
OL	Open Loop
PF	Proprioceptive Feedback
PIO	Pilot Induced Oscillation
PM	Precision Model
SM	(Hess's) Structural Model

Subscript

I	Lead
L	Lag

Symbols

δ_m	Manipulator Deflection
ω_c	Crossover Frequency
ω_n	NMS Natural Frequency
τ_e	Effective Time Delay
τ_I	Pilot Lead Time Constant
τ_L	Pilot Lag Time Constant
e	Error signal
f_t	Forcing Function signal
$Y\_(s)$	Transfer function
y_C	Controlled Element Output signal
s	Complex variable in Laplace Domain
t	Time - Representation in time domain

List of Figures

List of Tables

Part I

Literature Review

1

Introduction

The intricacies of modelling human behaviour in manually controlling a dynamic system have posed significant challenges, despite extensive research and progress in the past decades. Traditional system identification methods often fall short in accurately representing the human pilot. The human pilot is recognized as a nonlinear adaptive system, continuously adjusting based on the system's characteristics, environmental conditions, and numerous unquantifiable human variables.

Creating a comprehensive mathematical model of the human pilot is inherently challenging due to the complex, nonlinear, and adaptive nature of human behaviour. While qualitative and descriptive models, such as the skills, rules, and knowledge model proposed by Rasmussen [14], offer valuable insights, they are unable to provide the quantitative precision needed for a thorough understanding of the human-pilot system in a control task. Pilot models based in control system theory are necessary to accurately predict the human pilot's input during a control task.

Accurate pilot control modelling is crucial for several reasons. It allows for the analysis of the complete aircraft-pilot system, providing insights into aircraft pilot couplings (APCs) and pilot-induced oscillations (PIOs). Such modelling is essential for developing better-tailored human-machine interfaces (HMIs), including improved guidance systems that enhance overall flight safety and efficiency.

Historically, quasi-linear models have shown to be highly effective in identifying pilot characteristics. The crossover model proposed by McRuer [15] is among the most prominent models and able to predict the pilot's dynamic response given a control task with sufficient accuracy for many applications. This model approximates the neuromuscular system (NMS) and the manipulator using second-order dynamics and an effective time delay, and gives some guidance on equalization in the overall pilot-vehicle system. The precision model, meant to give further detail on the internals of this equalization and an estimation of the internal dynamics, models feedback in only the visual channel. This model does not provide detailed information on the internal mechanics of how and why this equalization occurs, and of relevance to this report, it does not explicitly account for proprioception by the human pilot, which is known to impact control behaviour [4]. There is no feedback path representing the force applied to the stick, nor the displacement to the human brain, and the model suggests that the pilot fully relies on only their visual senses for control. Such a model falls short in describing the human pilot dynamics taking into account the underlying structure and physiology. Experiments by Magdaleno et al. [13] demonstrated that pilots perform better with manipulators restrained by a spring, highlighting the potential impact of mechanical properties on pilot performance.

Hess's structural model was a significant attempt in this direction, incorporating elements of proprioceptive feedback to propose an additional internal loop responsible for equalization, assuming a more limited role for visual feedback [7]. This model has been reasonably successful in explaining human control adaptation with physiology in mind. Bachelder suggested some improvements to the structural model based on experimental data [9]. His experiments were limited, however, by both the limited sample size (N=1) and the equipment utilised. He later suggested a more generalized model that accounts for equalization to a much better capacity in both the visual and proprioceptive channels, using an optimization algorithm for parameter estimation [11] [16].

The goal of this project is to investigate the potential contribution of proprioceptive feedback towards equalization. Previous models, including the structural model and Bachelder's modified model, will be analysed to discover the most accurate model that can be used to simulate the pilot-aircraft system, keeping human physiology in mind and getting results that match experimental data.

This report reviews the models for proprioception in the context of the human pilot performing a manual control task that have been theorized and utilised, and aims to evaluate which models both reflect an accurate pilot-aircraft control loop, as well as representing an informative physiological model of proprioception in the human pilot.

To that goal, the research question of the thesis is presented.

Research Question

Can Proprioceptive Feedback account for equalization in the human pilot model?

1. Can a proprioceptive inner loop equalization account for pilot control adaptation to the degree established by the crossover model?
2. Is a model simulating equalization through proprioceptive feedback mathematically possible and physiologically plausible?
3. Can such a model be validated by experimental data, and provide an explanation for human control behaviours?

This report, looking at possible models based in human physiology (Chapter 2) discusses the literature available on various models used to model the human pilot in a manual control task, with a focus on proprioception. This review establishes guidelines on how these questions can be answered, setting up guidelines for the physiological characteristics of the operator already studied in the past, as well as past observations from experiments (sub-questions 2 and 3).

2

Pilot Modelling Overview

Human operator modelling has grown into an extensive field with applications in numerous engineering situations which involve designing systems interacting directly or indirectly with humans. In the context of pilot modelling, the primary application is in enhancing aircraft design, improving flight safety, and refining pilot training programs. Models are used to simulate pilot behaviour and interactions with the aircraft under various conditions, providing insights into handling qualities and the effectiveness of control systems. An understanding of human perception and cognition is necessary to understand our interaction with these systems.

Rasmussen's framework divides human control behaviour into three levels: skill-based behaviour, rule-based behaviour, and knowledge-based behaviour [14]. While knowledge-based and rule-based behaviour occur over larger time periods and involve decision making in novel and practised situations respectively, skill-based behaviour occurs in a much smaller time frame and involves highly practised actions in the control of an aircraft.

Manual control modelling focuses on the pilot's direct interaction with the aircraft's control systems. This involves the neuromuscular responses to control inputs, the sensory feedback from the aircraft, and the cognitive processes involved in decision-making. Figure 2.1 from a 2014 review of pilot models [1] shows a block diagram depicting the complex interactions involved between the pilot and the aircraft during control of the vehicle. The key components of the pilot model include:

1. Sensory models: Represent how pilots perceive visual, vestibular, and proprioceptive cues.
2. Biomechanical models: Simulate the physical movements and forces exerted by the pilot.
3. Control-theoretic models: Describe the pilot's control actions in response to perceived aircraft states

This report is largely concerned with Rasmussen's framework's 'skill' category wherein the pilot applies direct control actuation to the aircraft through their neuromuscular system based on sensory input, focussing on visual and proprioceptive cues. The first equalization model was proposed by Tustin in 1944 [17] using servomechanism theory and later developed by McRuer et al. who proposed a quasi-linear model of the human operator during a single target compensatory tracking task [15]. This laid the foundation for most models today [18]. McRuer's crossover theory model and precision model are further discussed in Chapter 3.

What is equalization?
Equalization refers to the human pilot's ability to adjust their dynamic response during manual control to obtain the desired closed loop behaviour (tracking the target signal closely) in the pilot-vehicle system. Depending on the controlled system (vehicle) characteristics, their sensory input and the target signals' frequency, the pilot can adapt their dynamic response to maintain closed loop stability. This is explained further in Chapter 3.

Role of Proprioception in Manual Control
Proprioception refers to the sense of self-movement and body position, crucial for pilots during manual control of the aircraft. Proprioceptive feedback comes from senses in the muscles and joints, providing information about limb position, movement and applied forces. In aviation, proprioception helps pilots feel

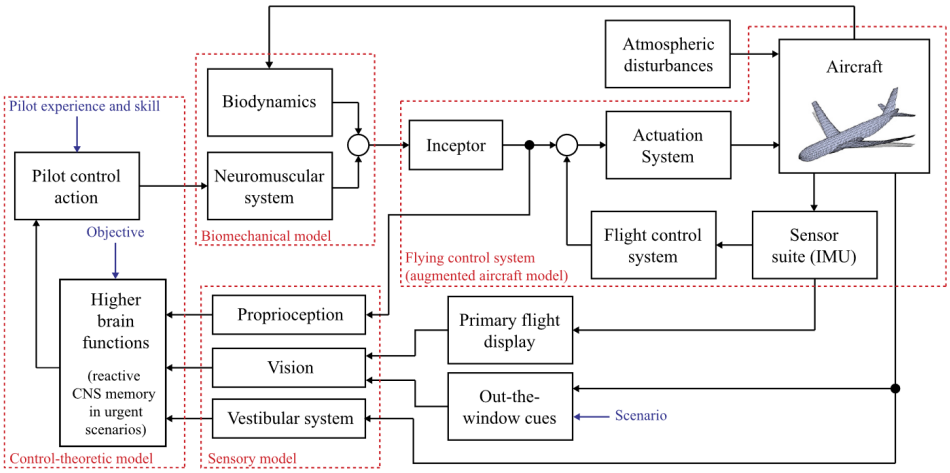

Figure 2.1: *Block diagram representing the pilot-vehicle system under manual control, Lone et al. 2014, Fig. 1 [1]*

the control forces and movements, contributing to their ability to maintain aircraft stability and execute precise manoeuvres.

Using proprioception, the pilot can sense the position and velocity of their arms as well as the force being applied as they use the stick to control the aircraft. This opens up a potential additional source of information, that can be used to improve manual control performance. Pilots may rely on proprioceptive cues for more precise control and reduce noise in their control inputs.

3

Established Manual Control Models

There has been extensive research in the modelling of the human ope rator in the context of the pilot-aircraft system. Through frequency domain analysis, **pilot behaviour during manual control** has been analysed using control systems theory and some successful mathematical models proposed.

In general as well as in the context of this report, quasi-linear models of the human operator have been extremely useful in modelling the pilot-vehicle system with minimal complexity and sufficient accuracy for most applications, and can be understood with classical control theory.

3.1. Crossover Model for Understanding Pilot Control Behaviour

McRuer et al proposed the crossover model [15] which was based on studies [19][20] that had observed that pilot control behaviour in the loop could be fitted well using a quasi-linear equalization model. This gave a method of understanding and predicting pilot manual control behaviour, especially in compensatory tracking systems. The model was based on pilots tasked with tracking a quasi-random signal, with different controlled element dynamics.

The crossover model assumes a linear equalization approximation of the human pilot, and is based on empirical evidence through signal tracking tasks. Although a human pilot is non-linear and adaptive, it was observed that pilot behaviour does not change significantly as long as the controlled element dynamics remain the same, for similar bandwidth quasi-random tracking tasks.

$$Y_{OL}(j\omega) = Y_p(j\omega)Y_c(j\omega) = \frac{\omega_c}{j\omega}e^{-j\omega\tau_e} \tag{3.1}$$

The crossover frequency of the model is defined by the frequency at which the open loop gain crosses over unit gain (0dB). The crossover model predicts the pilot model **near the crossover frequency**, such that the open loop dynamics exhibit a $-20dB/decade$ slope in that region, i.e., integrator dynamics.

This means that for different controlled system dynamics, the pilot adapts to obtain the net open loop response as close as possible to that shown in Equation 3.1 in the crossover region.

- For proportional controlled system dynamics (position control): $Y_C \approx K_C$, the pilot adapts towards dynamics such that $Y_P(j\omega) \approx (K_P/j\omega)e^{-j\omega\tau_e}$
- For integrator dynamics (velocity control) $Y_C(j\omega) = K_C/j\omega$, $Y_P(j\omega) \approx K_P e^{-j\omega\tau_e}$
- For double integrator dynamics (acceleration control) $Y_C(j\omega) \approx K_C/(j\omega)^2$, $Y_P(j\omega) \approx K_P(j\omega)e^{-j\omega\tau_e}$

The crossover model does not explain how these dynamics are created by the pilot, and based on what input, rather it gives an overall picture of the pilot-vehicle dynamics. The precision model gives further detail to the structure of the pilot dynamics, splitting these into the central nervous system (CNS), responsible for equalization, and the neuromuscular system (NMS) component.

To explain pilot equalization in further detail, other pilot models have been proposed in previous literature. This report is concerned with models that put emphasis on proprioception, and these are further discussed in Chapter 6 and Chapter 7. Since the crossover model is well established and has been repeatedly validated in studies over the past half a century, any models proposed during this project will be compared

to the general dynamics established by the crossover model. This has been incorporated through the first part of the research question of this project.

This means that any equalization model with realistic physiological parameters should be capable of providing integral parameters in the crossover region and high open loop gain in the low frequency region. Additionally the high frequency dynamics established by the precision model corresponding to the neuromuscular dynamics provide a benchmark as well, since it has proven to be a successful predictive model over several decades. Finally a plausible model must be robust to changes in system dynamics and forcing function bandwidth, to the same degree established by the crossover model [15].

3.2. Precision Model

A model of the human operator proposed by McRuer and Magdaleno based on empirical data [20] is called the precision model (PM) and is shown in Equation 3.2.

$$\overbrace{\underbrace{K_P}_{\text{Gain}}\underbrace{\frac{\tau_L j\omega+1}{\tau_I j\omega+1}}_{\text{Equalization}}\underbrace{\exp(-j\omega\tau)}_{\text{CNS Pure Delay}}}^{\text{Central Nervous System}}\overbrace{\underbrace{\frac{T_K j\omega+1}{T'_K j\omega+1}}_{\text{Low Frequency lag- lead}}\underbrace{\frac{1}{(T_{N_1}j\omega+1)}}_{\text{NMS Lag}}\underbrace{\frac{1}{[(\frac{j\omega}{\omega_N})^2+\frac{2\zeta_N j\omega}{\omega_N}+1]}}_{\text{Second Order Dynamics}}}^{\text{Neuromuscular System}} \tag{3.2}$$

In this model, a complex representation of the pilot was used in order to yield an adequate fit of empirical results. An approximate model form was proposed based on the approximations in Equation 3.3 and Equation 3.4. The high frequency terms have been approximated in the simplified precision model from third order to first order terms.

$$\frac{T_K j\omega+1}{T'_K j\omega+1} \approx \exp(-j\alpha/\omega) \qquad \text{where, } \alpha \doteq \frac{1}{T'_K} \pm \frac{1}{T_K} \tag{3.3}$$

$$\frac{1}{(T_{N_1}j\omega+1)((\frac{j\omega}{\omega_N})^2+\frac{2\zeta_N s}{\omega_N}+1)} \approx \frac{1}{1+T_N j\omega} \quad or \quad \exp(-j\omega T_N) \qquad \text{where, } T_N \doteq T_{N_1}+\frac{2\zeta_N}{\omega_N} \tag{3.4}$$

The simplified precision model is thus shown in Equation 3.5, with τ_e being the effective time delay incorporating NMS lag ($\tau_e = \tau + T_{N_1}$ when second order NMS dynamics are preserved in the open loop). The low frequency phase lag correction, given by the term $\exp(-j\alpha/\omega)$, can be omitted when low frequency dynamics are not relevant.

$$Y_P(s) = K_P\frac{\tau_L s+1}{\tau_I s+1}\exp(-j[\omega\tau_e+\alpha/\omega]) \qquad \text{where, } \tau_e = \tau + T_N \tag{3.5}$$

The lead and lag time constants, τ_L and τ_I, are important to equalization, and are adjusted by the pilot to obtain integrator-like dynamics in the open loop near the crossover frequency. The gain is adjusted to set the crossover frequency. Based on empirical results, McRuer et al. proposed verbal adjustment rules that can be used to compute the parameter values [15].

In its simplest application, this model can be applied to a pilot doing a single-axis manual control task using a compensatory display. The model can be used to determine the output to the stick given by the pilot through the neuromuscular system, using the formulation in Equation 3.2. The compensatory display only shows the pilot the error signal obtained by comparing the desired output with the measured output of the controlled element. A compensatory display was used by McRuer et al. to obtain the crossover model and the verbal adjustment rules, and later expanded to multiple outputs as well as different display types.

An assumption that the display is the only element through which the pilot is observing the output is inaccurate, as the vestibular and the neuromuscular systems amongst other systems also give the pilot information. In an experimental setting vestibular input can be absent when the setup does not provide motion cues, however, neuromuscular or proprioceptive feedback can still be present. The assumption in the use of the simplified precision model is that the pilot does not make use of this signal. The neuromuscular system and proprioception mechanisms are discussed further in Chapter 4.

4

Neuromuscular System Overview

The neuro-musculoskeletal system, usually called the neuromuscular system (NMS) is responsible for generating movement in our body to interact with the world around us. It is adaptable, and able to adjust reflexive responses and stiffness based on commands from the central nervous system. It acts as both an output system (for motion and force application) and a sensory system (perceiving force and displacement of the body) [21]. While the skeleton and joints give structure to the system, the muscles are responsible for generating forces to produce motion. The nervous system is responsible for carrying information back and forth between the muscles and the brain.

4.1. Signal Processing and Transmission

All signal processing and transmission in the system is done through neurons. These consist of a cell body, dendrites that receive signals, and an axon that sends signals to other neurons, muscles, or glands. Neurons communicate through electrical impulses and chemical signals across synapses, enabling complex processes.[21]

The central nervous system (CNS) processes incoming information (**afferent signals**) by receiving sensory inputs through specialized neurons that relay data to the brain or spinal cord. These signals are integrated and interpreted to produce a response. Outgoing information (**efferent signals**) is transmitted to the muscle-skeletal system through **motor neurons** after CNS processing, leading to actions like muscle contractions or glandular outputs. The speed of signal transmission depends on the distance and type of neurons involved, with delays ranging from milliseconds to a few seconds, especially in complex reflex arcs or higher cognitive processes [21].

The motor neurons carry signals as electrical impulses along their axons, which are insulated by myelin sheaths to increase transmission speed. This can increase the signal transmission speed by up to ten times as compared to non-insulated neurons. When the signal reaches the neuromuscular junction, it triggers the release of neurotransmitters, causing muscle fibres to contract. Signal transmission speed is about 10–100 meters per second, meaning responses can occur in milliseconds depending on the distance from the CNS to the muscle [21] .

The timings of neurons firing is considered less important in clinical research and the focus is usually on measuring the **firing rate** of neurons [21].

4.2. Muscle Actuation

Muscles are made up of **motor units**, each consisting of a motor neuron and the muscle fibres it innervates. These units process information by converting neural signals into muscle contractions, a process initiated by the firing of the motor neuron and the resulting depolarization of muscle fibres. Smaller motor units, which have fewer fibres and slower responses, are more **precise** and efficient for sustained, low-force tasks, such as posture maintenance. Larger motor units, with more fibres and faster responses, are more **powerful** but less precise, and are recruited for high-force, rapid movements.

Electromyography (EMG) is a technique used to measure the electrical activity generated by muscles during contraction. It detects the electrical signals produced when motor neurons activate muscle fibres. EMG can be performed using surface electrodes placed on the skin above the muscle, or intramuscular

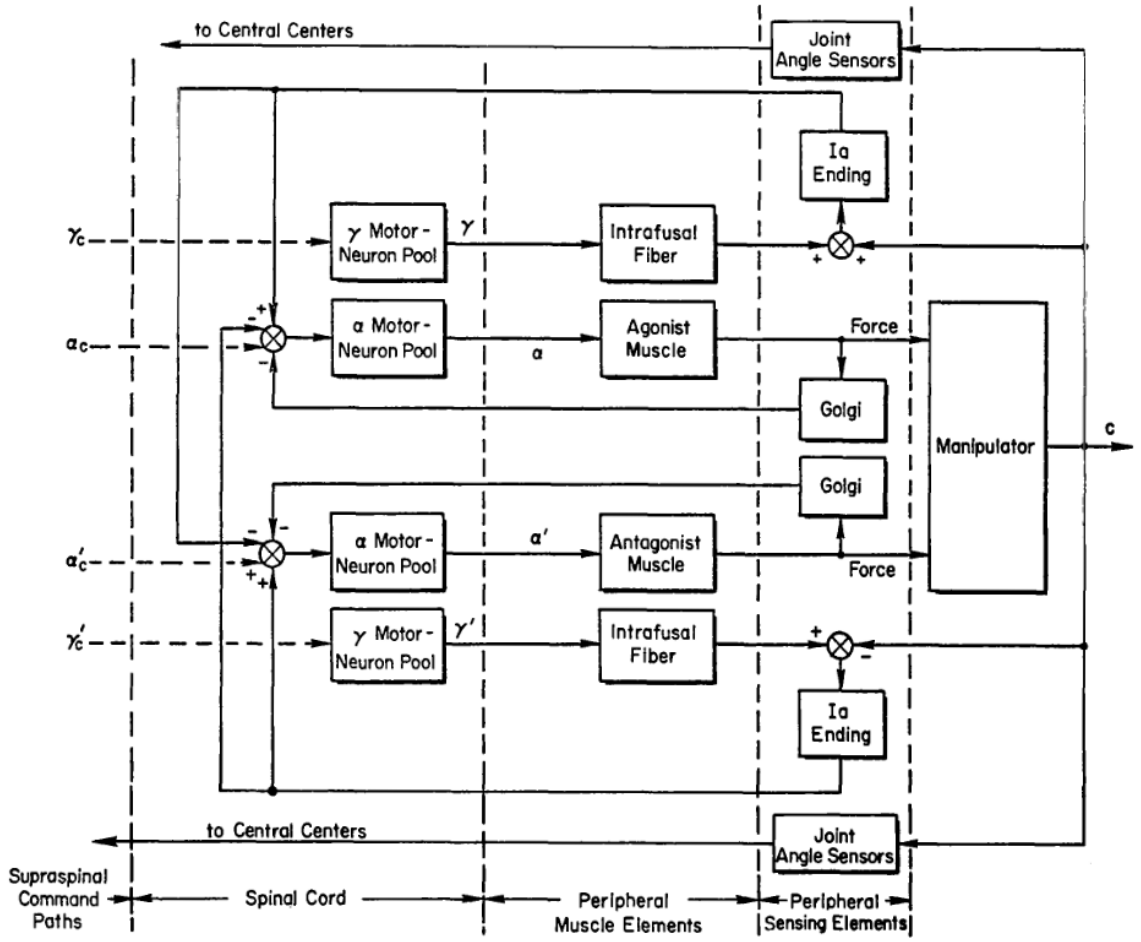

Figure 4.1: *Functional Diagram of the agonist-antagonist NMS elements involved in tracking (Magdaleno et al., 1971, Fig. 5) [2]*

electrodes inserted directly into the muscle. The former is used most often for research applications. The electrical signals are recorded and analysed, providing information about the timing, intensity, and pattern of muscle activation. This method is commonly used to study muscle function, diagnose neuromuscular disorders, and assess muscle response during various physical activities.

Muscle co-contraction or co-activation occurs when two opposing muscle groups (agonists and antagonists) contract simultaneously around a joint. This phenomenon helps stabilize the joint and control movements, especially during tasks requiring precision or when the body needs extra stability. Magdaleno and McRuer incorporated the agonist-antagonist pairing and co-contraction into their model of the NMS and consequently implicitly into the precision model [4] [2] (Figure 4.1).

In a study to identify the feedback component in the NMS during a pitch control task, Damveld et al. discovered unexpectedly high levels of co-contraction during the pitch control task as compared to the position control task [22].

In a study in 2020 Saliba et al. found that a strategy utilizing co-contraction significantly improved performance during a perturbation tracking task requiring only elbow flexion/extension. They reported significant improvements in performance even at low levels of co-contraction [23].

In Bachelder's experiment, muscle co-contraction is explained as a mechanism to improve stability and accuracy in challenging motor tasks. By increasing muscle stiffness, co-contraction enables near-instantaneous corrections to perturbations, thereby enhancing tracking performance [9].

Hess incorporates muscle co-contraction implicitly within his structural model of the adaptive human

pilot. He discusses the co-activation of agonist and antagonist muscle pairs, specifically through the concept of **alpha-gamma linkage**. This linkage is highlighted as necessary for the coordinated function of intrafusal and extrafusal muscle fibres, contributing to muscle stiffness and damping, which are vital for stabilizing the manipulator during control tasks. Co-contraction was proposed as a possible reason for the presence of washout characteristics in the proprioceptive feedback loop in Hess' structural model [7].

4.3. Proprioceptive Feedback organs

Proprioception refers to the body's ability to sense its position, movement, and the forces acting on its muscles and joints, providing awareness of the internal state. This information is crucial for coordinated movement and balance. **Golgi tendon organs** (GTOs) are sensory receptors located at the junction between muscles and tendons. They sense **muscle tension** and help prevent damage from excessive force by signalling the CNS to inhibit muscle contraction when tension is too high. **Muscle spindles** are located within the muscles and sense **muscle stretch** (type II) and the **rate of stretch** (type Ia, which has a higher transmission speed). Muscle spindles help regulate muscle length and movement speed. These spindles relay information about muscle length and velocity to the CNS, enabling fine control and adjustment of muscle contractions. The GTOs thus provide sensory feedback of force control, and muscle spindles relay muscle length and velocity feedback.

α**-motorneurons** are present in the spinal cord and responsible for innervating the contractile muscles based on signals from the brain (via upper motorneurons). γ**-motorneurons** are responsible for innervating the contractile fibres within the muscle spindles themselves.

As described in the neuromuscular system model by McRuer et al. (Figure 4.3), **alpha-gamma linkage** is the interaction between alpha motor neurons and gamma motor neurons within the muscle control system. It is essential for coordinated muscle movement, especially in activities requiring fine motor control and adaptive responses[4]. This mechanism utilizes proprioception to give internal feedback and is further discussed in Section 4.3 and McRuer's physiological model is discussed in Section 4.4.

Hess' structural model assumes **alpha-gamma linkage**, where both intrafusal (spindle) and extrafusal fibres co-activate, contributing to co-contraction. This mechanism enhances muscle stiffness and damping, which are critical for fine control during manual tasks [7].

Houk and Henneman, through experimentation on actively stimulated muscle, proposed a model for the GTOs suggesting that they "*constantly transmit to the spinal cord a filtered sample of the active forces being produced in the muscle. The dynamic properties of the filter are approximated by a linear mathematical model*" - Houk and Henneman, 1967, p. 480 [24]. The filtering process **favours rapid changes** in active force over slower changes, due to the receptor's dynamic properties. Hess' quasilinear models of proprioceptive feedback equalization also include washout characteristics, suggesting similar reasoning [6] [7].

Recent research at TU Delft suggests that the neuromuscular system is more sensitive to force changes than to position changes [25]. This was likewise observed by Bachelder [9] and Boogaard [3], with zero stiffness manipulators causing poorer tracking performance by a human operator.

In addition, there exist local feedback loops that help with muscle control through reflex actions. Muscle spindle feedback can directly excite alpha motor neurons to counteract muscle stretch (e.g., knee-jerk reflex). Moreover signals from Golgi tendon organs inhibit motor neurons through interneurons to prevent excessive force generation, which could damage muscles. Since interneurons also receive signals from the brain, which can translate to adaptable gains within these feedback loops. The brain can also generate an internal model based on an internal representation of the neuromuscular system and the environment. By generating expected sensory feedback (from muscle spindles and Golgi tendon organs), the system can pre-emptively adjust muscle activation. This combination of feed-forward and feedback control allows faster and more precise control [21].

4.4. Modelling the Neuromuscular and Proprioceptive Systems

Hill was the first to propose a mechanical muscle model able to present a simplified representation of muscle behaviour. The Hill-type model simplifies muscle behaviour using three components: the **Contractile Element**, which generates force based on activation and contraction velocity, following a force-velocity

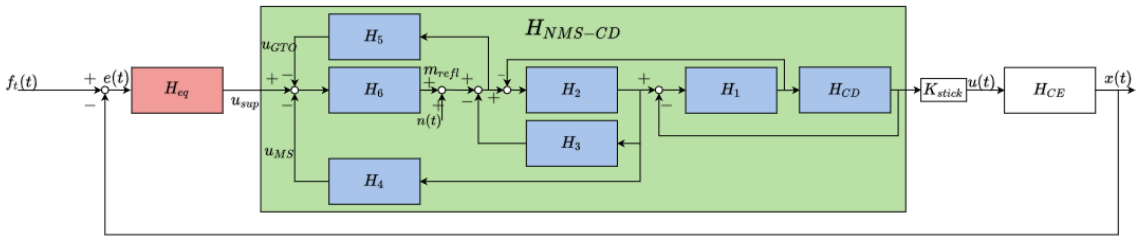

Figure 4.2: *Block diagram of the Human Operator (HO) and Control Device (CD) in a pursuit tracking task with the assumption that only the error signal is perceived from the visual display (Boogaard 2021, Fig. 9 [3])*

relationship; the **Series Elastic Element**, representing tendon elasticity with a non-linear stretch-force relationship; and the **Parallel Elastic Element**, modelling passive muscle stiffness. Additionally, the force-length relationship describes how muscles produce optimal force at intermediate lengths due to maximal filament overlap, while force diminishes at extreme lengths when muscles are overstretched or fully contracted [26]. This is a non-linear model, however for manual control tasks, muscle dynamics are often linearized to simplify analysis. The **contractile element** is approximated by a linear force generator with damping properties. The **series elastic element** and passive elasticity are represented as linear springs. This linearization is task-dependent and depends on muscle base force and the activation level of motorneurons, and system gains can be controlled by the CNS to a certain degree, showing the adaptive nature of the NMS. Depending on its applications, models based on Hill's can often seem too simple or too complex.

For general applications, a second order model of the combined NMS and stick dynamics as depicted in Section 3.2 is often sufficient.

In his structural model (Figure 6.2) Hess represented the neuromuscular system and manipulator dynamics as a second order system with the addition of the muscle spindle dynamics responsible for proprioceptive feedback and equalization [7].

Another more complex model developed in TU Delft incorporates local muscle feedback loops as well and is shown in Figure 4.2 [3]. The components of the model and their mathematical properties are shown in Table 4.1. An interesting property of this model is the lack of a lag term in the spindle feedback and no equalization terms for GTO feedback. This was a property suggested by van Paasen et al., as results from fitting tracking data to a model suggested that the neuromuscular feedback loop does not exhibit integrating open loop behaviour. The model could thus be simplified by limiting it to proportional and derivative control [27]. A lag equalization term has been presented in the structural model (Section 6.2), which would have to thus be **processed through the CNS**, with an additional inner loop signifying the internal neuromuscular feedback loop containing only low frequency washout characteristics (Section 6.2).

Table 4.1: *Mathematical Properties of the TU Delft NMS Model in Figure 4.2 [3]*

Description	Mathematical model
Grip dynamics	$H_1 = B_g j\omega + K_g$
Arm dynamics	$H_2 = \frac{1}{I_{arm}(j\omega)^2}$
Intrinsic muscle dynamics	$H_3 = B_i j\omega + K_i$
MS response	$H_4 = e^{-\tau_d j\omega}(K_v j\omega + K_p)$
GTO response	$H_5 = e^{-\tau_d j\omega} K_f$
Neuromuscular activation	$H_6 = \frac{\omega_{nm}^2}{(j\omega)^2 + 2\zeta_{nm}\omega_{nm} j\omega + \omega_{nm}^2}$
Manipulator	$H_{CD} = \frac{1}{I_{CD}(j\omega)^2 + B_{CD} j\omega + K_{CD}}$

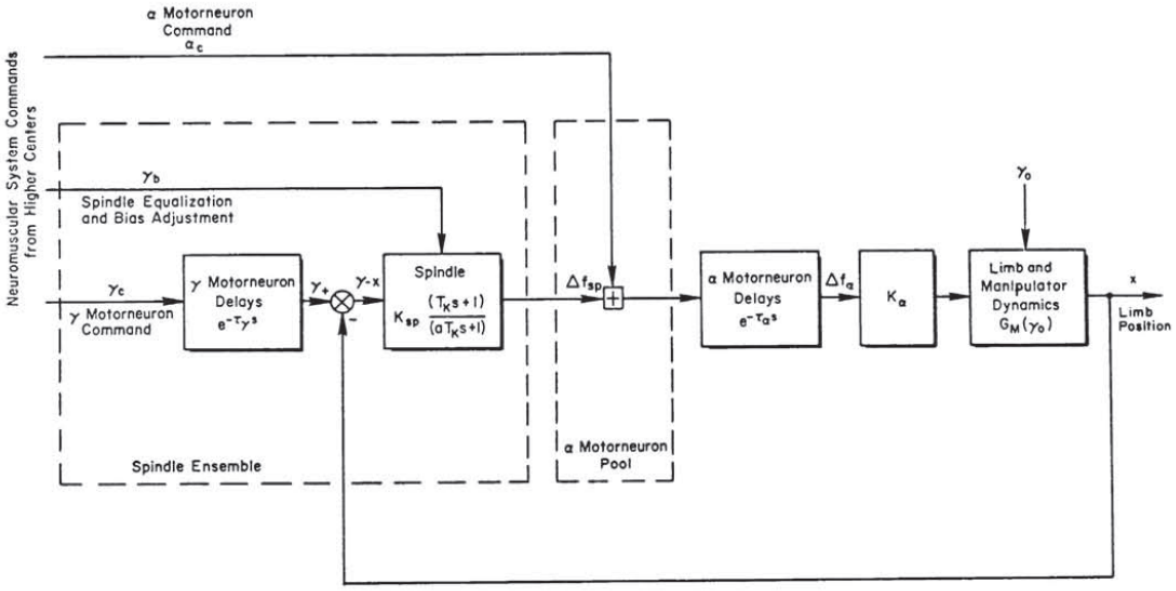

Figure 4.3: McRuer Neuromuscular Model [4]

McRuer et al. Physiological Model

McRuer et al. developed and validated a neuromuscular actuation system model and gave a detailed analysis of the physiological processes involved in actuation. They gave an explanation for the **adaptive nature** of the NMS, showing the CNS to be capable of modifying the system parameters and operating point through α motorneurons, and the muscle spindle acting as an **equalization element**, with adaptable parameters depending on the task [4]. Their precision model (Section 3.2) abstracts away from the detailed physiological components and mechanisms in order to present a less complex mathematical representation of the dynamics of the human operator as a system that fits the data obtained from compensatory tracking tasks.

The block diagram in Figure 4.3 shows the simplified neuromuscular system closed loop dynamics. According to the model, the muscle spindle provides:

1. Sensory feedback of the limb position
2. Lead/lag series equalization, parameters for which are provided by CNS via the gamma system
3. It's the source of part of the command to the system for actuation
4. A means for adjusting the steady state bias signal, adjusting the feedback gain and muscle tension

In the simplified model GTO force feedback is not visible, although the more detailed functional diagram in Figure 4.1 includes the feedback pathways involved for force feedback as well.

The model presents an equivalent single-loop feedback system composed of muscle, limb, and manipulator elements connected through sensory and equalization components. The dynamics are influenced by factors such as muscle tension and spindle feedback [4]. The authors asserted that such a simplified quasilinear model explained small perturbation behaviour of the NMS.

An experimental study by Magdaleno and McRuer in 1971 used single axis compensatory task data in order to study the neuromuscular dynamics. A mathematical model shown in Figure 4.4 was proposed for a controlled element exhibiting rate dynamics, with the retinal and central equalization changing for other controlled element dynamics based on the crossover model[2].

The model works as follows:

- The muscle/manipulator dynamics are modelled, based on experimental results, as a third order system with a gain and pure delay.
- The alpha motor neuron command α_c is sent by the CNS to the spinal cord.

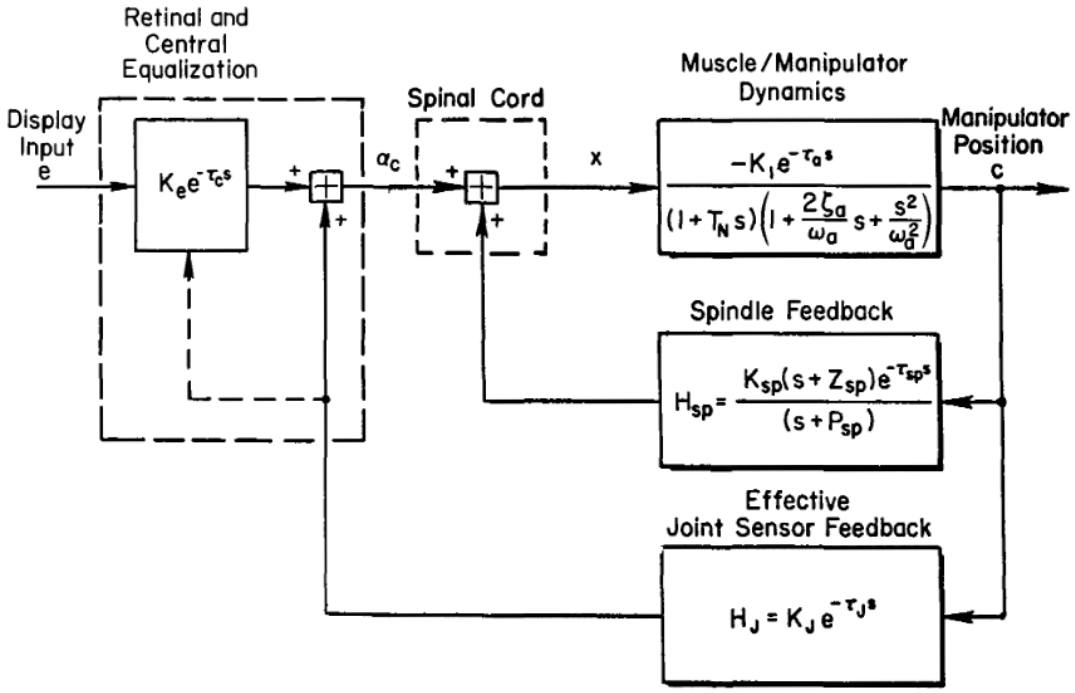

Figure 4.4: *Neuromuscular subsystems mathematical model for rate control ($Y_c = K_c/s$), Magdaleno and McRuer 1971, p. 60 Fig. 27 [2]*

- The gamma bias signal (γ_b in Figure 4.3 helps set up spindle feedback operating point equalization. The spindle equalization block is also meant to include golgi tendon feedback.
- The system includes joint sensor feedback, which acts as a gain and time delay filter for specific frequency ranges and ensures precise controlled movements. This is also sent to the CNS for bias adjustments, indicating in Figure 4.4, through the dotted feedback line, that it is used to adjust the delay parameter τ_c.

This same mechanism is also used to explain co-contraction and has been shown in Figure 4.1 with an agonist and antagonist muscle pair being sent signals separately from the central nervous system.

Another neuromuscular-manipulator model separates the feel system manipulator response in order to make distinct force and displacement feedback and was used to explain the differences between force and displacement sensoring inceptors, as well as explaining the roll ratchet phenomena [28]. Hess added this modification when using his structural model to understand aircraft handling qualities and adverse aircraft-pilot coupling (APC), and the revised structural model has been shown in Figure 7.1.

5

Smith's Adaptive Inner Loop Equalization Model

An inner loop model (Figure 5.1) was proposed by Smith that suggested an additional feedback from estimating the rate of change of the display signal. Although his study was not dedicated to modelling the pilot dynamics, but instead to establish a theory for predicting pilot opinion rating (POR), adding an additional inner loop for equalization accounting for human physiology provided a more realistic pathway to a measure for POR [5]. This model was credited by both Hess [6] and Bachelder and Aponso [11] to have first introduced the concept of an inner loop for equalization in the high frequency region.

The structure of the system for equalization remains essentially similar, however the model assumes that rate feedback for the inner loop is processed from the visual sensory input, i.e., **visual rate sensing**, without the need for an internal model of the controlled element dynamics. This suggests that (for a compensatory display) the rate feedback in Smith's model would be of the error in the vehicle output ($\dot{e_d}$ in Figure 6.1) vs the dual loop model assuming an estimate of the actual output feedback ($\hat{\dot{m}}$) rather than the error [6]. However, to obtain mathematical equivalence with the precision model (referred to as the servo model) when approximating, Smith suggests the target rate signal 'q_c' to be negligible compared to the actual output rate of the controlled element 'q' (shown in Figure 5.2). Using the symbols in Figure 6.1 this means assuming $\dot{m} \approx \dot{e}$.

Although this makes the models mathematically equivalent and therefore similarly applicable to empirical data, Hess argues that Smith's model is limited due to this necessary assumption, which implies assuming a limited bandwidth in the time rate of the target (forcing function) and disturbance signals [6]. Bachelder and Aponso similarly pointed out that visual rate feedback is also affected by a greater disturbance as compared to the system output and proprioceptive feedback, and an assumption of small disturbance is necessary to apply Smith's model [11].

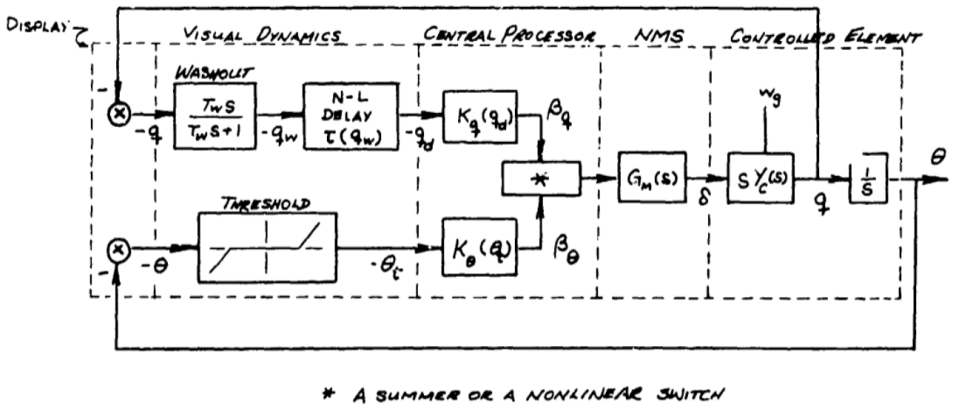

Figure 5.1: *Inner Loop model based on rate feedback (Smith 1976, p. 555 Fig. 1 [5])*

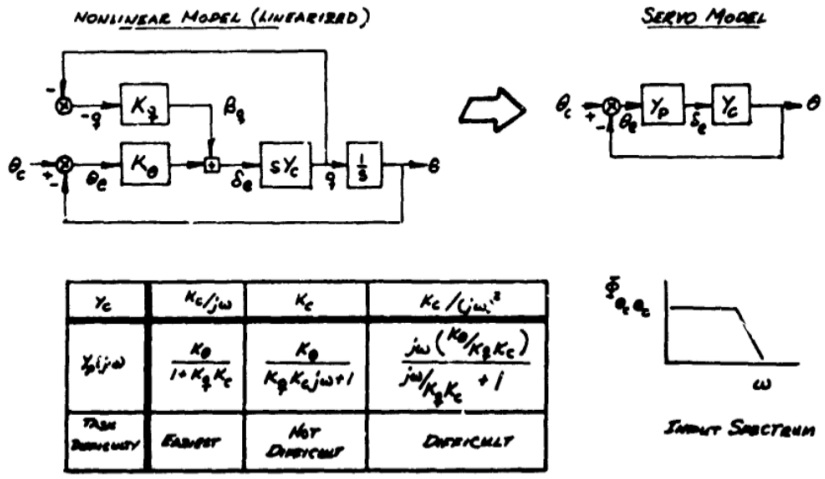

Y_c	$K_c/j\omega$	K_c	$K_c/(j\omega)^2$
$Y_p(j\omega)$	$\frac{K_\theta}{1+K_q K_c}$	$\frac{K_\theta}{K_q K_c j\omega + 1}$	$\frac{j\omega\left(K_\theta/K_q K_c\right)}{j\omega/K_q K_c + 1}$
TASK DIFFICULTY	EASIEST	NOT DIFFICULT	DIFFICULT

Figure 5.2: *Linearized approximation of the inner loop model (Figure 5.1)compared with the precision model (Smith, 1976, p. 555 Fig. 2 [5])*

Additionally according to Hess, when the displayed error is presented to the operator through an aural or tactile display, Smith's model could not be applied directly while a PF based inner loop model could.

6

Hess' Models utilizing proprioceptive equalization

Hess published his dual loop model in 1978 that attempted to explain in further depth **how** the human pilot equalization occurred that was hypothesized by previous models. He clarified that *"It is not the author's contention that the single-loop human controller models now in use are in any way incorrect, but rather that they contain an implicit but important internal loop closure which, if explicitly considered, can account for a good deal of the adaptive nature of the human controller in a systematic manner."* (Hess, 1978, p. 254 [6])

The key change in the equalization was through an additional inner loop that incorporated an internal model of the controlled element estimated by the pilot. This method was motivated by Smith's adaptive inner loop model.

A key feature of Hess' first dual loop and later developed structural model is the proprioceptive feedback and its usage in adaptive manual control. According to Hess single loop models like the precision model make the internal loop implicit, but studying the inner loop can shed some light on how the pilot adapts to different control situations, as the parameters would reflect to some degree how the pilot attempted equalization.

6.1. Dual Loop Model

The dual loop model was proposed in 1978 to study the **adaptive nature** of the pilot [6]. A block diagram showing the initial dual loop model is shown in Figure 6.1. The sensory feedback is through visual and proprioceptive channels.

The model assumes a compensatory tracking task, i.e., the display shows the relative error between the target signal and the output of the controlled system. In Figure 6.1 the **error signal '**e**'** is obtained from the difference between the target signal (not shown in the figure), and the **controlled system's output '**m**'** after including the **disturbance signal '**d**'**. The display dynamics are assumed by Hess to be negligible,

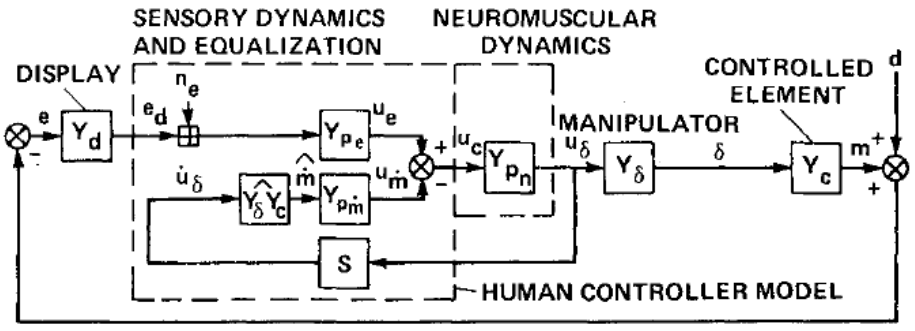

Figure 6.1: *Dual Loop Model (Hess, 1978 [6], p. 254)*

Table 6.1: Dual Loop Model description as shown in Figure 6.1 [6]

Block and dynamics	**Description and Parameters**	**Comment**
Y_d	Display dynamics	Assumed negligible
Y_δ	Manipulator dynamics	Assumed negligible
$Y_{p_e} = K_e(\tau_L s + 1)e^{-\tau_e s}$	Visual (outer loop) gain (K_e), equalization time constant (τ_L) and effective delay (τ_e)	$\tau_L = 0$ in all cases where proprioception is considered sufficient for equalization
$Y_{p_{\dot{m}}} = \frac{K_{pf}[(T_{\dot{m}}/\lvert T_{\dot{m}}\rvert)s]^k}{(T_{\dot{m}}s+1)^k}$	Proprioceptive (inner loop) gain ($K_{\dot{m}}$) and rate equalization	k=0, $\pm$1, $\pm$2 ... dictates washout characteristics and is fixed before fitting data
$\widehat{Y_\delta Y_c} = K_s s^n$	Estimated manipulator-controlled element dynamics, K_s=$\widehat{K_\delta K_c}$ (estimated gain) and n (estimated dynamics)	Both are considered adaptive parameters, however assumed known and not involved during identification
$Y_{p_n} = \frac{1}{(\frac{j\omega}{\omega_n})^2 + \frac{2\zeta_n j\omega}{\omega_n} + 1}$	Neuromuscular Dynamics, ω_n and ζ_n, are the NMS second order frequency and damping parameters	NMS delay is not included
$Y_p = \frac{u_\delta}{e_d} = \frac{Y_{p_e}Y_{p_n}}{1 + Y_{p_n}\widehat{Y_\delta Y_c}Y_{p_{\dot{m}}}s}$	Equivalent single loop controller dynamics	

Table 6.2: *Parameters of the Dual Loop model estimated using experimental data* (Hess, 1978 [6], p. 256)

$Y_\delta Y_c$	$\widehat{Y_\delta Y_c}$	K_e	τ_L, s	K_{pf}, s	$T_{\dot{m}}, s$	τ_e, s	ζ_n	$\omega_n, rad/s$
1.0	1.0	2.5	0	0.5	1.0	0.1	0.1	20
$1/s$	$1/s$	18.0	0	6.0	2.0	0.13	0.3	15
$1/s^2$	$1/s^2$	26.5	0	32.3	3.33	0.16	0.7	15
$2.82/s(s-1)^a$	$2.82/s^2$	5.5	0.33	10.0	5.0	0.15	0.1	15
$145/\Delta^b$	$10/s^2$	1.4	0	1.0	1.25	0.19	0.7	15
$2/s-2$	$2/s$	18.0	0	7.0	3.33	0.11	-	-

[a] Higher order controller model used ($k = 3$), [b] $\Delta = s^3 + 12.3s^2 + 11.6s$.

and the **displayed error signal** is represented as e_d. After accounting for the **remnant 'n_e'**, this signal is used for visual equalization in the block Y_{p_e}, and accounts for the **outer feedback loop** in the model. This error feedback through the visual channel is identical to the precision model. In this report focussing on dynamics involved in target tracking, disturbance rejection and remnant has not been addressed.

However, the precision model does not incorporate the additional inner loop feedback. This inner loop is based on the hypothesis that the pilot gets force feedback from the muscle input to the manipulator/stick (u_δ), which is **sensed as rate feedback through the GTOs**. Based on this rate feedback and an internal model that the pilot develops of the system ($\widehat{Y_\delta Y_C}$) they thus have an internal estimate of the rate of change of the vehicle output, $\hat{\dot{m}}$.

Equalization in the inner loop is acting on **rate sensed kinesthetic input** ($\dot{u_\delta}$) passed through an internal model to get an estimate of the rate of change of the controlled element output ($\hat{\dot{m}}$). This model assumes that the pilot is directly able to sense the force they apply on the stick and is able to accurately estimate the rate of change of this force $\dot{u}_\delta$ to use for equalization. In addition, it is also assumed that the pilot is able to get a reasonably accurate internal 'idea' of what the controlled element dynamics are.

Hess suggests that this internal model is able to approximate the manipulator and controlled element dynamics as $\widehat{Y_\delta Y_c} = K_s s^n$ in the region beyond the crossover frequency, and maintains a similar idea when he proposes the structural model in 1980 [7], however excluding the manipulator dynamics as the manipulator position is also sensed via spindle feedback (see Section 6.2). Based on these model dynamics the pilot is able to anticipate how the model would react to the input, i.e. they have an estimate of (1) the order of the dynamics, and (2) an estimation of the gain for $\dot{m}/u_\delta$ as shown in Figure 6.1. This internal model is used for equalization in the inner loop.

Equalization on proprioceptive input occurs in the block $Y_{p_{\dot{m}}}$ in Figure 6.1, explained further in Table 6.1. Of note is that this equalization only involves a lag term and no lead term. Mathematically since the input to the block is the **rate** sensed (estimated) output from the controlled element it introduces the differential element necessary to make up for the lack of a lead, **making rate sensing in the inner loop mathematically equivalent to a lag in the single loop model**.

In the table, the value of k being 1 implies a lag term in the input, however larger values of k are introduced to include washout characteristics (high pass filter) to explain performance data in more difficult tasks. $k = 3$ is used when $Y_\delta Y_c = K_c/s(s-1)$ in Table 6.2.

Visual feedback processing in the CNS is represented in block Y_{p_e}. Any **equalization within this block** only occurs if the proprioceptive feedback loop is unable to provide the necessary lead equalization, in which case $Y_{p_e} = K_e(\tau_L s + 1)e^{-\tau_e s}$. In all other cases $\tau_L = 0$.

Adaptive behaviour by the pilot occurs by changing the parameters K_e (outer loop/visual feedback gain), $K_{\dot{m}}$ (inner loop/proprioceptive feedback gain) and $T_{\dot{m}}$ (inner loop lag time constant) along with the internal model $\widehat{Y_\delta Y_C}$. If the inner loop is insufficient for equalization (e.g. when proprioceptive feedback is weak), only then an outer loop (visual) lead with time constant τ_L is employed.
The quality of the sensory inputs dictate the relative loop utilization of the outer and inner loop, quantified by the respective gains K_e and $K_{\dot{m}}$. When the inner loop is utilized more, the lag time constant $T_{\dot{m}}$ is larger.

The pilot adapts such that the order of $\hat{\dot{m}}/u_\delta = s\widehat{Y_\delta Y_c}$ is given by $sK_s s^n, n \in \mathbb{Z}$, where K_s (estimate of controlled element gain) and n (are determined by the behaviour of the system beyond the open-loop crossover. This means that

1. for proportional control, $Y_c = K_c$, the pilot uses the differential element in the inner loop for equalization $(U_{\dot{m}}(s)/U_\delta(s) = sK_c\frac{K_{pf}[(T_{\dot{m}}/|T_{\dot{m}}|)s]}{(T_{\dot{m}}s+1)})$,
2. for integral control, an equivalent gain with washout dynamics $(U_{\dot{m}}(s)/U_\delta(s) = s\frac{K_c}{s}\frac{K_{pf}[(T_{\dot{m}}/|T_{\dot{m}}|)s]}{(T_{\dot{m}}s+1)})$,
3. and for double integrator control an integrator in the model estimation is necessary to create a lag term in the inner loop $(U_{\dot{m}}(s)/U_\delta(s) = s\frac{K_c}{s^2}\frac{K_{pf}[(T_{\dot{m}}/|T_{\dot{m}}|)s]}{(T_{\dot{m}}s+1)})$.

The neuromuscular system is approximated using second order dynamics with the natural frequency ω_n and damping ζ_n, similar to the precision model. The neuromuscular delay, which was incorporated into

an effective delay in the precision model, cannot be seen the same way here as the **inner loop does not include a delay** beyond the lag component in the equalization block $Y_{p_{\dot{m}}}$.

6.1.1. Validation and Results

This model was fitted to experimental data with four different model dynamics, $Y_C = K$, K/s, K/s^2, $K/s(s-1)$, with increasing pilot workload.

For the first three cases the data used is the same as that obtained by Kleinman et al. in their study proposing and validating the optimal control model in 1970 [29]. The experiment involved a single axis compensatory tracking task, with an error display only. The sum-of-sines forcing function was introduced through a disturbance, amplitudes dictated by noise spectra with 1st order dynamics introduced as a velocity disturbance for both K/s and K/s^2 dynamics, and 2nd order for position disturbance in the case of proportional dynamics (K), with a break frequency of 2 rad/s. Kleinman et al. published more details about the experiment in a separate study [30] which mentions experiments were performed with **three** subjects who were trained pilots, after thorough training in the task. It was stated that the error due to the large remnant and disturbances made high frequency (beyond 2 rad/sec) describing function data less accurate. The spectra however were considered accurate up to roughly 36 rad/sec. The input to the manipulator was measured and the describing functions obtained were averaged over the three subjects.

Data for the fourth controlled system dynamics ($K/s(s-1)$) was taken from a study by Elkind et al. who used the same data for parameter calibration before a different task was conducted [31]. This experiment also involved a compensatory display with the subjects being four trained pilots, extensively trained in the task beforehand.

In all cases the pilots were asked to minimize the means square tracking error.

Hess mentioned the manipulator to be an isometric force device, leading to the assumption that manipulator dynamics are negligible. Data fitting of the model was done with this assumption. Moreover it was assumed that $k = 1$ for the first three control tasks ($Y_c = K_c, K_c/s, K_c/s^2$ and $k = 3$ for the fourth ($Y_c = K_c/s(s-1)$). The parameters used for data fitting were therefore as mentioned in Table 6.1. Identification results are as mentioned in Table 6.2. **The fitting was not rigorous**, however the parameters obtained when substituted provided a satisfactory approximate fit of the data.

According to Hess this model provides approximately similar describing functions to those measured in the experimental tracking tasks, with the parameters being within reasonable constraints (Table 6.2).

For the first three cases, equalization is done purely through proprioceptive feedback ($\tau_L = 0$). For the fourth system, however, a lead similar to the simplified precision model is present in the visual compensation block Y_{p_e} which contributes towards equalization, with a lead time constant $\tau_L = 0.33s$.

6.1.2. Verification of Pilot Internal Estimation Model

To check the hypothesis of the pilot approximately estimating controlled element dynamics as $\widehat{Y_\delta Y_c} = K_s s^n$, Hess fitted two other controlled element dynamics datasets as well.

The first dataset for $Y_c = K_c/s^3 + 12.3s^2 + 11.6s$ was borrowed from Levison et al., 1976 [32]. The second for $Y_c = K_c/(s-2)$ was borrowed from Jex and Allen, 1970 [33].

Table 6.2 shows the assumed approximations of the controlled element dynamics by the pilot, along with the parameters obtained after fitting the dual loop model. The estimated and exact dynamics for the first model show approximately identical gain for frequencies at and beyond crossover ($\omega_c = 1.8 rad/s$), however significant difference in phase. Due to rate sensing and the high pass filter, this is also the frequency domain where the inner loop feedback is likely to be concentrated.

For the first case, the model was fitted with a similar method to the systems before, however for the second case, a model with no second order NMS dynamics was used ($Y_{p_n} = 1$ in Figure 6.1 and Table 6.1) due to no data being available in the high frequency (>10 rad/sec) band. The DL model was able to approximately match experimental data with the parameters shown in Table 6.2.

A more detailed analysis of the results, along with results from the structural model, is presented in Section 6.2.

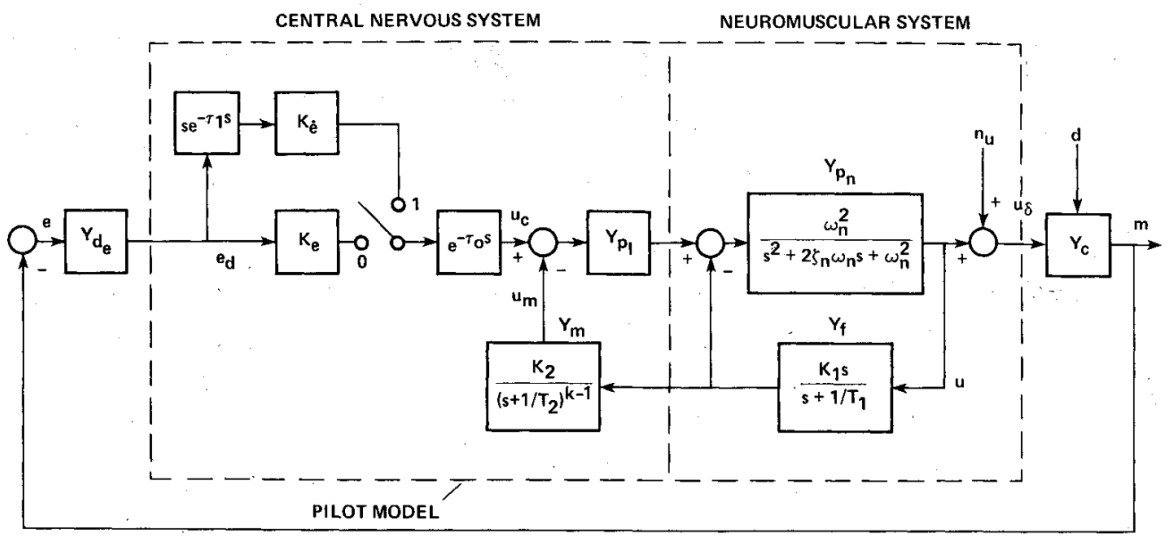

Figure 6.2: *Structural Model, Hess 1980, p. 417 Fig. 1 [7]*

6.2. Structural Model

Hess later updated the DL model, proposing the structural model (SM) [7]. The goal of the model was to develop further the understanding obtained from the dual loop model of the mechanism of pilot equalization and adaptation. The SM attempts to clarify further the nature of the internal model of controlled element dynamics sensed by the pilot, and better explain adaptive behaviour. It also includes an element to better explain non-linear pilot behaviour (pulsive control for more difficult tasks).

In a study in 1984 Hess showed time delays in the vehicle dynamics leading to a significant lead generation by the pilot and causing regression in pilot-vehicle crossover frequencies. This was hypothesized to be a major factor in increasing pilot workload and causing pilot induced oscillations (PIOs) [34]. He also provided an analytical analysis of PIOs using the optimal control and crossover models [35]. In his **revised structural model in 1990**, Hess incorporated cockpit inceptor force-feel system dynamics in order to help design better inceptors to mitigate pilot-induced oscillations [8] [36]. The revised model also included an extension to the SM first proposed in 1990 to include vestibular motion cues [37].

6.2.1. The Main Elements of the Structural Model

In the SM (Figure 6.2) the controlled element, Y_c, is being controlled by the pilot in a single axis compensatory display control task. The SM was also extended to a pursuit tracking task in 1981 [38]. Hess offers a clear demarcation showing the control dynamics implemented by the CNS and the NMS dynamics. Of note, equalization based on proprioception seems to occur through the CNS, however the delay associated with signal transfer and processing (pure delay, included in the block labelled $e^{-\tau_o s}$ in figure) is not incorporated into the PF inner loop, suggesting that although the inner loop equalization is capable of adaptive behaviour controlled by the CNS, the information processing and equalization itself occurs locally in the NMS.

The controlled element dynamics Y_c and the display dynamics Y_{d_e} are the same as the dual loop model (Y_c and Y_d in Figure 6.1), with the display dynamics assumed as negligible during data fitting. Also similar to the dual loop model, this model has two loops aimed for equalization, an external loop based on visual compensatory feedback and an internal loop based on proprioceptive feedback.

A departure from the dual loop model was the **removal of manipulator dynamics as a separate structure**. The dual loop model hypothesized that the operator received force feedback and internally modelled the manipulator and controlled system models as a combined element, in this new model it is assumed to be implicit within the controlled element dynamics. Practically, since the DL model was validated only with an **isometric controller assumption** and no manipulator dynamics, the results do not differ. Although **force feedback is the assumed information source for proprioceptive equalization**, verification of this assumption was not within the scope of this experiment. Although force feedback was hypothesized, this study did not confirm it, and Hess addressed this in further detail in a later study (see

Section 7.2). Later studies citing this model have often mistakenly attributed u_δ to be the manipulator deflection feedback, although this does not make a difference in the mathematical model due to the isometric manipulator assumtion.

The remnant is hypothesized to arise from non-linearities and time variations in the pilot model, due to, for example, incorrect parametrization. The remnant is therefore injected into the pilot output as a pure process noise.

Visual feedback from the display (Y_{d_e}) is processed either through a direct equalization gain (gain K_e) or through a visual rate sensing region with a delay (gain $K_{\dot{e}}$ and delay τ_1), the latter meant for higher workload tasks.

Hess introduced a visual rate sensing component in the visual sensory model, and in a unique approach included a switch component rather than adding weighted attitude vs rate perception directly. Rate sensing had an additional delay associated (τ_1) in addition to the visual processing and signal delay τ_0. τ_1 depends on what kind of feedback was available to the pilot. Hess noted that in the case of aural or tactile displays, rate would have to be derived internally and the time delay would be larger, while for direct rate perception the sampling delay would be negligible. During data fitting, a conservative sampling delay of $\tau_1 = 0.2s$ and a central processing delay of $\tau_0 = 0.14s$ were estimated with the assumption that rate was perceived via the central (foveal) vision. Later experiments have shown rate perception to take significantly greater delay when through central vision as opposed to peripheral vision [39].

McRuer's differential displacement model in 1967, a model describing lead generation through visual rate perception, was used [40], to select a rough delay of $\tau_1 = 0.2$ seconds.

A similar switching approach was also used by Hess in his revised structural model in 1997 [36], while adding a noise signal to visual rate perception as well, however excluding the time delay τ_1 in this model. In this publication a central processing delay of $\tau_0 = 0.2s$ as an estimate of the crossover model's effective time delay τ_e. This can be seen in Figure 7.1.

Hess maintained that choosing some parameters such as the effective time delay and NMS dynamics as invariable before applying estimation techniques on the other parameters that exhibited higher variability and adaptiveness allowed consistently accurate results despite the analytical simplification. In the revised model, also included in the visual perception dynamics was a low frequency integral compensation to exhibit the pilot's trimming behaviour. It was considered a minor compensation at a low frequency and assumed negligible for the purposes of this study ($\epsilon \equiv 0$).

The switch between proportional and rate sensed visual feedback is parametrized by a probability term for the system being in either control mode, introducing some flexibility and adaptability not present in the dual-loop model. The probability term P_1 varies depending on the nature of the task and the difficulty of control. Hess provides specific values for different controlled-element dynamics:

- Simple control tasks (K_c and K_c/s dynamics): $P_1 \approx 0.05$, meaning almost no error rate control is used.
- More complex control tasks (K_c/s^2 and $K_c/s(s-1)$ dynamics): P_1 increases to around 0.2, indicating increased reliance on error rate feedback.
- Highly complex control tasks ($K_c/s(s^2 + 1.414s + 1)$): P_1 is set at 0.25, meaning error rate feedback plays a significant role.

When it comes to proprioceptive equalization, the SM makes the proprioceptive equalization dynamics more explicit and the internal model implicit, with Y_m taking a different form depending on the estimated controlled element dynamics and representing the adaptive behaviour of the pilot based on sensed controlled element behaviour. While Y_m is the equalization block, Y_f represents the muscle spindle feedback and acts as both a differentiator at low frequencies (as in the dual loop model) as well as providing washout characteristics. This helps smooth out long-term changes in system behaviour and focus the control response on more immediate, higher-frequency inputs.

The neuromuscular dynamics are once again modelled as a second order system, with the addition of spindle feedback characteristics incorporated in an additional local feedback loop. Although not as significant as a series lag term or a pure delay element at higher frequencies, **this does introduce a delay at lower frequencies** upon loop closure. There is no other explicit delay element present.

An additional new element of the model is the block for pulsing logic, Y_{P_I}. This block is useful for explaining the pulsing behaviour of the pilot in high workload tasks, as Hess explained in a separate publication[41]. For easier tasks $Y_{P_I} = 1$.

6.2.2. Equalization

The structural model utilizes the same equalization pathway as the dual loop model, with $Y_{pf} \approx sK_{pf}\hat{Y}_c$. This structure in the inner loop enables an equivalent open loop expression corresponding to the crossover model, excluding delays. The mechanism assumes an internal derivative followed by an estimation of the order of the controlled element dynamics. However the internal model estimation is written in a different formulation.

The model assumes that the pilot perceives the controlled element dynamics similarly to the dual loop model (see Table 6.1). When sensing a proportional control task, the pilot uses a lead in the inner loop ($Y_m = K_2(s + 1/T_2)$). For integral control, Y_m is a pure gain, and for a controlled element with double integrator dynamics, a lag is used $(Y_m = \dfrac{K_2}{s + 1/T_2})$.

While Y_m is responsible for dynamic equalization based on the internal model of the controlled element, Y_f represents the feedback provided by the muscle spindle and incorporates a differentiator for low frequency signals. The format for these dynamics were not directly addressed, with Y_f being generally attributed to GTO and MS dynamics, with the force vs position feedback using either organ not directly addressed.
Hess observed that the parameter T_2 was necessary (in place of having pure s^k dynamics to replicate the controlled element) in order to match the model with experimental data. This suggests that equalization in the inner loop is only applied to a certain frequency region, suggesting that low-frequency sensory input from the muscle spindles/GTOs is not processed for dynamic equalization. An assumption of $T_1 \approx T_2$ was used to fit the model to experimental data, implying that the time constant is dependent on the (adaptive) behaviour of the muscle spindles.

The model assumes that the CNS adjusts its control behaviour through **constant gains** applied to the error and error rate signals. These gains are represented as K_e (for the error) and $K_{\dot{e}}$ (for the error rate). By adjusting these gains, the CNS is effectively equalizing the control system response to match the desired behaviour.
The operator can switch between error-based control and error-rate-based control, with equalization applied differently in each mode. The switch is controlled by a probability parameter P_1, which determines how often the system relies on error rate rather than error. This probabilistic switching provides flexibility in how the operator equalizes the system [7].

In his study modelling pilot induced oscillations (PIO), Hess suggested that during such an event the pilot regressed to using only error rate control without proprioceptive feedback for equalization, leading to the undesirable behaviour [36].

6.2.3. Validation

In validation of the dual loop model, Hess neglected the manipulator dynamics, hence the DL model does not directly say much about force vs position feedback. The SM also assumes negligible control stick dynamics, leaving the question of force vs position feedback open.

Data used for the first three cases ($Y_c = K_c, K_c/s, K_c/s^2$) is the same as that used for the DL model (Table 6.2).

For the case of $Y_c = K_c/s(s - 1)$ and $K/s|_{peripheral}$, a study in 1971 by Levison et al. provided the data [42]. And for $Y_c = K_c/s(s^2 + 1.414s + 1)$ data from another study by Levison in the same year was used [43].

Only the parameters $K_e, K_{\dot{e},K_2,T_1}$ and P_1 were adjusted fit the measured frequency response. Other parameters were assumed to be known beforehand being a non-adaptable property of the physiology, or based on the known controlled element dynamics in the case of k. The introduction of the switch between the two visual pathways made the process of model fitting much more complicated.

Table 6.3: Pilot model parameter values for the Structural model [7]

	Model Parameters											
Controlled-element dynamics	k	K_e	$K_{\dot{e}}$	K_2	P_1	T_1	K_1	τ_0	τ_1	ζ_n	ω_n	ρ
K	0	11.1	2.13	2.0	0.05	5.0	1.0	0.14	0.2	0.707	10.0	0.38
K/s	1	22.2	3.42	2.0	0.05	5.0	1.0	0.14	0.2	0.707	10.0	0.38
K/s^2	2	26.2	10.5	10.0	0.20	2.5	1.0	0.14	0.2	0.707	10.0	0.38
$K/s(s-1)$	2	89.6	28.6	30.0	0.20	1.0	1.0	0.14	0.2	0.707	10.0	0.38
$K/s(s^2+1.414s+1)$	3	116.0	13.0	35.0	0.20	0.85	1.0	0.14	0.2	0.707	10.0	0.38
$K/s\|_{peripheral}$	1	12.6	2.52	0.75	0.25	5.0	1.0	0.14	0.2	0.707	10.0	0.38

Fitting was a complicated process mainly due to the switching behaviour for which a mathematical approximation had to be used. A non-rigorous parameter estimation methodology similar to the already mentioned dual loop model fitting was used to obtain the parameter values.

The parameter values obtained via fitting the data are shown in Table 6.3.

6.2.4. Later Development and Applications

The Task-Pilot-Vehicle (TPV) model, a computer-based simulation model that helps in designing and testing aircraft flight models, was used to simulate the pilot vehicle multi-axis control model of a rotorcraft based on Hess' structural model in 2010 [44].

Modifications to the structural model by Efremov et al. improved agreement with calculated error variance, as well as evaluating the influence of newer task variables (control element gain coefficient and the acceptable accuracy range) on pilot-vehicle interactions. It was successfully applied to predictive display design (for spacecraft docking with the ISS) and to developing a lateral flying qualities prediction criterion that incorporated motion cue effects [45].

7

Force vs Position Feedback

To understand how proprioceptive feedback can be modelled, the distinction between the pilot sensing force feedback vs position feedback from the stick is crucial. Some experiments have been conducted to analyse this by modifying the stick dynamics between a free-moving stick and a stick having various spring constraints. In a 1966 study analysing manipulator restraints and their effect on the pilot's performance, Magdaleno and McRuer found that in tasks with more difficult dynamic s (double integrator control), pilot performance was best at an intermediate spring stiffness. With no spring however, increasing stick inertia caused performance to degrade significantly for proportional and double integrator control dynamics. This experiment had only one subject due to limitations on the number of runs they could conduct [13]. In another study in 1971, Magdaleno and McRuer obtained results suggesting a central processing delay constant of 66ms and 82ms when fitting their NMS model to tracking tasks conducted with isometric and isotonic inceptors respectively, suggesting force feedback improved performance, however could not confirm statistical significance due to limited data and only two subjects present. They also noted **a greater average tension in agonist-antagonist muscle pairs reduced response delay** when using higher quality muscle tension data from a foot rudder inceptor based manual tracking task, with describing function data being nearly identical to a hand manipulator inceptor [2].

In another 2017 study, Fu et al. performed an experiment analysing pilot's discrimination strategy by analysing the just noticeable difference (JND) in human haptic perception, and found that results validated a model suggesting force differences being the deciding factor [25].

Recent experiments at TU Delft suggest a correlation between the availability of force feedback, the theoretical activity occurring in the golgi tendons, and the tracking performance of the pilot, however statistical significance is still limited [3].

Finally, Bachelder and Aponso also published a study in 2021 comparing stiff and free joysticks, and concluded force feedback to be the prioritized feedback source, as well as proposing further additions to Hess' inner loop equalization models [9] [16]. However the single subject limitation amongst other issues limits the applicability of the experiment itself.

There is indication that research so far leads to a likely inference of force feedback being more accurate, and employed to a greater degree by the pilot for control, as compared with position feedback, though further studies and more experimental data is necessary to draw conclusions.

7.1. McRuer and Magdaleno's study

McRuer and Magdaleno conducted an experiment in 1966 studying the effects of different manipulator dynamics on the pilot's dynamics [12]. A single trained pilot with experience in similar tracking tasks was involved in the experiment. Their previous publication extensively studying pilot dynamics in compensatory systems ([20]) was cited to have established this pilot as representative of a population of pilots, and he was also the single subject in another study on compensatory and pursuit displays due to the same limitations [46].

The setup involved a compensatory display and two different forcing functions to compare results with different forcing function bandwidth, the first being a 6-4 input with the first 6 sine waves having a greater amplitude and a bandwidth roughly $2\ rad/sec$, and the second forcing function the same amplitude for all

10 waves, and frequency ranging from $0.314\ rad/sec$ to $14.03\ rad/sec$. Three controlled element dynamics, proportional, integrator and double integrator ($Y_c = K_c, K_c/s, K_c/s^2$) were studied.

The tracking task was performed with different manipulators. The first was a pressure manipulator, which measured the pilot's force input using a strain gauge, with the stick itself remaining immobile. The second manipulator was a spring restrained manipulator with minimal inertia, damping and nonlinearities. The final manipulator employed a knob on an unrestrained and nearly frictionless wheel, with the intention to approximate a free moving controller. The experiment was performed with [12].

The model McRuer used to analyse the results was the approximate precision model (Equation 3.5), with α used to parametrize low frequency lead-lag and T_N (Equation 3.4) used to parametrize high frequency delay of the neuromuscular system. In terms of these parameters the results indicated:

1. The pressure control manipulator consistently showed lower RMS error, as has been confirmed by multiple studies before and since then.
2. For every controlled element Y_c the free-moving manipulator had greater high frequency phase lag, suggesting a greater neuromuscular delay (T_N) compared to the pressure manipulator.
3. Low frequency amplitude ratio and phase lag remained the same for $Y_c = K_c/s^2$ and with the low bandwidth FF for $Y_c = K_c$, suggesting that α did not change between the free moving and pressure manipulators for these control tasks. For $Y_c = K_c/s$ and with high bandwidth FF for $Y_c = K_c$ however, there was a greater low frequency phase lag for pressure control as compared with the free moving controller, suggesting a larger value for α for the pressure controller.

Overall they found that the phase curve in the open loop frequency response shifted towards higher frequencies when going from free-moving to pressure sensing manipulators [12].

Magdaleno and McRuer also published a parallel study analysing the effects of manipulator restraints with a focus on the pilot's describing function and performance rather than dynamics. In general a spring manipulator was found to be better for pilot performance, with pilot performance remaining largely invariant to changes in the spring rates for easier tasks, and being optimal at an intermediate spring rate for harder tasks. An interesting result obtained was that for a purely inertial (no spring) manipulator, increasing the manipulator inertia over the pilot's limb inertia degraded performance considerably. Pressure control manipulators were found to be nearly as effective for control as spring restrained manipulators. Additionally the pilot's performance did not show significant difference between optimal pressure and spring restrained control conditions [13].

They also discovered that, specifically for a proportional control task $Y_c = K_c$, the operator's performance did not degrade significantly with the free moving manipulator with high inertia as compared with a pressure manipulator. This suggested that the force-displacement dynamics of the manipulator were largely compensated through position feedback in such a task [13].

Gordon-Smith also conducted a study in 1970, during which the effect of the manipulator on manual control was also studied. This study observed a slight decrease in the natural frequency (15 rad/sec for the free moving manipulator vs 18-20 rad/sec for the pressure manipulator) of the neuromuscular system observed, and a very significant increase in the phase lag over a wide frequency region when switching to a free moving manipulator.

While only a single controlled element (integral) was used, the experiment had 8 subjects and the results were recorded for three different forcing function bandwidths ($\omega_i = 1.5rad/sec, 2.5rad/sec, 4rad/sec$). The changes in the neuromuscular system natural frequency were more significant as bandwidth increased, with a very large decrease in natural frequency as well as damping observed for the largest forcing function bandwidth. The differences in phase lag in the high frequency region remained consistent throughout, however there was also a noticeable change in the low frequency region for the higher bandwidth of 4 rad/sec, corresponding to McRuer and Magdaleno's observations of the 'phase umbrella' [10].

7.2. Hess' Revised Model

In 1990 Hess published a study analyzing manipulator and feel system effects in manual control [8]. In this study he proposed a revised version of the structural model (Figure 7.1) which included feel system dynamics (with the previous structural model assuming isometric manipulator with direct proportional

Table 7.1: *Model Parameters in the Revised Structural Model, Hess 1990, Table II, p. 925 [8]*

Neuromuscular System	**Manipulator-Feel System**	**Sensing**	**Vehicle (Y_c)**	G_1	G_2	K_e	τ_0 (sec)
$\frac{e^{-0.05s}}{(s/20)^2+2(0.7)s/20+1}$	$1/s^2$	Position	$1/s$	10.0	0	28.0	0.05
$\frac{e^{-0.05s}}{(s/20)^2+2(0.7)s/20+1}$	$1/s$	Force	$1/s$	10.0	0	5.89	0.05
$\frac{(s+1)e^{-0.05s}}{(s/20)^2+2(0.7)s/20+1}$	$1/s^2$	Position	$1/s^2$	5.0	$\frac{50}{10s+1}$	11.27	0.05
$\frac{e^{-0.05s}}{(s/20)^2+2(0.7)s/20+1}$	$\frac{1}{(s/14)^2+2(0.7)s/14+1}$	Position	$\frac{1}{[s(0.15s+1)]}$	1.0	0	6.25	0.05
$\frac{e^{-0.05s}}{(s/20)^2+2(0.7)s/20+1}$	$\frac{1}{(s/14)^2+2(0.7)s/14+1}$	Force	$\frac{1}{[s(0.15s+1)]}$	1.0	0	6.25	0.05

dynamics included into the controlled element). Besides other goals of the study related to vestibular control and biodynamic feedback, models for various manipulator/feel system dynamics were proposed, and Hess attempted to qualitatively match the model dynamics to data from previous studies analyzing different manipulator dynamics and their effects on pilot control. This included McRuer and Magdaleno's study [12], a study by Gordon Smith in 1969 [10], and a study by Aponso and Jonhnston in 1988 [47].

This model was fitted only to integrator and double integrator controlled element dynamics, as well as $Y_c = 1/[s(0.15s+1)]$ dynamics which is meant to simulate roll subsidence mode of an aircraft in forward flight, with the goal to study the roll ratchet phenomena.

When modelling the feel system, Hess used similar manipulator dynamics for pressure, spring or free moving manipulators, while also including force as well as displacement sensing control for the spring manipulator. While displacement sensing remains the same, force sensing has the switch S_3 in Figure 7.1 in the 'up' position, with force rather than stick displacement acting as input to the controlled element. This was only applied to data from Aponso and Johnston's study with $Y_c = 1/[s(0.15s+1)]$.

When adapting to the changing manipulator dynamics, the pilot is able to adjust through proprioceptive compensation blocks and inserting a lead 'T_{L_n}' in the open loop neuromuscular dynamics, which is present in the case of the free moving manipulator [8].

For the former two cases, although the model was able to qualitatively show the changes in high frequency phase lag observed by both McRuer and Magdaleno [12], and Gordon-Smith's [10] studies, it should be noted that the model's frequency response does not show a slope of -20 dB per decade in the crossover region, as can be seen in the experimental data.

In their study in 1988, Aponso and Johnston found that force sensing improved the pilot's high frequency performance by reducing the lag in open loop [47]. This was with the controlled element dynamics corresponding to $Y_c = 1/[s(0.15s+1)]$. The model was able to show this behaviour when comparing force and position sensing as well.

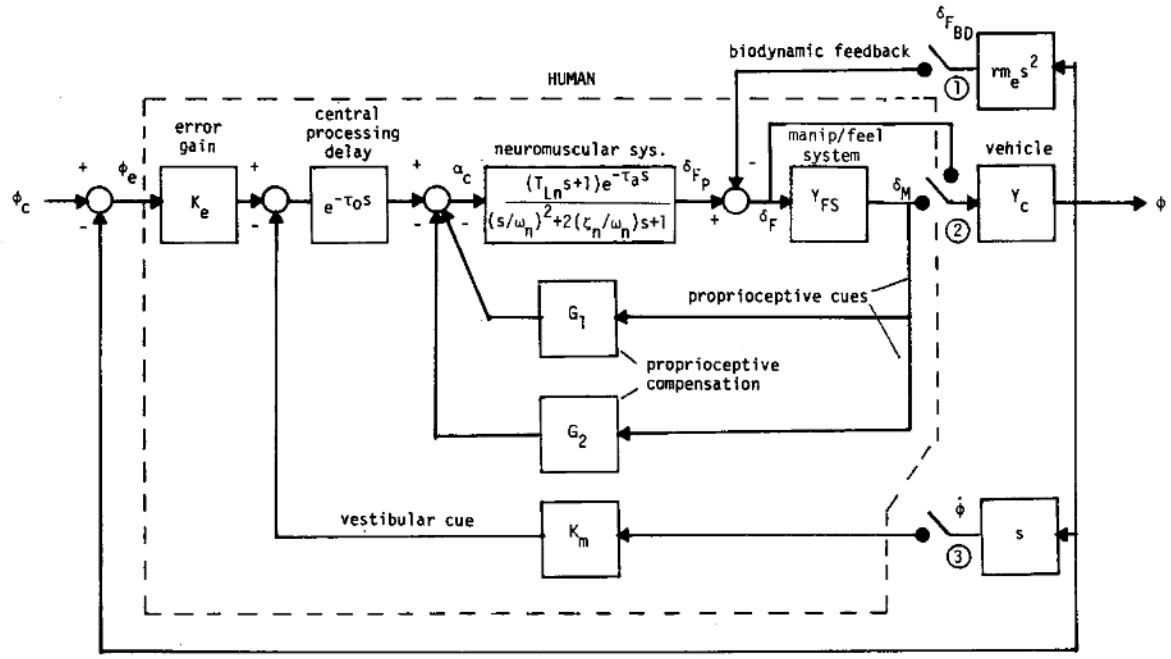

Figure 7.1: *Revised Structural Model, Hess 1990, p. 924 Fig. 1 [8]*

7.3. Bachelder and Aponso's Results

Bachelder and Aponso published a study of the neuromuscular-feel system interdependence, modelled using Magdaleno and McRuer's mechanical model of the neuromuscular system [4]. They proposed a model that included a generalized version of the proprioceptive equalization in the structural model [9].

The model used by Bachelder for the neuromuscular system, derived from the mechanical model proposed by Magdaleno and McRuer [13] [2] is shown in Equation 7.1.

$$G_{NMFS} = \frac{\delta}{\beta} = \frac{k_I k_T}{\Delta}, \tag{7.1}$$

Here:

$$\Delta = \left[\left(m_L s^2 + k_T + k_I\right)\left(b_m s + k_m + k_T\right) - k_T^2\right] \cdot \left(m_F s^2 + b_F s + k_F + k_I\right) - k_I^2\left(b_m s + k_m + k_T\right)$$

m_F, b_F and k_F represent the inertia, damping and spring stiffness of the feel system respectively. k_I represents the interface dynamics, k_T represents muscle-tendon stiffness/compliance, m_L, b_m, k_m are parameters representing the limb inertia and muscle dynamics. Under the approximation of the feel system inertia m_F and damping b_F being negligible, this effectively resolves into third order dynamics. Force feedback through the golgi tendons occurs from within this block rather than the output.

Through this linked model of the neuromuscular-feel system, a more reliable proprioceptive feedback signal expression is established and the impact of proprioceptive feedback can be studied. The transfer function described by this system, G_{NMFS} is used along with the known manipulator dynamics G_{FS} The open loop neuromuscular system dynamics are obtained through this model and the known manipulator dynamics. The proprioceptive force/displacement feedback loop is closed around this model (Figure 7.2).

This model was manually fitted to data from Gordon Smith's study in 1970 [10] and a similar NMS peaking and high frequency lag with free moving feel system dynamics and displacement feedback could be observed when compared with position feedback and spring manipulator [9].

A rough experiment was also conducted in the same study, using a Microsoft sidewinder joystick, comparing the pilot dynamics with spring centering and free moving manipulator dynamics. Similar trends to previous studies were observed in regards to rms error and pilot performance [9].

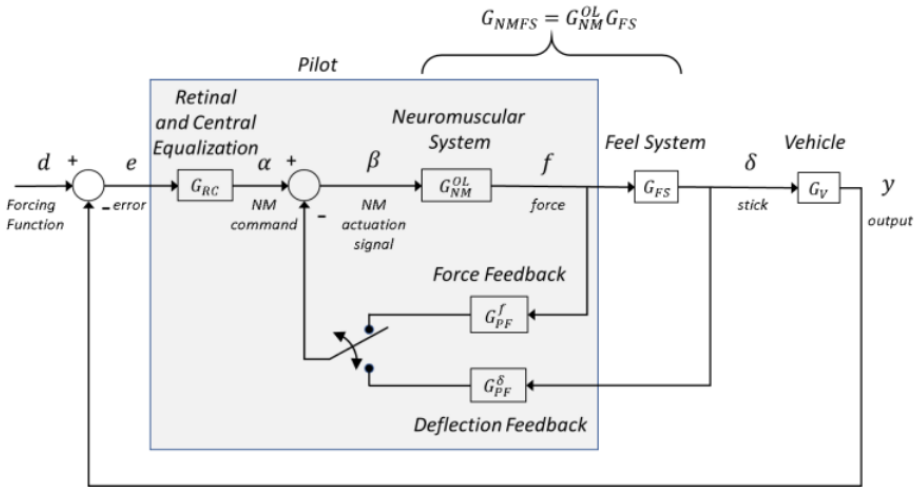

Figure 7.2: Neuromuscular System Model feedback structure (see Equation 7.1), Bachelder and Aponso 2021 [9]

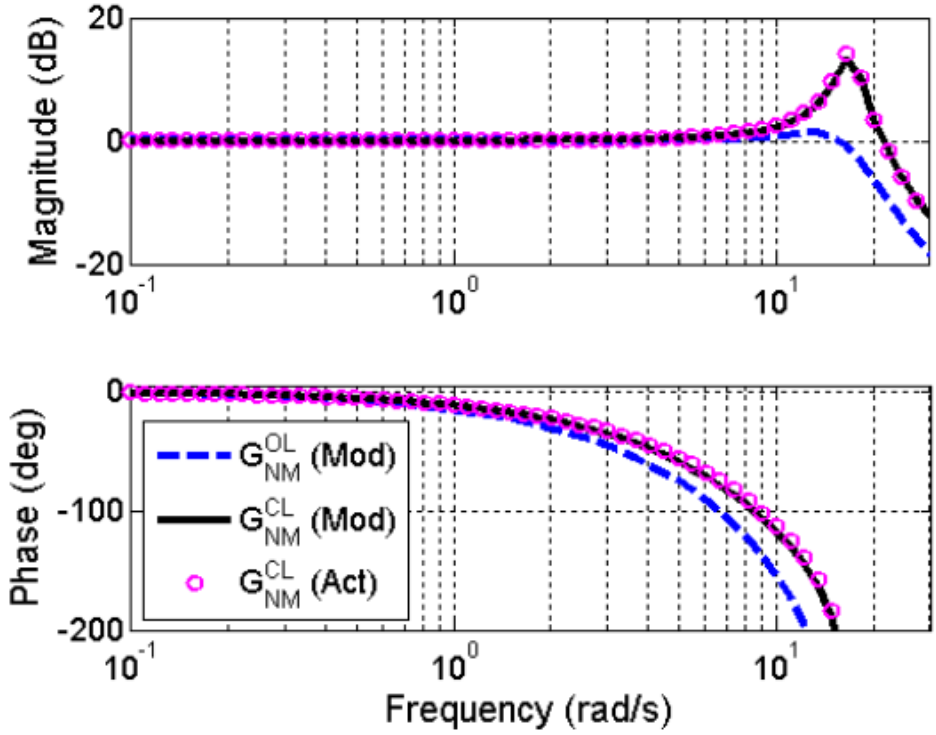

Figure 7.3: *Fitting the neuromuscular system model to data from Gordon-Smith's study in 1970 [10], free moving manipulator and integral control task, Bachelder and Aponso 2021, Figure 19 [9]*

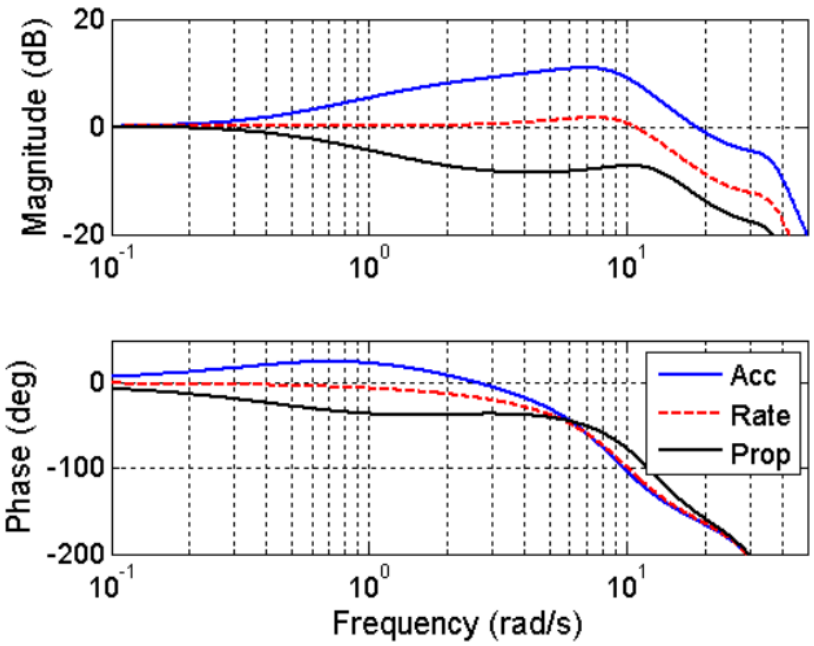

Figure 7.4: *Modeled closed loop NMS dynamics indicating equalization, Bachelder and Aponso 2021, Figure 26 [9]*

The improvement in tracking error was significant for double integrator control, smaller for single integrator control, and a slightly larger tracking error was observed with a spring centered manipulator during proportional control.

They also observed that the PSD of the stick deflection showed peaks not only at the forcing function peak frequencies but there were also additional peaks visible at frequencies close to 7 rad/sec, which is lower than the typically observed 10 rad/sec, and hypothesized it to be due to joystick characteristics employing less tension, similar to what would be expected with thumb/forefinger control on a gamepad controller.

This experiment, however, was also unreliable due to forcing function frequencies not fitting into the run length (the forcing function SOS frequency ranged from 0.048 to 4.65 rad/sec, but the length of each run was 60 seconds, too short to accurately identify lower frequencies [9]) and a single subject involved in the experiment with a manipulator not intended for precision tasks. Although the observed describing function was not printed in the published study, the crossover frequency and phase margin for each control task and both manipulators were printed. Interestingly for integral dynamics, the crossover frequency appeared to be much lower for the free moving manipulator in a range that would be expected when controlling a double integrator system. The slightly worse crossover frequency for the free moving compared with the spring manipulator during double integrator control seems more expected, however does not line up with observations by McRuer and Magdaleno who observed that the pilot was able to adapt to the manipulator to maintain the same crossover, with some differences only beyond the crossover frequency. Keeping this in mind, results from the frequency analysis of this experiment's data can be erroneous.

The model in Figure 7.2 was used in conjunction with the 7 rad/sec open loop NMS natural frequency and a damping ratio of 0.7 to obtain the dynamics of the closed loop neuromuscular system. The closed loop NMS dynamics, including proprioceptive equalization, proposed by Bachelder and Aponso can be seen in Figure 7.4.

Muscular co-contraction (COC): As discussed in Chapter 4, during manual control tasks, it is expected that the agonist-antagonist muscle pair being used for manipulation would be simultaneously under tension to improve precise movement. For harder tasks/greater precision requirements, a greater average tension in the muscle pair is present. Studies have shown that introduction of muscular co-contraction improves performance and reduces pilot error [23] [2].

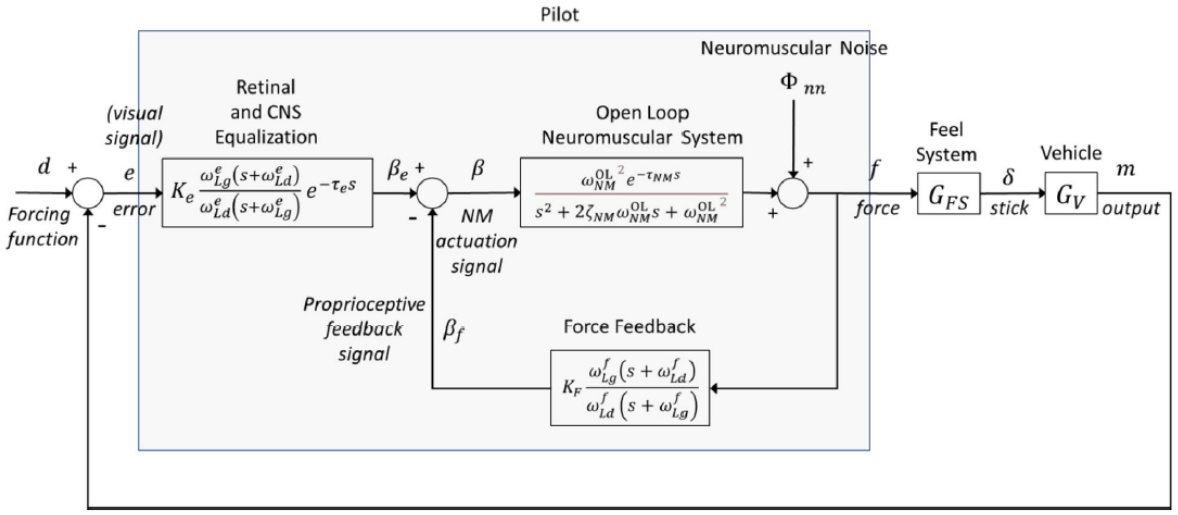

Figure 7.5: *A Generalized Equalization Model assuming force feedback, Bachelder and Aponso 2022, Figure 8, [11]*

This study also observed a high correlation between stick RMS in the high frequency NM region (supra active control and the low frequency active control region, with both showing a linear increase with the crossover frequency. It was proposed that this along with past neurophysiological research suggested:

- ω_c and COC are directly related, both being higher for a 'high-gain' pilot.
- The stick displacement power in the active control region for a given crossover frequency is proportional to the force power driven by the feel system characteristics.

It can also be noted that McRuer and Magdaleno also observed the 'phase umbrella' shifting with changes in manipulator dynamics. An absence of force feedback in a free manipulator lead to both an increase in high frequency time delay and a *decrease* in high frequency time delay in the low frequency region in some cases (as discussed in Section 7.1). Low frequency data is of course highly erroneous, and cannot be a reliable indication.

When it comes to proprioceptive equalization, Bachelder and Aponso concluded that force feedback based equalization was the preferred method for the inner loop feedback control proposed by Hess, i.e. the feel system is outside the inner loop. While Hess assumed neuromuscular system parameters to be fixed while proprioceptive feedback and pilot gain parameters were adaptive, their conclusions indicated an adaptive open loop NMS natural frequency. This study concluded feel system dynamics and pilot performance to be significantly interdependent.

The closed loop NMS frequency imposed a limit on the lead/lag terms in the proprioceptive feedback equalization dynamics, with the open loop pilot dynamics (and thus the closed inner loop of the NMS) known to have a peak in the high frequency region.

In rate command systems, equalization through the NM system happens more effectively due to the proportional nature of force feedback. However, for acceleration commands, higher-level cognition is required for integral control, meaning equalization becomes more challenging and often relies on a **pulsive control strategy** rather than continuous adjustment [41].

8

Conclusions

In regards to modelling the neuromuscular system, significant studies have already been conducted and an accurate mechanical model of the neuromuscular dynamics discounting proprioceptive feedback loops are well known. Proprioception is known to occur via force feedback through GTOs, as well as limb position and velocity feedback through muscle spindles.

Quasi-linear models of a pilot during manual control have been established and give an accurate approximation and prediction of the pilot's control response in the feedback loop. The crossover model gives an accurate prediction of the overall pilot response, including equalization and delay, especially in the region of open loop crossover. The precision model gives a more accurate mathematical model, and includes neuromuscular limitations, fitting well to experimental data. These models do not necessarily say that all equalization occurs through visual feedback, the degree to which other sensory cues such as proprioception and motion cues are used for this equalization are less well known.

The structural model suggests an alternative formulation for equalization through proprioceptive feedback. Although it fits experimental data, it is not a predictive model, and instead meant to provide insight into the adaptive behaviour of the pilot. It has been employed to understand pilot limitations through study of pilot performance measures, as well as model undesirable behaviours such as pilot induced oscillations and the roll ratchet phenomena.

Whether equalization truly occurs only through proprioception cannot be confirmed directly with ease, but the impact of manipulator dynamics on the pilot's control behaviour can provide some insight into the degree to which manipulator dynamics are used during control. Multiple studies comparing pressure and/or spring centering manipulators to free moving manipulators have shown that when the free moving manipulator is used pilot performance worsens (the mean square tracking error increases), suggesting force feedback to be integral to the control behaviour. For a free moving manipulator when compared with a pressure or spring centering manipulator:

1. Phase lag for a very wide band in the high frequency region is larger for all controlled system dynamics, suggesting a larger equivalent NMS delay T_n.
2. The natural frequency as well as damping of the NMS dynamics decreases, with the difference becoming more significant for higher bandwidth forcing functions.
3. Phase lag in the low frequency region is observed to be smaller, with the decrease becoming more significant for an integrator or proportional control task, as well as becoming more significant for a higher bandwidth forcing function. (Error margins are higher in this region)

Considering the increase in the high frequency delay, an increase in the neuromuscular lag in the formulation of the precision model is suggested but cannot be explained. The structural model attempts to explain this behaviour, however significant approximations and assumptions regarding the dynamics of the NMS are made that are not explained through a mechanical model.

Bachelder and Aponso also attempt to explain this behaviour and suggest a model of the pilot describing function that includes both proprioceptive and visual equalization occurring in different frequency bands. A rough experimental setup was used to confirm the impact of the manipulator dynamics on the pilot's describing function, and this mixed equalization model used to explain this behaviour. The neuromuscular

dynamics natural frequency can be used to estimate the equalization parameters in the proprioceptive loop, suggesting that the impact of the changes in proprioceptive feedback can be observed through changes in the neuromuscular peak in the pilot's describing function. Their study proposed muscular co-contraction, a phenomena known to improve human motor control accuracy, to be key to the pilot's adaptive behaviour as well and impacting the change in the natural frequency of the open loop NMS dynamics. They propose a method of identifying the equalization parameters through comparison of the closed loop NMS poles with the observed high frequency peak in the pilot's frequency response function.

Although these experiments suggest that force rather than position feedback seems to be of greater importance for control, their experiment also seemed to suggest that position feedback was slightly better when the control task was for proportional control ($Y_c = K_c$). This improvement in the tracking error, although also observed in McRuer's study, is much less than the improvement in integral/double integrator control tasks with a spring inceptor.

9

Next Steps

The research questions posed in Chapter 1 are repeated below for convenience.

Research Question

Can Proprioceptive Feedback account for equalization in the human pilot model?

1. Can a proprioceptive inner loop equalization account for pilot control adaptation to the degree established by the crossover model?
2. Is a model simulating equalization through proprioceptive feedback mathematically possible and physiologically plausible?
3. Can such a model be validated by experimental data, and provide an explanation for human control behaviours?

Based on gathered literature, a preliminary analysis can be conducted studying the impact of an inner equalization loop on simpler mathematical models (Question 1)

1. A short mathematical analysis of inner loop feedback based equalization can be conducted in the frequency domain, and results compared with expected pilot equalization characteristics based on the crossover model.
2. A similar analysis with a model comparable to the (revised) structural model can be conducted by including the presence of second order neuromuscular system dynamics and delay, and studying the differences from the (simplified) precision model.

In an approach matching the mixed equalization model presented in Section 7.3, a full mechanical model of the neuromuscular system utilizing recent findings will be included to study the affects of inner loop equalization better. Proprioceptive equalization will be used to attempt replication of experimental trends observed for human operators in different control tasks and with different manipulators. The mathematical and physiological limitations of such a model can thus be analysed based on established empirical results (Questions 2 and 3).

Finally, if a proprioceptive equalization based model is able to replicate these empirical trends, such a model will also be compared with a model implementing purely visual equalization and restricted to only reflexive proprioceptive feedback, in order to analyse potential advantages of one over the other.

Bibliography

[1] Lone, M., and Cooke, A., "Review of pilot modelling techniques," *48th AIAA Aerospace Sciences Meeting Including the New Horizons Forum and Aerospace Exposition*, 2010, p. 297.

[2] Magdaleno, R. E., and Mc Ruer, D. T., "Experimental validation and analytical elaboration for models of the pilot's neuromuscular subsystem in tracking tasks," Tech. rep., NASA, 1971.

[3] Boogaard, M., "Proprioceptive Qualities in Manual Control," Master's thesis, Technische Universiteit Delft, 2021. URL `https://resolver.tudelft.nl/uuid:8365c5d2-b52c-4b57-8a5e-ba8fc7115807`.

[4] McRuer, D. T., Magdaleno, R. E., and Moore, G. P., "A neuromuscular actuation system model," *IEEE Transactions on Man-Machine Systems*, Vol. 9, No. 3, 1968, pp. 61–71.

[5] Smith, R. H., "A unifying theory for pilot opinion rating," *Proceedings of the 12th Annual Conference on Manual Control*, 1976, pp. 542–558.

[6] Hess, R. A., "Dual-loop model of the human controller," *Journal of guidance and control*, Vol. 1, No. 4, 1978, pp. 254–260.

[7] Hess, R. A., "Structural model of the adaptive human pilot," *Journal of guidance and control*, Vol. 3, No. 5, 1980, pp. 416–423.

[8] Hess, R. A., "Analyzing manipulator and feel system effects in aircraft flight control," *IEEE Transactions on Systems, Man, and Cybernetics*, Vol. 20, No. 4, 1990, pp. 923–931.

[9] Bachelder, E. N., and Aponso, B. L., "The Feel System is an Extension of Both the Vehicle and Neuromuscular Systems," *47th European Rotorcraft Forum*, 2021.

[10] Gordon-Smith, M., "An investigation into certain aspects of the describing function of a human operator controlling a system of one degree of freedom(Analysis of describing function of human operator controlling system of one degree of freedom)," 1970.

[11] Bachelder, E. N., and Aponso, B. L., "Human pilot control adaptation: A physiological interpretation," *AIAA SCITECH 2022 Forum*, 2022, p. 2446.

[12] McRuer, D. T., and Magdaleno, R. E., *Human pilot dynamics with various manipulators*, Vol. 66, Air Force Flight Dynamics Laboratory, Research and Technology Division, Tech Report, 1966.

[13] Magdaleno, R. E., and McRuer, D. T., *Effects of manipulator restraints on human operator performance*, Vol. 66, Air Force Flight Dynamics Laboratory, Research and Technology Division, Air Force Systems Command, United States Air Force, 1966.

[14] Rasmussen, J., "Skills, rules, and knowledge; signals, signs, and symbols, and other distinctions in human performance models," *IEEE transactions on systems, man, and cybernetics*, , No. 3, 1983, pp. 257–266.

[15] McRuer, D. T., and Jex, H. R., "A review of quasi-linear pilot models," *IEEE transactions on human factors in electronics*, , No. 3, 1967, pp. 231–249.

[16] Bachelder, E. N., and Aponso, B. L., "Handling Qualities and Aircraft Pilot Coupling: New Evidence of Neuromuscular Origins," *AIAA SCITECH 2022 Forum*, 2022, p. 0890.

[17] Tustin, A., "An Investigation of the Operator's Response in Manual Control of a Power Driven Gun." *CS Memorandum*, Vol. 169, 1944.

[18] Pool, D. M., Zaal, P. M. T., Damveld, H. J., van Paassen, M. M., and Mulder, M., "Pilot equalization in manual control of aircraft dynamics," *2009 IEEE International Conference on Systems, Man and Cybernetics*, IEEE, 2009, pp. 2480–2485.

[19] Licklider, J. C. R., “Quasi-linear operator models in the study of manual tracking,” *Developments in mathematical psychology*, 1960, pp. 171–280.

[20] McRuer, D. T., “Pilot Dynamics in Compensatory Systems,” *Air Force Flight Dynamics Lab. Tech. Report*, 1965.

[21] van Paassen, M. M., “Neuromuscular System,” *Course AE4316, Technische Universiteit Delft*, 2022.

[22] Damveld, H., Abbink, D., Mulder, M., Mulder, M., Van Paassen, M. M., Van der Helm, F., and Hosman, R. J., “Identification of the feedback components of the neuromuscular system in a pitch control task,” *AIAA Modeling and Simulation Technologies Conference*, 2013, p. 7915.

[23] Saliba, C. M., Rainbow, M. J., Selbie, W. S., Deluzio, K. J., and Scott, S. H., “Co-contraction uses dual control of agonist-antagonist muscles to improve motor performance,” *BioRxiv*, 2020, pp. 2020–03.

[24] Houk, J., and Henneman, E., “Responses of Golgi tendon organs to active contractions of the soleus muscle of the cat.” *Journal of neurophysiology*, Vol. 30, No. 3, 1967, pp. 466–481.

[25] Fu, W., van Paassen, M. M., and Mulder, M., “The influence of discrimination strategy on the jnd in human haptic perception of manipulator stiffness,” *AIAA Modeling and Simulation Technologies Conference*, 2017, p. 3668.

[26] Hill, A. V., “The heat of shortening and the dynamic constants of muscle,” *Proceedings of the Royal Society of London. Series B-Biological Sciences*, Vol. 126, No. 843, 1938, pp. 136–195.

[27] Van Paassen, M. M., Van Der Vaart, J. C., and Mulder, J. A., “Model of the neuromuscular dynamics of the human pilot’s arm,” *Journal of aircraft*, Vol. 41, No. 6, 2004, p. 1482–1490.

[28] Xu, S., Tan, W., Efremov, A. V., Sun, L., and Qu, X., “Review of control models for human pilot behavior,” *Annual Reviews in Control*, Vol. 44, 2017, pp. 274–291.

[29] Kleinman, D. L., Baron, S., and Levison, W. H., “An optimal control model of human response part I: Theory and validation,” *Automatica*, Vol. 6, No. 3, 1970, pp. 357–369.

[30] Baron, S., Kleinman, D. L., Miller, D. C., Levison, W. H., and Elkind, J. I., “18. Application of Optimal Control Theory to Prediction of Human Performance in a Complex Task,” *Annual NASA-University Conference on Manual Control*, Vol. 215, Scientific and Technical Information Division, Office of Technology …, 1969, pp. 367–387.

[31] Elkind, J. I., Levison, W. H., and Ward, J. L., “Studies of multivariable manual control systems-A model for task interference,” Tech. rep., NASA, 1971.

[32] Levison, W. H., Baron, S., and Junker, A. M., “Modeling the effects of environmental factors on human control and information processing,” *Aerospace Medical Research Laboratory, AMRL-TR-76-74*, 1976.

[33] Jex, H. R., and Allen, R. W., “Research on a new human dynamic response test battery,” *Proceedings of the sixth annual conference on manual control*, Wright Patterson AFB OH, 1970, pp. 743 – 777.

[34] Hess, R. A., “Effects of time delays on systems subject to manual control,” *Journal of Guidance, Control, and Dynamics*, Vol. 7, No. 4, 1984, pp. 416–421.

[35] Hess, R. A., “Analysis of aircraft attitude control systems prone to pilot-induced oscillations,” *Journal of Guidance, Control, and Dynamics*, Vol. 7, No. 1, 1984, pp. 106–112.

[36] Hess, R. A., “Unified theory for aircraft handling qualities and adverse aircraft-pilot coupling,” *Journal of Guidance, Control, and Dynamics*, Vol. 20, No. 6, 1997, pp. 1141–1148.

[37] Hess, R. A., “Model for human use of motion cues in vehicular control,” *Journal of Guidance, Control, and Dynamics*, Vol. 13, No. 3, 1990, pp. 476–482.

[38] Hess, R. A., “Pursuit tracking and higher levels of skill development in the human pilot,” *IEEE transactions on systems, man, and cybernetics*, Vol. 11, No. 4, 1981, pp. 262–273.

[39] Hosman, R. J. A. W., and Mulder, M., “Perception of flight information from EFIS displays,” *Control engineering practice*, Vol. 5, No. 3, 1997, pp. 383–390.

[40] McRuer, D. T., Wolkovitch, J., Hofmann, L., Weir, D. H., Jex, H. R., Phatak, A., and Moore, G., *New approaches to human-pilot/vehicle dynamic analysis*, Air Force Flight Dynamics Laboratory, Air Force Systems Command, United States Air Force, 1968.

[41] Hess, R. A., "A rationale for human operator pulsive control behavior," *Journal of Guidance and Control*, Vol. 2, No. 3, 1979, pp. 221–227.

[42] Levison, W. H., Elkind, J. I., and Ward, J. L., *Studies of multivariable manual control systems: A model for task interference*, National Aeronautics and Space Administration, 1971.

[43] Levison, W. H., "The effects of display gain and signal bandwidth on human controller remnant," *AMRL-TR*, Vol. 70, 1971, p. 93.

[44] Heffley, R., "Use of a task-pilot-vehicle (tpv) model as a tool for fight simulator math model development," *AIAA Modeling and Simulation Technologies Conference*, 2010, p. 7620.

[45] Efremov, A. V., Tjaglik, M. S., Tiumentzev, U. V., and Wenqian, T., "Pilot behavior modeling and its application to manual control tasks," *Ifac-Papersonline*, Vol. 49, No. 32, 2016, pp. 159–164.

[46] Wasicko, R. J., McRuer, D. T., and Magdaleno, R. E., *Human pilot dynamic response in single-loop systems with compensatory and pursuit displays*, Vol. 66, Air Force Flight Dynamics Laboratory, Research and Technology Division, Air Force Systems Command, Wright Patterson Air Force Base, Ohio, 1966.

[47] Aponso, B. L., and Johnston, D. E., "Effect of manipulator and feel system characteristics on pilot performance in roll tracking," *15th Atmospheric Flight Mechanics Conference*, 1988, p. 4326.

[48] Hess, R. A., "A unifying approach to human pilot modelling," *IFAC Proceedings Volumes*, Vol. 17, No. 2, 1984, pp. 2609–2613.

Part II

Technical Report

Proprioceptive Equalization in Pilot Manual Control Modeling

Savneek Bhatia*, Prof.dr.ir.Max Mulder† and Dr.ir.M.M.van Paassen‡
Control and Simulations Department, Faculty of Aerospace Engineering,
Delft University of Technology, Delft, The Netherlands

Pilot manual control behavior has traditionally been modeled using purely visually driven quasi-linear frameworks. The role of proprioception and manipulator feedback (force and position) in shaping pilot dynamics for equalization has been theorized in literature, however well-grounded models that check all boxes remain elusive. This project investigated the feasibility of proprioceptive equalization utilizing a mechanical model of the neuromuscular system (NMS) originally developed at TU Delft (van Paassen et al., 2004 [1]). Frequency domain analysis and root locus methods reveal that muscle spindle and tendon feedback may affect characteristics near the region of crossover, but cannot independently achieve the integrator-like open-loop characteristics required for effective equalization. A mixed equalization strategy based on combining force feedback with visual compensation is shown to be physiologically plausible and theoretically effective in reducing pilot effort. Qualitative comparison against experimental trends supports the conclusion that proprioception contributes to neuromuscular stabilization and performance enhancement; however, it could not conclusively prove the possibility of equalization.

I. Nomenclature

δ	=	Manipulator Deflection
ω_c	=	Crossover Frequency
ω_n	=	Natural Frequency (of the NMS)
τ	=	Visual Channel Time delay
CE	=	Controlled Element
CL	=	Closed Loop
FS	=	Feel System
GTO	=	Golgi Tendon Organs
I (subscript)	=	Lag
L (subscript)	=	Lead
MS	=	Muscle Spindles
NMS	=	Neuromuscular System
OL	=	Open Loop
PF	=	Proprioceptive Feedback

II. Introduction

Manual control tasks, particularly in aerospace applications, rely heavily on the pilot's ability to adapt and compensate for system dynamics to maintain stable and precise performance. Traditional models, such as McRuer's crossover model [2], have provided critical insights into this adaptive behavior, illustrating how pilots shape open-loop dynamics to achieve integrator-like behavior near the crossover frequency. Such mathematical models primarily attribute pilot equalization to visual feedback pathways, effectively modeling pilot behavior during compensatory tracking tasks under specific conditions.

However, other models have suggested that visual feedback alone may not fully capture the complexities of human manual control. Physiologically motivated models, such as Hess's structural model, propose that proprioceptive

*MSc. Student, Control and Simulations section, Faculty of Aerospace Engineering, Delft University of Technology, Delft, The Netherlands
†Professor, Control and Simulations section, Faculty of Aerospace Engineering, Delft University of Technology, Delft, The Netherlands
‡Professor, Control and Simulations section, Faculty of Aerospace Engineering, Delft University of Technology, Delft, The Netherlands

feedback—information from muscle spindles and Golgi tendon organs—plays a critical role in forming an internal feedback loop that aids in achieving the desired crossover dynamics. Such models have often been used successfully to analyze subjective handling qualities [3], pilot induced oscillations (PIOs) [4], the roll ratchet phenomena [5], aircraft pilot coupling (APC) events [3], and pulsive control behaviour in double integrator control tasks [6] [7]. Other applications of the structural model by Hess and its modifications have included predictive display design, development of flying qualities criteria, and flight simulator fidelity of rotorcraft [8].

While promising, these proprioceptive models show deficiencies in predictive accuracy and physiological plausibility, particularly concerning limitations of such an equalization approach. In particular, such a model is referred to as a descriptive model, providing insight after fitting parameters to available data.'Unification' attempting to use proprioceptive feedback models as predictive models for equalization have been attempted, however not without limitations [9].

Experimental results have also indicated that force feedback is extremely important during manual control tasks, with pilots being sensitive to force feedback [10] [11]. Given the limitations of purely visual or proprioceptive models, recent research has suggested the potential for mixed equalization strategies [12], leveraging both visual and proprioceptive feedback. Understanding how pilots integrate these sensory pathways is crucial for advancing pilot models, especially as manipulator dynamics, such as stiffness, are known to significantly influence pilot performance and subjective handling qualities [13] [14].

This study investigates the potential role of proprioceptive feedback in pilot manual control equalization, building upon previous structural models to develop a more nuanced understanding of how manipulator characteristics interact with neuromuscular dynamics. A simplified mathematical framework is introduced to explore the feasibility and limitations of proprioceptive equalization. This is followed by utilizing a detailed mechanical model of the neuromuscular system to capture the interaction between muscle forces, manipulator feedback, and sensory pathways. The focus lies in understanding the mathematical characteristics of different control strategies in the frequency domain. Through root locus analysis, frequency response studies the mathematical feasibility of different control strategies is established, and qualitative fitting to experimental trends is attempted to verify that the model is an accurate representation of the physical characteristics of the pilot's response function.

Since a proprioceptively equalized control model depends significantly on the feedback from the manipulator, the impact of changing manipulator characteristics on the pilot's describing function is likely to shed more light on such a model. Proprioceptive feedback can be through the force being exerted, sensed by golgi tendon organs (GTOs), or through the displacement, assumed to be sensed by the muscle spindles (MS). For a pressure manipulator, no position feedback is available as the manipulator is fixed in place, and for a free moving manipulator no force feedback is available as force exertions required for displacement are negligible (assuming small mass and damping). Attempts at using the (revised) structural model to explain pilot behavior when using different manipulators have been unable to establish the model in a motivated way [5] as the model is not able to achieve integrator dynamics near crossover during an acceleration control task, and no attempt being made for a proportional control tasks, something that is shown to also be unsatisfactory in Section IV.

Many studies have shown a manipulator with force feedback available (i.e. a pressure manipulator or a manipulator with a stiff spring) to be integral in achieving the best performance from the pilot, with spring as well as pressure manipulators repeatedly showing better performance (smaller tracking errors) and smaller phase lags when compared with free moving manipulators [13] [15] [16] [11]. Fu et al. observed force feedback to be the deciding factor in human haptic perception [10]. Houk and Henneman, through experimentation on actively stimulated muscle, proposed a model for the GTOs suggesting that they "*constantly transmit to the spinal cord a filtered sample of the active forces being produced in the muscle. The dynamic properties of the filter are approximated by a linear mathematical model*" - Houk and Henneman, 1967, p. 480 [17].

Experimental studies on the effects of manipulator dynamics can thus provide valuable information on studying proprioceptive feedback.

Ultimately, this work aims to clarify whether proprioceptive feedback can meaningfully contribute to pilot equalization strategies in the region of crossover and under what conditions it becomes a significant factor, providing insights that could inform both pilot modeling efforts and the design of future manual control systems.

III. Literature Background - Equalization

McRuer' crossover model, a quasi-linear model of pilot control behavior in the frequency domain, is one of the most prevalent and useful models in predicting pilot behavior during a manual control task. Through empirical analysis it

was observed that the pilot implemented their effort to obtain integrator-like dynamics in the open loop in the region of crossover, ω_c, with the open loop characteristics thus appearing in the form of $H_p(j\omega)Y_c(j\omega) \approx (\omega_c/s)e^{-\tau_e s}$. The non-linear and adaptive pilot behavior can be approximated as a linear model during a compensatory tracking task, with the frequency response obtained using quasi-random sum of sine forcing functions that the pilot is tasked to follow. This result was obtained under specific conditions: compensatory control with continuous (sum of sines) input signals in controlled environments and with trained pilots as subjects [2].

The model includes the concept of equalization. Human operators adjust their control strategies to compensate for controlled element (CE) dynamics, shaping the system to achieve integrator-like behavior around the region of gain crossover. This equalization is assumed to be achieved through central nervous system processing and is a consistent feature across various tasks.

The precision model, by the same authors, proposed an expression for pilot dynamics that included equalization through visual feedback (from the display). The simplified precision model (Equation 1) shows a visual lead (τ_L) and/or lag (τ_I) term being used for equalization, with the effective time delay (τ_e) also including neuromuscular limitations (T_N) along with visual processing delays, τ. When more complexity is required in the model, the (extended) precision model is often used, and second order neuromuscular dynamics, observed to occur at a frequency much higher than crossover, are included in the open loop [18].

$$Y_P(s) = K_P \frac{\tau_L s + 1}{\tau_I s + 1} \exp(-j\omega\tau_e) \qquad \text{where, } \tau_e = \tau + T_N \tag{1}$$

Although an extremely successful model, it relies on visual feedback based compensation to be the primary pathway for equalization used by the pilot. Lead and lag estimation is done on the error signal based on visual feedback. Taking an alternative approach, the dual loop and later the structural model proposed by Hess suggests that proprioceptive feedback is the primary pathway for equalization. This is an inner loop model, building upon a previous model by Smith in 1976 [19] which had proposed visual rate estimation to be the pathway for generation of a similar inner loop used for equalization. The structural model, on the other hand, proposed that proprioceptive feedback of the input control force (sensed through golgi tendon organs, GTO) and stick displacement (sensed by muscle spindles, MS) is used in conjunction with an internal estimate of the controlled element dynamics by the pilot to generate an inner loop, leading to the expected open loop crossover dynamics [20] [21].

This means that to achieve the same dynamics as the precision model in the open loop, lag or lead is utilized in an internal loop based on manipulator force and position feedback from proprioceptive organs. An inner loop lead leads to a lag term in the open loop and vice versa.

The structural model is not a predictive model, and is instead called a descriptive model. Although such an inner loop was able to exhibit the necessary crossover dynamics, it was largely validated with assumptions of isometric manipulator and force feedback, and is able to replicate but not predict pilot response characteristics. Additionally, Hess used physiologically implausible parameter values, such as a proprioceptive lag of 2.5 seconds for double integrator control and lead of 5 seconds for proportional control [21].

A deeper analysis on the mathematics of proprioceptive equalization can help better understand the two different approaches to explaining equalization.

Work by Bachelder and Aponso. proposed a mixed feedback model of the pilot with both proprioceptive and visual feedback being used for equalization [12]. It was applied to estimation of pilot handling qualities and undesirable oscillatory behaviors [14] [22]. They discovered force feedback to be the preferred pathway to contribute towards equalization, while stick displacement feedback is used when force feedback is unavailable (e.g. for a light and free moving manipulator). Although a promising model, validation has been extremely limited. A more detailed version of the mixed equalization model was fitted to past data from Gordon-Smith in 1970 [16], for integrator controlled element dynamics [23], based on which along with their own rough experiment approximations were made a generalized equalization model was proposed (Part I, Section 7.3).

IV. Simplified Mathematical Analysis

To understand the potential for proprioceptive equalization in current quasi-linear models, a simple model structure shown in Figure 1 is considered. u_δ can be either the force (with manipulator dynamics included in the CE, Y_c), or it can be deflection (with manipulator dynamics included in G_{NMS}). Hess' structural model assumed the former, and during verification assumed that the manipulator was isometric (with a stiff spring and comparatively negligible inertia and

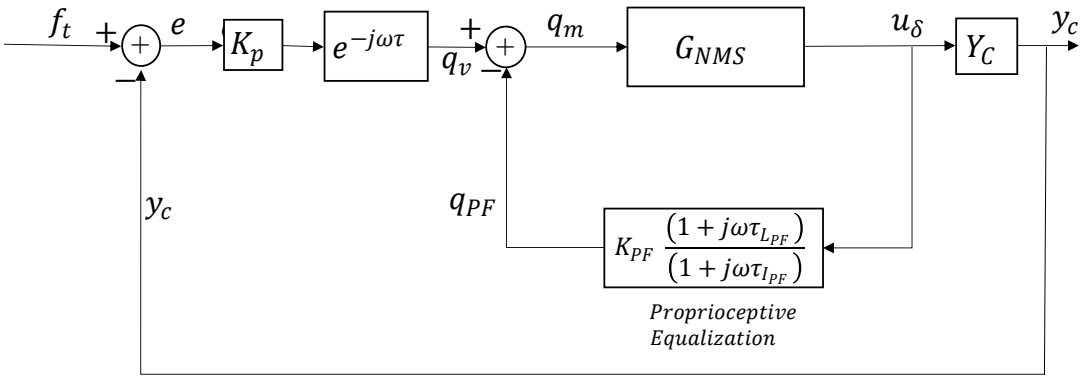

Fig. 1 A simplified form of a proprioceptive feedback equalization model

damping, ensuring that the feel system dynamics are constant, $G_{FS} = K$). This also means that while force feedback was hypothesized, the model itself was not verified with this in mind, and either could have been present [21]. A later study by Hess attempted to fit a revised version of the structural model, with different feel system dynamics considered, however was not satisfactorily able to do so as proportional control tasks were not considered, an assumption of a lead in the NMS dynamics for the case of free manipulators was proposed with little reasoning, and the case of free manipulator and double integrator CE dynamics could not exhibit integrator dynamics in the crossover region [5]. In this section, differentiating force vs deflection feedback is not relevant as the goal is only to study the mathematical properties of inner loop equalization.

For $k = 0, 1, 2$, the controlled element exhibits proportional, integrator and double integrator dynamics respectively. The structural model suggests that based on the pilot's estimate of these dynamics, an internal model is created. While his previous dual loop model explicitly used this internal estimate of the plant dynamics [20], the structural model makes it implicit and suggests the proprioceptive equalization dynamics change based on the pilot's estimate of the order of the controlled element dynamics as well as gain as shown in the figure [21].

A. A Mathematical understanding of inner loop equalization

The NMS and FS dynamics are neglected ($G_{NMS} = 1$) to study the mathematics of inner loop blocks and the effect on the outer loop, and the open loop expressions are shown in Table 1. Such an approach is not new and a similar analysis was also conducted by Hess in 1984 [9], however his study assumed a pure derivative term in the proprioceptive feedback block along with the estimated plant dynamics, which overly simplifies the dynamics and neglects limitations involved in introducing lead or lag. Here it is assumed that equalization takes on a lead or lag term with a time constant of τ_{PF}, corresponding with the latest revised structural model [3], and the generalized equalization model [12].

Table 1 shows the main results (see Appendix A for the complete analysis) showing that:

- For $Y_c = K_c$ a lead in the inner loop, acting on the proprioceptive feedback, is transformed into a lag in the pilot's response characteristics (from error e to control input u_δ to the CE), however with a time constant that is smaller than the lead time in the inner/proprioceptive loop. This means that a slightly larger proprioceptive lead time constant is necessary (compared with the visual lag time constant) to achieve the same open loop equalization.
- for $Y_c = K_c/s^2$, although a lag in the inner loop is transformed into an equivalent open loop lead, it also adds an open loop lag term that limits the compensation that can be provided.

The limitation for $Y_c = K_c$ dynamics could be compensated for by simply assuming a larger lead time constant is being produced in the inner loop. Additionally in both CE dynamics cases a large proprioceptive feedback gain K_{PF} would minimize these limitations, which would in turn also lead to a proportional increase in the pilot's open loop gain K_p on the visual feedback to achieve the same open loop dynamics.

These terms highlight essential limitations in inner loop equalization. Lag production in the pilot's response requires larger lead time in the inner loop, and a lead in the pilot's open loop response cannot be obtained purely through inner loop equalization without an additional lag term being introduced, especially considering realistically smaller values of K_{PF}.

The second limitation is an intrinsic mathematical limitation in proprioceptive feedback equalization, it shows up

Table 1 Summary of the open loop responses (from error e to output y_c) comparing visual and proprioceptive inner loop equalization models while neglecting NMS and FS dynamics (Figure 1)

Plant Dynamics	Visual Equalization	Proprioceptive Equalization
$Y_c = K_c$	$Y_{OL} = K_p K_c \frac{1}{1+\tau_I j\omega} e^{-j\omega\tau_e}$	$Y_{OL} = \left(\frac{K_p K_c}{1+K_{PF}}\right) \frac{1}{1+\left(\frac{K_{PF}}{1+K_{PF}}\right)\tau_{L_{PF}} j\omega} e^{-j\omega\tau_e}$
$Y_c = K_c/s$	$Y_{OL} = K_p K_c \frac{1}{j\omega} e^{-j\omega\tau_e}$	$Y_{OL} = \left(\frac{K_p K_c}{1+K_{PF}}\right) \frac{1}{j\omega} e^{-j\omega\tau_e}$
$Y_c = K_c/s^2$	$Y_{OL} = K_p K_c \frac{1+\tau_L j\omega}{(j\omega)^2} e^{-j\omega\tau_e}$	$Y_{OL} = \left(\frac{K_p K_c}{1+K_{PF}}\right) \frac{1+\tau_{I_{PF}} j\omega}{(j\omega)^2\left(1+\left(\frac{\tau_{I_{PF}}}{1+K_{PF}}\right) j\omega\right)} e^{-j\omega\tau_e}$

in the parameters used by Hess to validate his structural model, with proprioceptive gain increasing from $K_{PF} = 2.0$ for proportional and integral control to $K_{PF} = 10.0$ for double integrator control to compensate for this unintended lag term. This is still insufficient, however, and a visual rate estimation algorithm was also introduced by Hess in his structural model which likely corrected for this [21].

Equalization for the integrator dynamics are trivial for both cases and do not offer new insights besides showing the larger visual gain term that would be necessary to compensate for the inner loop gain.

B. Simplified Model with second order neuromuscular system dynamics

As mathematical limitations of purely proprioceptive equalization have been highlighted in the previous section, a major result is that producing a lead in the pilot's response, needed for $Y_c = K_c/s^2$ dynamics, purely through proprioception and a visual gain is actually impossible even with idealized neuromuscular dynamics. However due to the nature of the loop closure of the proprioceptive inner loop, it stands to reason that neuromuscular dynamics would significantly affect the impact of the proprioceptive feedback, likely creating further limitations. Second order dynamics in the open loop often describe a good approximation of neuromuscular limitations of the pilot, with a natural frequency of the order of 10 rad/sec. When considering these dynamics for the neuromuscular system, the effects of the inner loop closure were analyzed (see Appendix B). The root locus plots in Figure 2 show effect of closing the inner loop with different proprioceptive equalization dynamics, around a second order NMS block (Equation 2), corresponding with different CE dynamics, and are able to effectively summarize the main results of this analysis.

$$G_{NMS}(j\omega) = \frac{\omega_n^2}{(1+j\omega T_{N_1})[(j\omega)^2 + 2(\zeta_n\omega_n)j\omega + \omega_n^2]};\ T_{N_1} = 0.025sec,\ \omega_n = 10rad/sec,\ \zeta_n = 0.6; \tag{2}$$

1. Proportional Control

For the proportional control task, $Y_c = K_c$, the inner loop is closed with a proprioceptive feedback lead ($\tau_{L_{PF}} = 0.6sec$) and the resulting root locus plot is shown in (Figure 2a). This control task has the most jarring effects, with a small proprioceptive lead significantly shifting the second order NMS poles. While this results in the open loop lag necessary for equalization, it also causes the NMS dynamics to disappear. This would imply a significantly reduced time delay when position feedback is available, which does not happen. This suggests that this model might be a poor approximation to study spindle feedback.

2. Integrator Control

For the integrator control task, $Y_c = K_c/s$, inner loop closure with a pure gain (Figure 2b) causes the NMS dynamics' natural frequency to be pushed away, thereby improving the pilot response. A side effect is the reduction of damping, although it is not significant enough to counteract the advantages of increasing natural frequency, ω_c. This proprioceptive

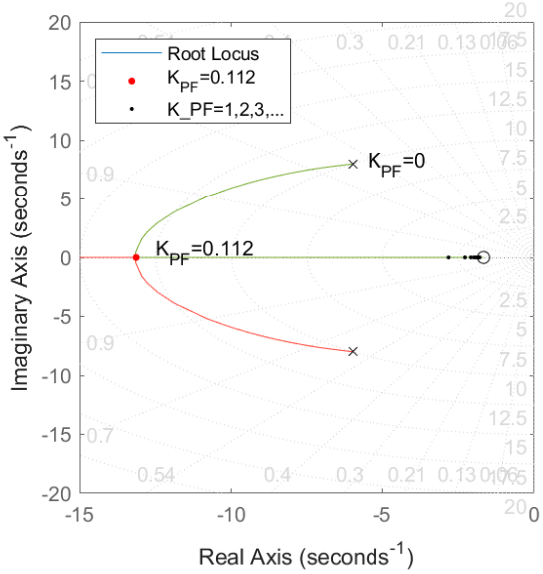

(a) Proportional Dynamics, $Y_c = K_c$, PF lead

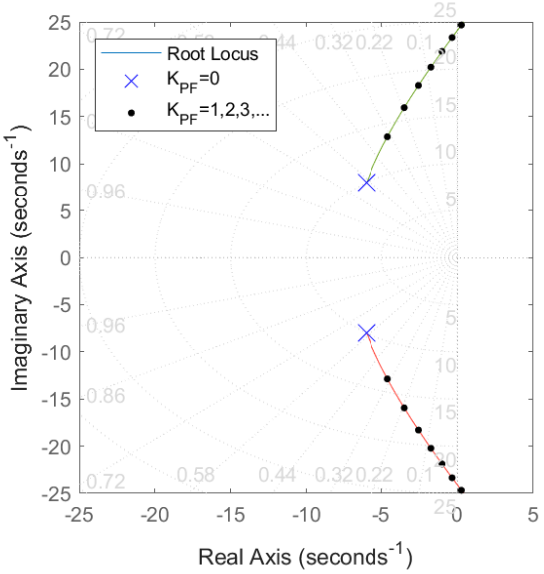

(b) Integrator Dynamics, $Y_c = K_c/s$, PF gain

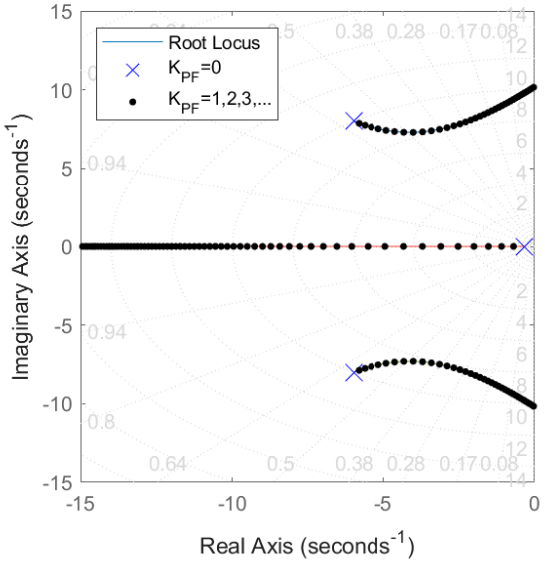

(c) Double Integrator Dynamics, $Y_c = K_c/s^2$, PF lag

Fig. 2 Root Locus plots showing the effect of the inner loop closure around second order neuromuscular dynamics

feedback gain thus helps stabilize high frequency control behavior and reduces the phase lags in the crossover region, and is not significantly limited by the neuromuscular system poles for small enough values of gain. For larger values of gain, the poles become increasingly undamped and finally enter the right half plane and the system becomes unstable. Instability does not occur when $T_{N_1} = 0$, and the system becomes unstable more quickly for larger values of T_{N_1}.

3. Double Integrator Control

For the double integrator control task, $Y_c = K_c/s^2$, loop closure around second order dynamics with a lag term ($\tau_{I_{PF}} = 3sec$, corresponding with the desired open loop lead in the visual response) in the proprioceptive feedback loop has worse effects. Figure 2c highlights

- the same limitation observed with idealized NMS dynamics, i.e., there is a lag term introduced in the pilot's response as an unintended consequence, which can only be removed with unrealistically high values of K_{PF}.
- an additional limitation introduced by the presence of 2nd order dynamics, which is the fact that introduction of proprioceptive feedback causes these poles' natural frequency and damping to reduce, leading to larger phase lag in the crossover regions. Since this is an undesirable behavior, if proprioceptive feedback (force or position) shows these dynamics, then this method of equalization would not be preferred.
- The lag time constant is too large to be physiologically possible, once again showing that purely proprioceptive equalization for $Y_c = K_c/s^2$ CE dynamics is not possible.

For further details, see Appendix B.

4. Conclusions

An inner loop lead for equalization in proportional control tasks is unrealistic due to the second order NMS dynamics disappearing as a result of the inner loop feedback, likely due to a poor approximation of the NMS dynamics for such an application. While the NMS dynamics in the pilot's response are well represented by second order dynamics when considering visual equalization in the precision model, it is likely a poor approximation when considering proprioceptive feedback as well.

An inner loop lag contributing to acceleration control tasks is also unlikely due to it appearing to be a bad control strategy for these dynamics of the G_{NMS}, making the second order poles less stable. Additionally it is also impossible in the absence of any visual lead as shown in the previous section.

Under an assumption of negligible FS dynamics (isometric manipulator) force and displacement sensing are equivalent, but with the spindles sensing muscle stretch and velocity, and the Golgi tendon organs (GTOs) sensing stress in the tendons rather than the actual force on the manipulator, a significant portion of the approximated NMS dynamics become relevant. It is likely that force and position sensing by these organs also has some unknown sensory dynamics by nature. A better understanding of the NMS is thus necessary.

V. Mechanical Model of the Neuromuscular System

Bachelder and Aponso initially used a mechanical model of the NMS [23]. After showing the validity of such a model, later publications switched to a generalized model, while specifying that the second order NMS dynamics are directly dependent on the manipulator and can change for different feel system dynamics. Such an approach takes into account that the force being sensed by the pilot is also acting as an input to the stick.

A similar approach of utilizing a mechanical model of the neuromuscular system is attempted here. The model shown in Figure 3 was developed in TU Delft in 2004 [1] and is an actuation model with 5 independent state variables: the muscle stretch (x_m), the position and velocity of the limb ($x_l, \dot{x_l}$) and the position and velocity of the manipulator ($\delta, \dot{\delta}$), all considered in terms of angular deflection. The input to the mechanical system, q_m is the muscle activation, in this case the angular moment produced by the muscle. There is a parallel damping element b_m to this input, a series elastic component k_{SEC}, which can be considered as the tendon connecting the muscle to the limb/bone. An additional parallel elastic component k_{PEC} is also present in the model, resisting limb displacement. The limb has an inertia I_{arm} .

Contact dynamics between the hand and the stick are given by the spring constant k_C and damping term b_C.

In general a manipulator exhibits second order dynamics due to inertia, damping and a spring constant. Varying these properties will change the dynamics of the combined neuromuscular and feel system (NMS-FS). The contact force F_C is applied on the manipulator/feel system, which has its own spring constant and damping, k_F and b_F, and inertia I_F, with respect to its own axis of rotation. A **free moving manipulator** has no spring attached and hence, when damping is negligible, exhibits double integrator dynamics, which is used as the input to the controlled element (CE). A

pressure manipulator, on the other hand, is clamped in place. Force applied on the manipulator is then used as the input to the controlled element, generally through the use of a strain gauge on its surface.

All parameter values have been presented in Table 2. For a complete state space representation of the model used, see Appendix C.

This model is quite similar to the model used by Bachelder and Aponso (from Magdaleno, 1971 [24]). Besides the major difference of using angular coordinates, which would not change the dynamics expressions, this model also includes a damping term in the skin contact/grip (b_c) and has some differences in the positioning of the parallel elastic component in the muscle. Both models abstract away from muscular co-contraction, with the entire muscle activation input only represented by a single (angular) force input, q_m, which is a drawback when considering that changes in the feel system dynamics will also affect muscular co-contraction. It can, however, be assumed that lower spring constants/natural frequency of the manipulator increases co-contraction and can be approximated as an increase in the stiffness of the parallel elastic component of the muscle (k_{PEC}), along with a decrease in the sensitivity of the force feedback by the golgi tendon organs (GTOs) which sense the tension in the series elastic component (k_{SEC}) in this model.

The structure of the model is shown in Figure 4, with the limb and the feel system/manipulator shown separately to better see the effect of changing feel system dynamics on the overall system. This can be seen in Figure 3 where the top view of the arm on the left represents the model G_{NMS}, which is also dependent on the manipulator displacement, $\delta\ L_F$, as a state variable. However the converse is not true, and the response from F_c to δ is independent of the pilot's neuromuscular system dynamics. This structure is inspired by what was used by Bachelder and Aponso in 2021 [23], however it differs from the later generalized model [12] due to the dependency on the feel system being included.

Another major difference is in the fact that proprioceptive feedback does not directly sense the control force and stick displacement but instead assumptions are made, grounded in physiology, that the GTOs sense the force in the tendons, here the series elastic component ($F_{gto} = k_{SEC}(x_l - x_m)$), and the spindles sense the stretch in the muscles x_m. This creates significant differences in the feedback dynamics and can shed further light on the limitations of the feedback data from the force and position sensing organs.

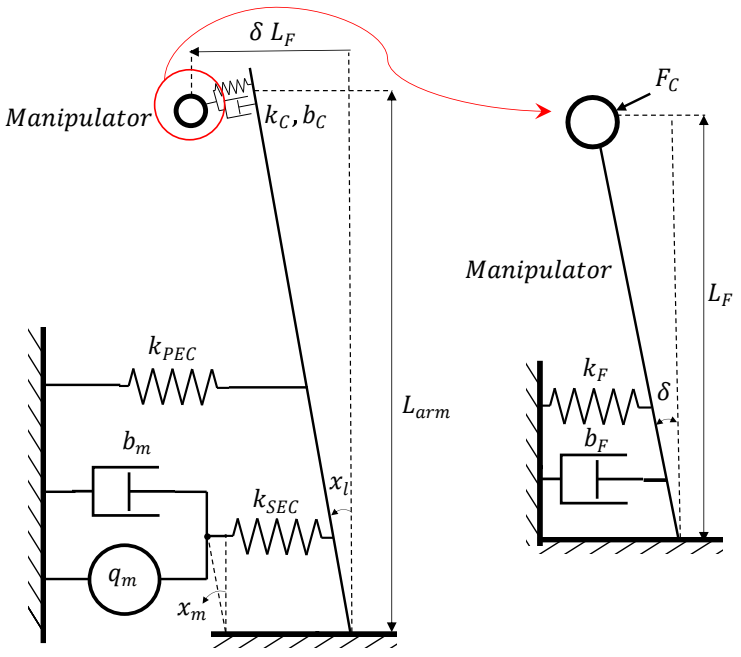

Fig. 3 Mechanical Model of the Neuromuscular and Feel System, with the top view of the pilot's arm gripping the manipulator (left) and a head on view of the manipulator (right), based on van Paassen et al. 2004 [25]

A. Effect of NMS dynamics in the frequency domain

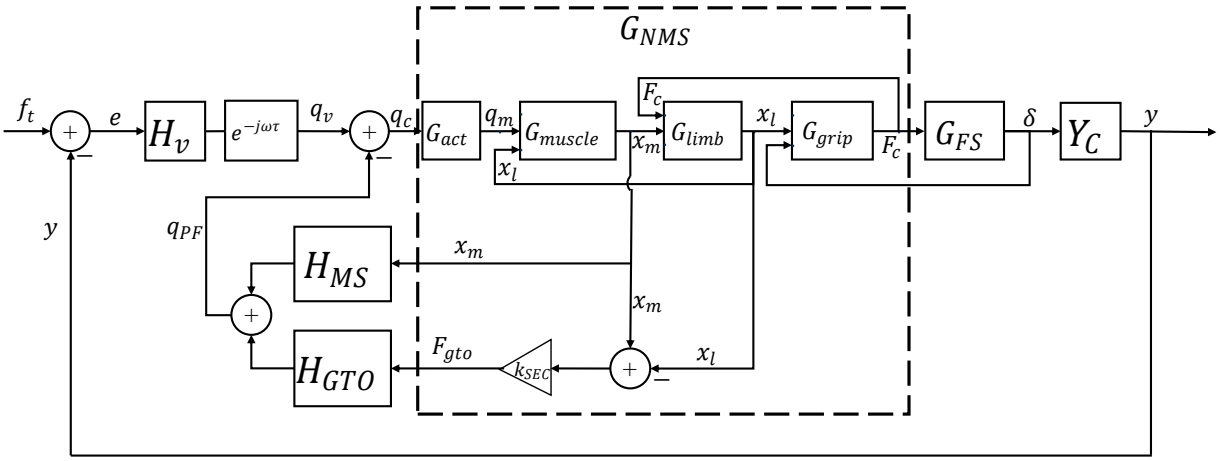

Fig. 4 Model Diagram of the Proprioceptive and Visual feedback Loops, and the NMS-FS hardware model from Figure 3

Table 2 Neuromuscular System Parameters for (Figure 3

Parameters	Notation	Value
Parallel Elastic Component	k_{PEC} $[N\ m\ rad^{-1}]$	9.14*
Series Elastic Component	k_{SEC} $[N\ m\ rad^{-1}]$	30
Muscle damping	b_m $[N\ m\ s\ rad^{-1}]$	0.538
Manipulator Length	L_F $[m]$	0.1
Manipulator Inertia	I_F $[kg\ m^2\ rad^{-1}]$	0.0065
Limb (Arm) Length	L_{arm} $[m]$	0.36
Limb Inertia	I_L $[kg\ m^2\ rad^{-1}]$	0.0417
Contact spring rate	k_C $[N\ m\ rad^{-1}]$	300
Contact Damping	b_C $[N\ m\ s\ rad^{-1}]$	7.01
Manipulator Spring Rate	k_F $[N\ m\ s\ rad^{-1}]$	1.48**
Manipulator Damping	b_F $[N\ m\ s\ rad^{-1}]$	0.01

* For a free moving manipulator $k_{PEC} = 18.28 Nm/rad$ due to co-contraction
** For (stiffer) manipulators with different spring constants, $k_1 = 1.48 Nms/rad$, $k_F = k_1, 5k_1, 25k_1$
** For free and fixed (pressure sensing) manipulators, $k_F = 0$ and $k_F = 73k_1$ respectively (non-ideal clamp)

In order to compare the dynamics of the mechanical model with the previous approximations, a brief analysis of the dynamics of the neuromuscular system is shown, and pole positions of the NMS response are depicted in Figure 5.

The system is analyzed by varying the manipulator natural frequency, with $k_F = k_1$ corresponding to a manipulator natural frequency of 15 rad/sec. For successively stiffer springs, k_F is increased and shown as a multiple of k_1, which corresponds with a feel system natural frequency of $\sqrt{k_1/I_F} \approx 15 rad/sec$. The manipulator characteristics vary from a freely moving manipulator ($k_F = 0$), to a clamped (pressure control) manipulator ($k_F = 73k_1$, as the clamped stick still has some leeway), for which F_c is considered the input to the controlled element rather than δ due to pressure sensing control.

1. Pole-Zero Analysis of the NMS

A key observation arises from the pole-zero map of the dominant poles of the neuromuscular and feel system, presented for the open-loop system from q_m to δ (Figure 5).

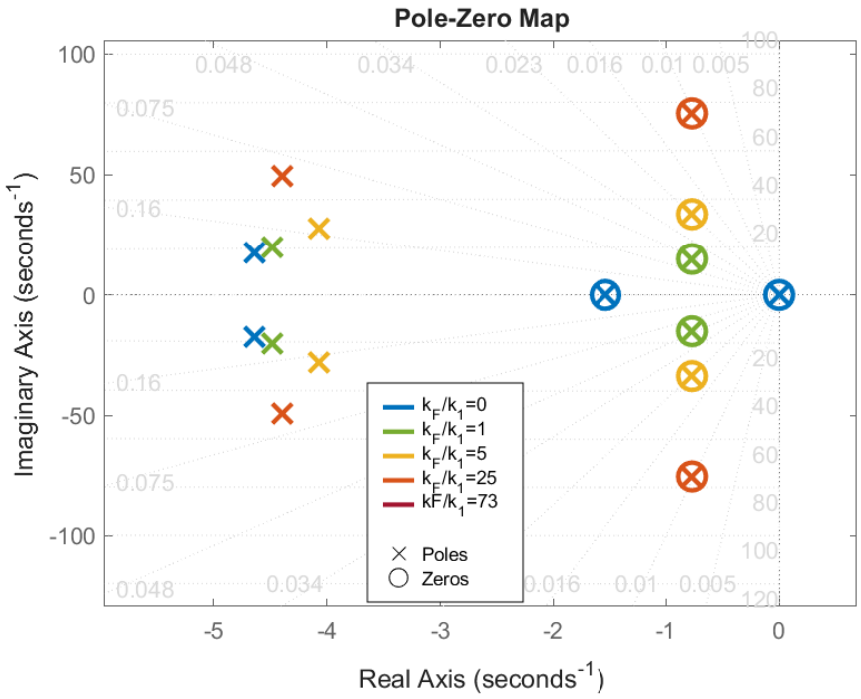

Fig. 5 Dominant poles of the NMS-FS model (q_m to δ) with the added pole-zero cancellations corresponding to the feel system poles

The pole-zero plot shows that the neuromuscular-feel system has dominant second order poles, with lag terms present at higher frequencies. This means that a second order approximation with a small lag is quite accurate when considering the output to be the stick deflection, δ. However, when considering force feedback, the expression $G_{NMS} = F_c/q_m$ is separate and consists of the same dominant poles as well as zeros that cancel out with the feel system poles. This pole zero cancellation has been intentionally shown in the pole-zero plot.

These cancellations reveal a limitation in the second order approximation when considering force feedback, and also imply the same limitation in the general model used by Bachelder. In the open inner-loop, there are zeros as well as poles in the transfer function from q_m to F_c, which are likely to significantly affect the open-loop dynamics if an inner-loop closure is made using force feedback F_c. These zeros are present in the mechanical model initially used by the same authors [23] as well. For the slightly different model used there, the negligible damping in the feel system and assumed zero damping in the contact force result in the same zeros lying on the imaginary axis. The presence of these zeros within the inner loop can fundamentally change what happens when force feedback is used.

2. Comparing actual F_c and δ with the sensed F_{gto} and x_m

After establishing these dynamics, the dynamics from q_m to the muscle stretch, x_m, (assumed to be sensed by muscle spindles) and the force in the tendon/series elastic component,$F_{gto} = k_{SEC}(x_l - x_m)$ (assumed to be sensed by GTOs), are studied.

Figure 6 shows the frequency response functions of the system, comparing the actual outputs of the stick position and force with the sensed muscle spindle and Golgi tendon organ (GTO) outputs, for various manipulator stiffness characteristics.

A reduction in the feel system's natural frequency (i.e., a reduction in the manipulator spring rate) causes significant lag in the neuromuscular system output when no proprioceptive correction is assumed. In contrast, increasing the spring constant raises the natural frequency of the dominant neuromuscular poles, reducing the phase lag.

The effect of co-contraction for the free moving manipulator by increasing k_{PEC} can be clearly observed as a decrease in the static gain of the frequency response function of stick deflection. Figure 6a. Additionally, small changes

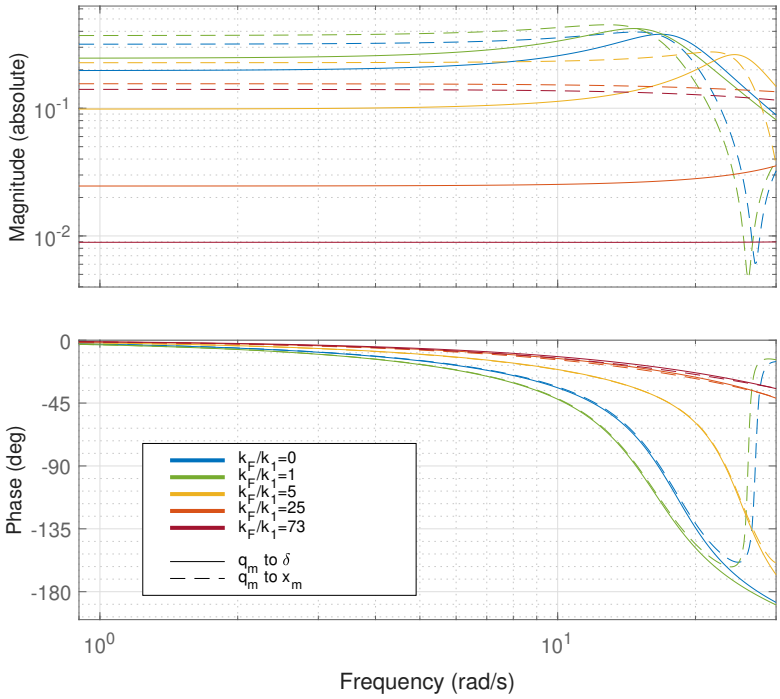

(a) Stick deflection δ and sensed muscle stretch x_m

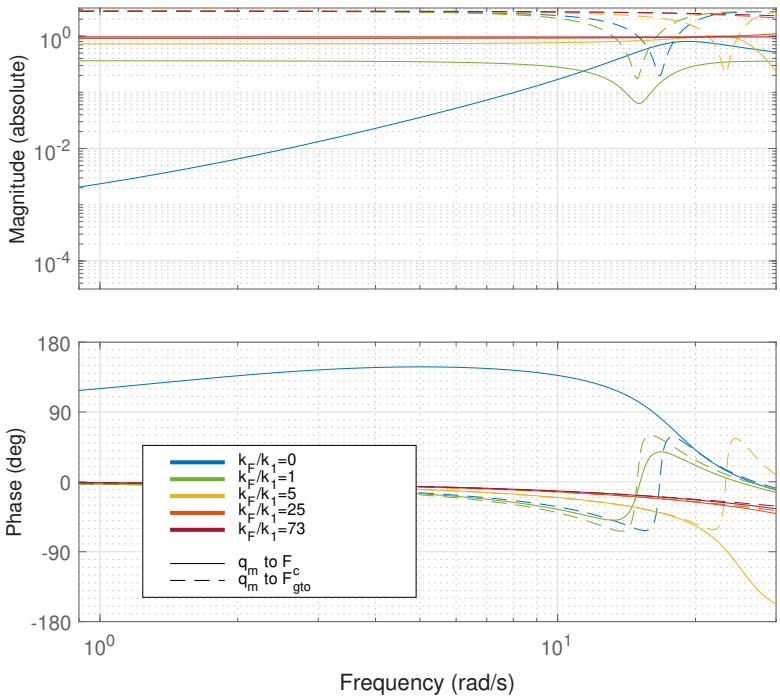

(b) Control Force F_c and sensed force in tendon F_{gto}

Fig. 6 Bode Plots showing the frequency response of the open inner-loop NMS dynamics from q_m to stick displacement and force, compared with sensed muscle stretch (q_m to x_m) and sensed tendon force (q_m to F_c)

in the system's natural frequency occur, pushing it to a higher frequency and reducing phase lag in the high-frequency region. The observed improvements from increasing the stiffness of the PEC through co-contraction are particularly beneficial for lighter manipulators, while being unnecessary for heavier manipulators. For the latter, the lower mean force in the muscles will increase the force feedback sensitivity, assumed to be the difference between agonist and antagonist muscles pairs, facilitating easier force sensing by the Golgi tendons.

For scenarios where the feel system natural frequency ω_n is much larger than the neuromuscular system's natural frequency, the force sensed by the Golgi tendons and the stick displacement show nearly identical dynamics. For the manipulator with the least stiffness, $k_F = k_1$, the force sensed by the GTOs lags slightly behind the actual contact force on the manipulator.

When $k_F = 0$ (free moving manipulator), force sensing through the GTOs is not possible. For other manipulator restraints, the phase curves from q_m to F_c, and to F_{gto} are quite similar regions that are most relevant ($\omega < 20 rad/sec$). Specifically, for $k/k_1 = 0, 1, 5$, a notable attenuation in the high-frequency region is observed. This attenuation arises due to the poles and zeros in the transfer function being closer, forming the 'trough' in the frequency response. This shows that the presence of the zeros in the NMS frequency response function is an important factor, especially for a $k_F = k_1$, at these frequencies, which are also likely to affect the phase lag in the pilot response function.

In these systems with lower spring stiffness, spindle feedback would then be a much more effective control strategy since neuromuscular and feel system dynamics do not interfere with force and position feedback.

The findings highlight key characteristics of the neuromuscular and feel system's behavior (in the absence of proprioceptive feedback), particularly the effects of system stiffness and natural frequency on phase lag and force sensing. Reducing the feel system's natural frequency leads to greater time lag, while increasing the spring constant reduces this lag. This has been one of the most significant observations in studies that compared effects of changing manipulator dynamics. This suggests that the improvement in performance with the increase in spring stiffness can be more confidently attributed to the mechanical properties of the system rather than the availability of force feedback for control. These observations also explain observed improvements in performance when co-contraction is employed for systems where phase lag due to the manipulator's characteristics is significant.

This model does suggest that assumptions of the sensed GTO force and muscle stretch being approximately equal to the force on the stick and its deflection are valid mostly when manipulators with higher natural frequency are used. For manipulators with lower stiffness, an additional phase lag term in contact force feedback to the pilot can provide a good approximation to what is sensed by the GTOs.

An interesting effect of there being only two dominant poles in this model of the neuromuscular system is that approximations can give identical results in the frequency region of relevance. Unsurprisingly, the overall response from q_m to δ can be easily reduced to second order dynamics and a small lag term. However, in addition to this, another good approximation is the for the block G_{NMS} shown in Equation 3. Since G_{FS} has second order dynamics which can be measured relatively easily, including these without adding additional unknown parameters to pilot models is possible. This introduces a significant change in force feedback loops closed with F_c as compared to the approximate second order dynamics used previously by Hess and others. This also suggests that the generalized model shown in **??** is only a good approximation when the feel system dynamics can be safely approximated as a gain with isometric manipulator assumptions. See Appendix C for more information about the second order approximations that can be made for this model.

$$G_{NMS}(j\omega) = \frac{F_c(j\omega)}{q_m(j\omega)} = \frac{\omega_n^2}{(1 + j\omega T_{N_1})\left((j\omega)^2 + 2\zeta_n\omega_n\, j\omega + 1\right)} \frac{1}{G_{FS}(j\omega)} \tag{3}$$

VI. Analyzing GTO and MS Feedback

As the mechanical model of the NMS is established, it is necessary to understand the effect of force and position feedback on the pilot's response. In this section, the potential changes in open-loop behavior that arise when equalization feedback is introduced through either Golgi Tendon Organ (GTO) or Muscle Spindle (MS) feedback pathways, are explored. The response q_v to δ when the inner PF loop is closed is considered in the presence of various proprioceptive feedback scenarios depending on different control tasks, and for different manipulator spring dynamics. This inner loop closure incorporates a neuromuscular activation lag of 0.01 second (in the block G_{act}) and a proprioceptive compensation delay of 0.025 seconds.

$$G_{act}(j\omega) = K_{act}/(1 + j\omega T_{act}); K_{act} = 0.3\ Nm, T_{act} = 0.01\ s \tag{4}$$

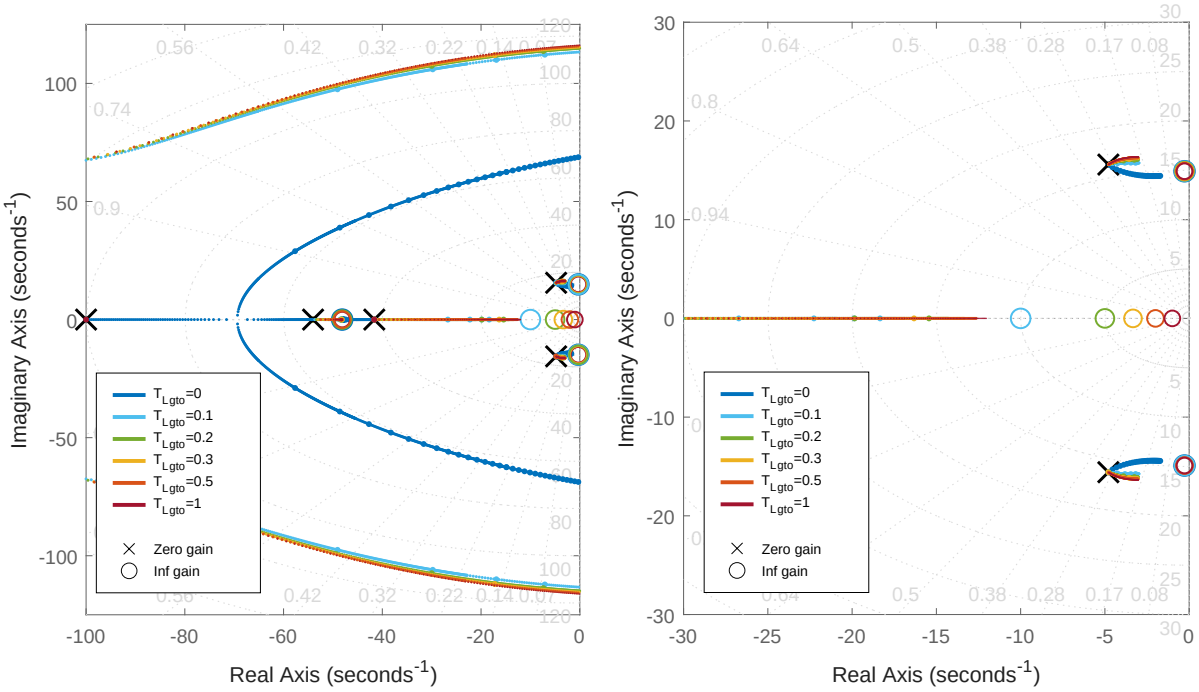

(a) Root Locus, GTO Lead **(b) Dominant Poles (zoomed in)**

Fig. 7 Root Locus Plot, closing the inner loop with a GTO lead, (from q_v to δ), $k_F = k_1$

$$H_{gto} = K_{gto}\,\frac{1 + j\omega T_{L_{gto}}}{1 + j\omega T_{I_{gto}}} e^{-j\omega\ \tau_d}; \tau_d = 0.025\ s \tag{5}$$

$$H_{ms} = K_{ms}\,\frac{1 + j\omega T_{L_{ms}}}{1 + j\omega T_{L_{ms}}} e^{-j\omega\ \tau_d}; \tau_d = 0.025\ s \tag{6}$$

The key plots, showing the effect of the inner loop closure on the pilot's response characteristics (from q_m to δ) that are representative of the results are shown here. For all plots and analysis of the proprioceptive feedback loops, see Appendix D.

A. Golgi Tendon Organ (GTO) Force Feedback

The effects of introducing GTO lead (meant to introduce an open loop lag in the pilot's response for proportional CE dynamics), and of GTO lag (meant to introduce an open loop lead in the pilot's response for double integrator CE dynamics) are considered through root locus plots in Figures 7 and 8, and Bode plots (as in Figure 11).

The response of the neuromuscular system with a force feedback through the GTOs was analyzed. The presence of a pair of zeros in the open-loop response from q_c to F_{gto} significantly alters the pilot response characteristics when the loop is closed via force feedback, as compared to when the zeros were absent, resulting in similar results as discussed in section IV.

1. Proportional Control Dynamics, $Y_c = K_c$: GTO Lead

In the root locus plot (Figure 7) it can be seen that introducing a GTO lead has a destabilizing effect on the dominant poles of the NMS. The second order poles become less damped and move towards the right half plane, before the model becomes unstable. The necessary lag in the pilot response, required for proportional equalization, is not achieved within stability bounds.

Incorporating a lead element within the GTO feedback block implies the estimation of jerk for equalization—an approach that is physiologically implausible. From a mathematical standpoint, when GTO feedback is employed

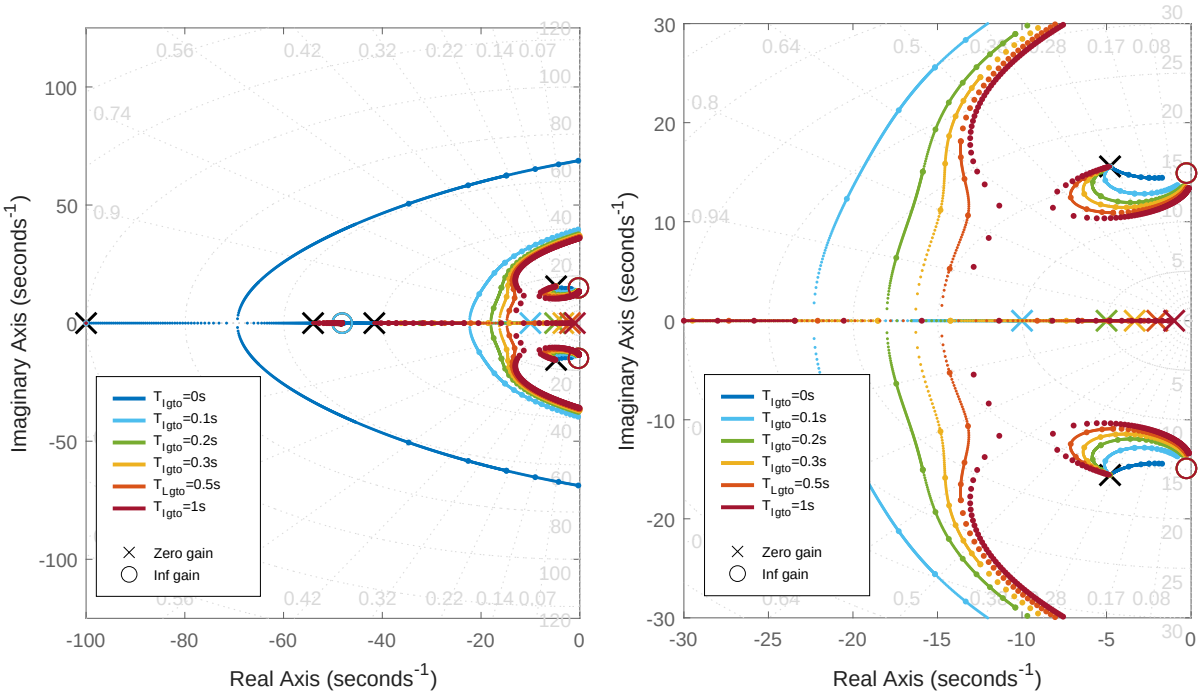

(a) Root Locus, GTO Lag **(b) Dominant Poles (zoomed in)**

Fig. 8 Root Locus Plot, closing the inner loop with a GTO lag, (from q_v to δ), $k_F = k_1$

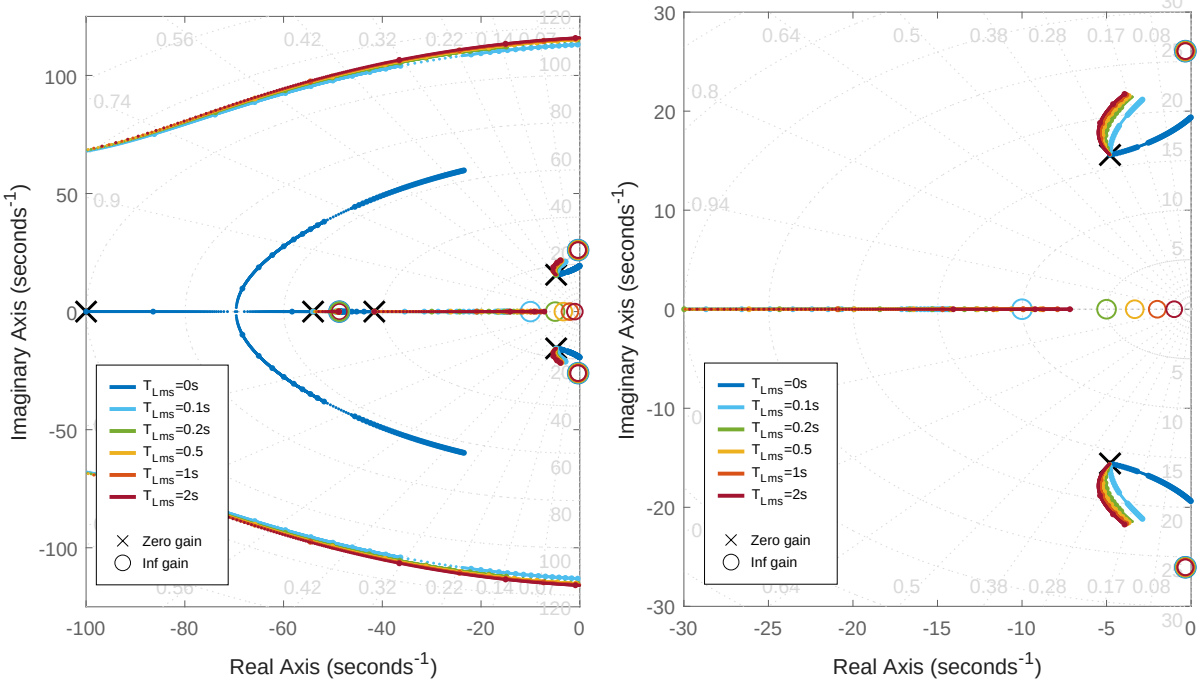

(a) Root Locus, MS Lead **(b) Dominant Poles (zoomed in)**

Fig. 9 Root Locus Plot, closing the inner loop with a MS lead, (from q_v to δ), $k_F = k_1$

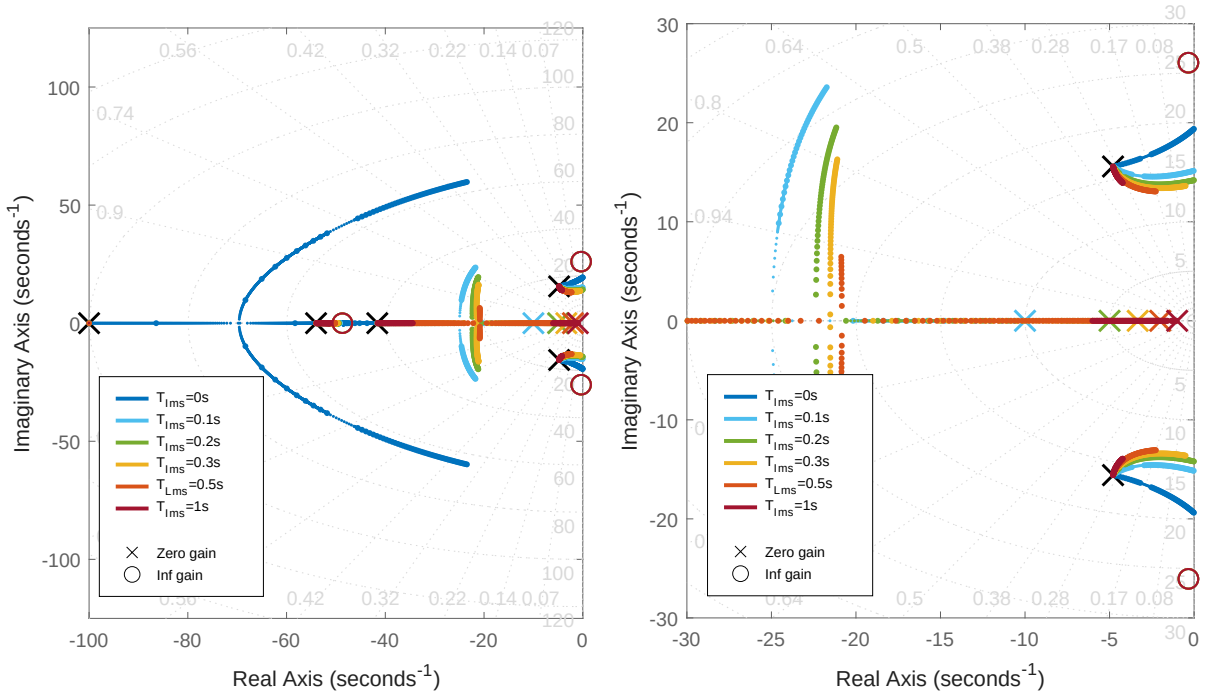

(a) Root Locus, MS Lag **(b) Dominant Poles (zoomed in)**

Fig. 10 Root Locus Plot, closing the inner loop with a MS lag, (from q_v to δ), $k_F = k_1$

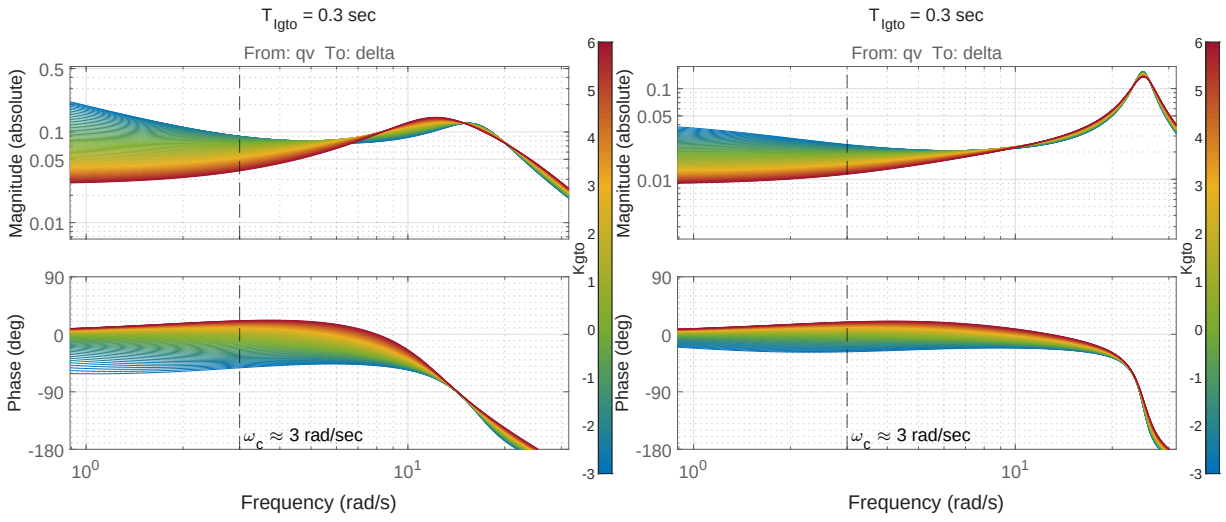

(a) $k_F = k_1$ **(b)** $k_F = k_1$

Fig. 11 FRF from q_v to δ with a GTO lag, with $T_{I_{gto}} = 0.3s$

for equalization of the feel system, the resulting closed-loop neuromuscular system response (from q_v to δ) exhibits instability over a broad range of gain values. Frequency response plots (Appendix D) confirm that force feedback gain does not yield either a lead or a lag in the pilot's open-loop response. Furthermore, for small gain values where the system remains stable, significant phase lags are produced due to non dominant poles moving towards the right. All this shows that a GTO force feedback lead is unlikely to contribute effectively to crossover equalization.

2. Double Integrator Control Dynamics, $Y_c = K_c/s^2$: GTO Lag

Introducing a lag into the force feedback channel, meant for double integrator CE dynamics equalization, however, avoids large instabilities and does not cause undesirable peaking in the open-loop response. Figure 8 shows that the effect of small GTO gain on the NMS poles is stabilizing up to a certain range, increasing the damping of the poles. However, the pole corresponding with the lag term cannot be removed entirely, and is still significant for this range of gain values. This corresponds with the results obtained in section IV.

For stiffer springs however, such as $k_F/k_1 = 5$ (Figure 11), the natural frequency of the dominant pole also increases. The frequency response functions in Figure 11 show that a small lag, on the order of 0.2 to 0.3 seconds, is sufficient to generate a limited open-loop lead in the pilot response characteristics. It is also evident that lag-based force feedback may serve to **reduce phase lag**. Therefore, if force feedback is available, and if the introduction of a small delay is physiologically plausible, it is likely that trained pilots may utilize this mechanism for equalization. The presence of a lag term, at a larger frequency, however also impacts the dynamics near the crossover region and once again ensures that pure proprioceptive equalization for a double integrator control task through a GTO lag is not possible, but it can be a significant contributor towards equalization in conjunction with a visual lead term.

This means that without a visual lead also present, it would still be impossible to equalize purely through proprioceptive feedback as the system would be unstable when controlling double integrator controlled element dynamics ($Y_c = K_c/s^2$). A mixed equalization with a significant contribution through a proprioceptive lag is however plausible, and can be a significant contributor to equalization.

Key Results:

- Lag in the GTO feedback pathway appears capable of producing an open-loop lead near the region of crossover, which would contribute towards equalization in harder tasks such as double integrator control, however some contribution from a visual lead would still be necessary to ensure stability as the GTO by itself also introduces a slightly higher frequency lag term.
- The NMS dynamics implement an upper limit to how high the GTO lag can be increased, which wasn't present when simplified NMS dynamics were being discussed. For weaker (lower spring stiffness) manipulators, a GTO lag by itself appears to increase damping for very small gain, followed by reduced damping lower natural frequency of the NMS dominant poles, with eventual instability. This puts an upper limit on the compensation that force feedback can provide, with greater compensation being possible for stiffer manipulator characteristics.
- GTO lead causes instability and is not able to contribute towards equalization near the region of crossover.

B. Muscle Spindle (MS) Feedback

1. Proportional Control Dynamics, $Y_c = K_c$: MS Lead

Based on the root locus plots in Figure 9, a lead in the spindles has a stabilizing effect on the dominant NMS poles, increasing the natural frequency. However, it is also clear that no condition within stability bounds is able to bring about a lag term significant enough to affect equalization. Interestingly, a pure gain in the spindle appears to have the worst affect on the system, reducing the damping in the dominant poles leading to instability. In contrast, a lead term minimizes this decrease in damping, maintaining it somewhat at the same location for smaller lead times. This has an overall beneficial stabilizing effect, showing the presence of spindle feedback to be valuable in improving performance, even though it cannot not induce equalization.

FRF plots (Appendix D) suggest that a small lead on MS feedback remains stable over a wide range of gain values and effectively damps the neuromuscular peak. However, this improvement comes at the cost of increased phase lag. An MS lead beyond a lead time of 0.2 seconds does not remain stable. Moreover, MS-based leads are unable to produce any substantial equalization lead in the crossover frequency region.

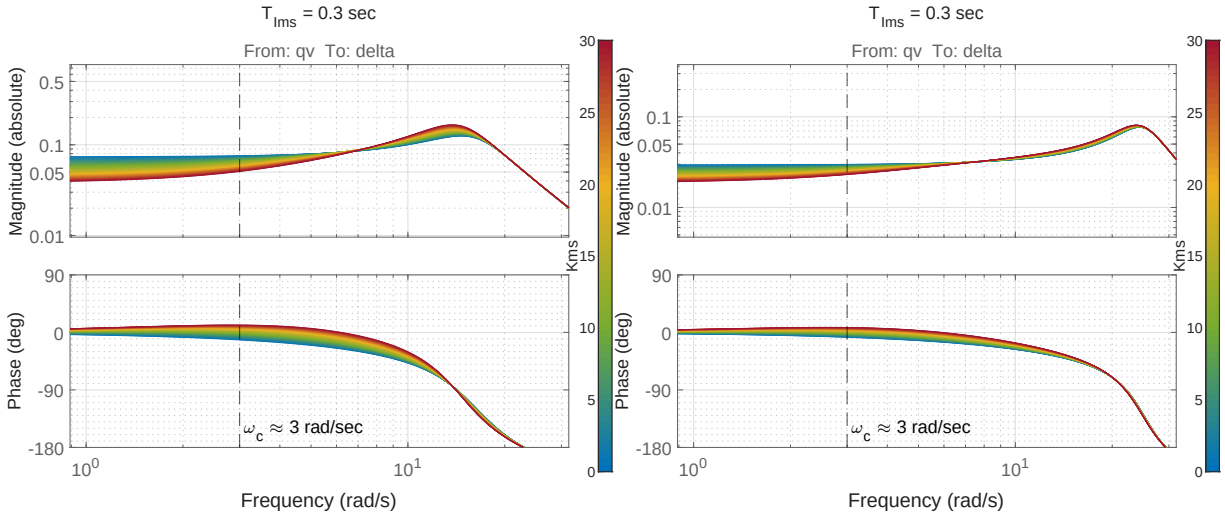

(a) $k_F = k_1$ **(b)** $k_F = 5k_1$

Fig. 12 FRF from q_v to δ with a MS lag, with $T_{I_{ms}} = 0.3s$

2. Double Integrator Control Dynamics, $Y_c = K_c/s^2$: MS Lag

A lag term does not significantly affect stability and can induce minor changes in the crossover region only (Figures Figure 10 and Figure 12). While this may be mathematically correct, studies have suggested that the role of MS lag is very limited [1].

Additionally, based on the root locus plot, a small lag into the MS feedback channel accentuates the neuromuscular peak, although not significantly. The FRF shows reduced time delay. As the lag time constant is increased, mid- and low-frequency characteristics are affected more strongly. This results in some lead in the crossover region and a slight reduction in low-frequency lag.

Overall, the mechanical model suggests that changes in spindle feedback dynamics lead to relatively minor alterations in the crossover and open-loop behavior, which would likely be more helpful in suppressing NMS characteristics than implementing crossover equalization. In contrast, variations in GTO gain and lag result in more significant system-wide changes.

Prior modeling work from 2004 indicated that MS feedback could be approximated as containing no lag, only lead elements [25].

Muscle Spindles are insufficient for effective equalization, but can play a significant role in smoothing the neuromuscular response.

VII. Utilizing Proprioceptive Feedback for Equalization

In scenarios where equalization is primarily visual, proprioceptive feedback, whether from force or position, may be utilized to flatten the neuromuscular system response near the crossover region and enhance gain margin. With the precision model, Visual equalization provides an open loop lag in the pilot's FRF for proportional control tasks, a pure gain for integrator tasks, and an open loop lead in the pilot's FRF for double integrator tasks.

For proprioceptive or mixed equalization, on the other hand, the design objective becomes to introduce appropriate dynamic characteristics into the crossover region through the neuromuscular feedback loops, with visual compensation compensating for any deficiencies.

In both cases, the main goal is to obtain integrator like dynamics in the region of crossover, a relatively high gain for lower frequencies and minimize disturbance arising from the neuromuscular system's poles at higher frequencies. In all control scenarios, parameters are manually selected to satisfy these criteria, specifically for a system with a relatively light, spring-restrained manipulator where $\sqrt{k_F/I_F} \approx 15$ rad/s.

Based on the results from Section VI, proprioceptive feedback appears to be limited to the following effects:

- MS feedback alone does not substantially modify open-loop behavior without risking instability. Similarly, a GTO-based lead does not significantly alter system dynamics, and may in fact induce instability.

- Adjusting GTO gain values can meaningfully affect the open-loop response but may reduce the damping of the dominant neuromuscular poles.
- Including a lag in GTO feedback—interpreted as the pilot estimating stick velocity from applied forces—can substantially improve open-loop delay and provide the necessary lead associated with double-integrator-type control.

A. Integrator Control Dynamics, $Y_c = K_c/s$

Such a system is considered trivial for equalization, as the necessary integrator dynamics near crossover are provided by the CE, and the pilot must tweak their necessary gains only to get the best performance. As proprioceptive feedback gains are used to improve performance even in the case of visual equalization, two separate scenarios are not necessary.

With the neuromuscular system as defined previously, and the controlled element dynamics such that $Y_c(s) = K_c/s$, $K_c = 24.3\ cm/rad$. I.e. stick deflection of 6 degrees causes the target on the display to move at roughly 2.5 cm (or 1 inch) per second.

Using the mechanical model and manually estimating the pilot's control parameters to obtain crossover dynamics dictated by McRuer's verbal adjustment rules [2], the resulting parameters necessary are shown in Table 3, with the open loop response in Figure 15. For the case of integral dynamics, additional cases of manipulator dynamics are also considered and analyzed in section VIII.

Equalization for integral dynamics highlighted that spindle feedback was a significant contributor to reducing undesirable high frequency dynamics, while also performing fine adjustments of slope near crossover. GTO gain was also helpful in the crossover region, however not necessary.

B. Proportional Control Dynamics, $Y_c = K_c$

For this system it is necessary to produce an open loop lag in order to achieve integrator crossover dynamics. This can be done by directly introducing a lag on visual feedback. For equalization through proprioceptive feedback, the structural model proposes an inner loop derivative or lead term. Experimental evidence has suggested that pilot performance in proportional feedback does not deteriorate, and in fact improves, when force feedback is not available (for free moving manipulators) [15]. This suggests that if proprioceptive equalization is used, it would be through a lead on position feedback. As has already been observed, it was not possible for muscle spindles to equalize alone, and no stable system could be achieved without a visual lag term.

The same control sensitivity is used, $K_c = 24.3\ cm/rad$, such that a stick deflection of 6 degrees causes the target to move 2.5 cm.

When attempting equalization through **only visual feedback**, a visual delay of $\tau = 0.16\ s$ was used along with a visual equalization term:

$$H_v = \frac{K_p}{1 + j\omega\tau_{I_{vis}}}; K_p = 1.64,\ \tau_{I_{vis}} = 0.6s \tag{7}$$

When attempting proprioceptive equalization, with no visual compensation, the model could not be stabilized with required higher PF lead time constants. In Figure 13, with the same visual delay of $\tau = 0.16\ s$:

$$H_v = K_p = 1.57 \tag{8}$$

$$H_{MS} = K_{ms}(1 + j\omega\tau_{L_{ms}})e^{-j\omega\ \tau_d}; K_{ms} = 5, \tau_{L_{ms}} = 3\ s;\ \tau_d = 0.025\ s \tag{9}$$

When attempting **mixed equalization** however, it was possible to achieve better phase lags in the crossover region and beyond while also reducing the need for visual compensation as can be seen in Figure 13. The blocks used in this case, with the same visual delay $\tau = 0.16\ s$:

$$H_v = \frac{K_p}{1 + j\omega\tau_{I_{vis}}}; K_p = 1.48,\ \tau_{I_{vis}} = 0.4s \tag{10}$$

$$H_{ms} = K_{ms}(1 + j\omega\tau_{L_{ms}})\ e^{-j\omega\ \tau_d}; K_{ms} = 4, \tau_{L_{ms}} = 0.5\ s;\ \tau_d = 0.025\ s \tag{11}$$

It is interesting to note that it was possible to reduce, but not eliminate, visual equalization with the use of MS lead.

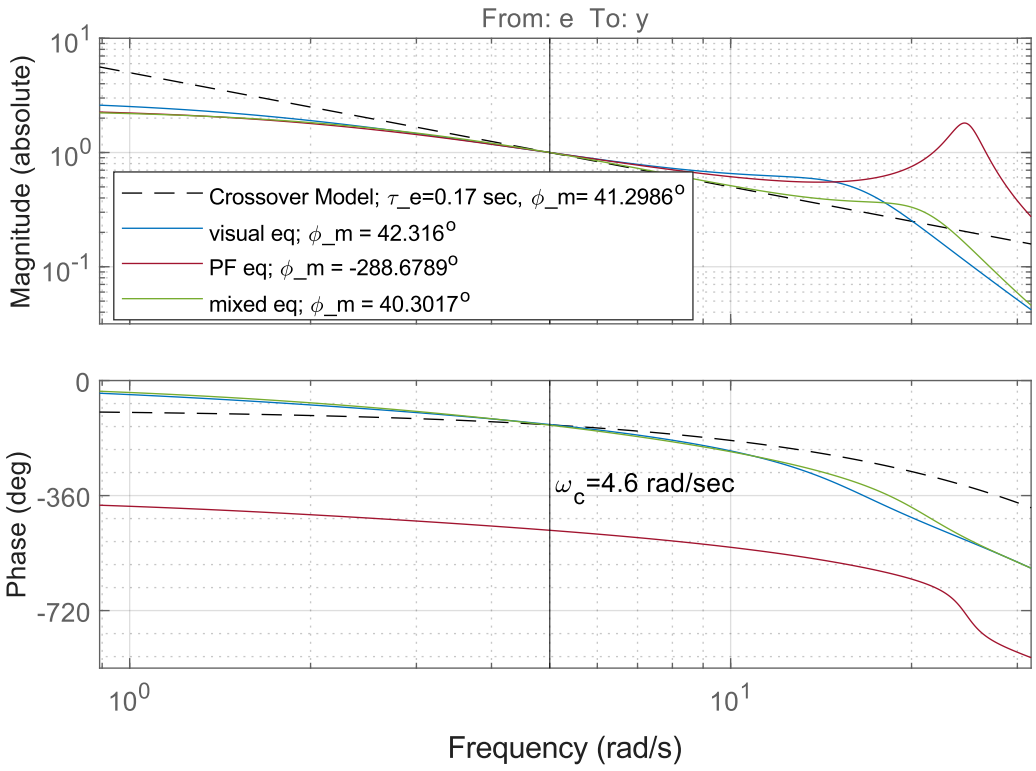

Fig. 13 Proportional Equalization through visual and mixed feedback

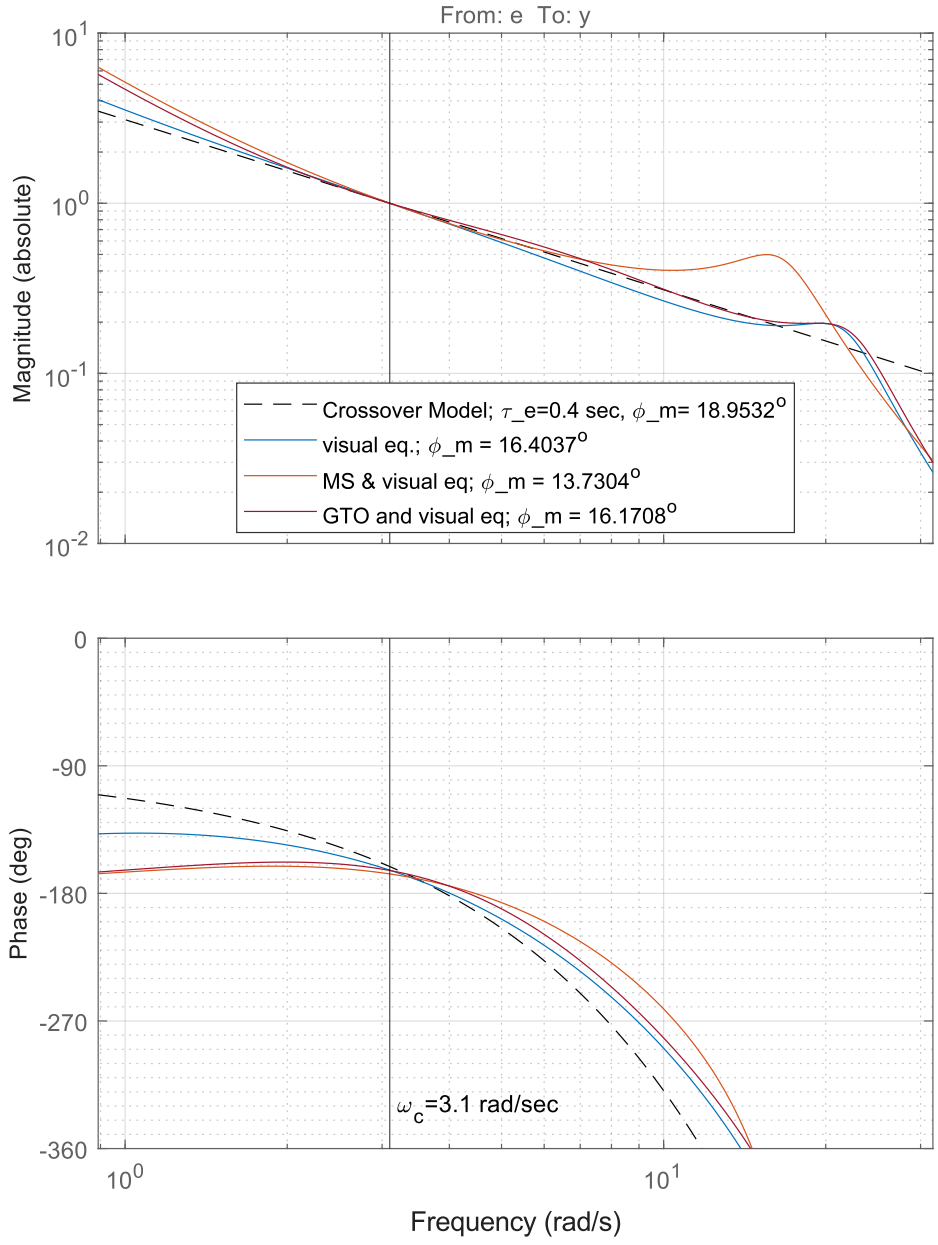

Fig. 14 Double Integrator Control through visual and mixed feedback

C. Double Integrator Dynamics, $Y_c = K_c/s^2$

For this system it is necessary to produce an open loop lead in the pilot's FRF in order to achieve integrator like crossover dynamics. This can be implemented as a lag on force feedback in the inner loop to achieve similar results. The structural model used a lag time as high as 2 seconds, which is physiologically implausible in the short time frames at which the neuromuscular cues are processed. Nevertheless, a mixed equalization method is still attempted here, and results can be seen in Figure 14.

The controlled element sensitivity was set to $K_c = 29.2\ cm/rad$. To minimize variables while also ensuring a realistic response, the spindle characteristics were fixed according to Equation 12

$$H_{ms} = K_{ms}(1 + j\omega\tau_{L_{ms}})e^{-j\omega\ \tau_d}; K_{ms} = 10, \tau_{L_{ms}} = 0.3\ s;\ \tau_d = 0.025\ s \tag{12}$$

When equalizing with **purely visual compensation**, it was possible to achieve the required crossover characteristics with parameters shown in in Equation 13

$$H_v = K_p(1 + j\omega\tau_{L_{vis}}); K_p = 0.96,\ \tau_{L_{vis}} = 2\ s, \tau = 0.25\ s \tag{13}$$

Purely proprioceptive compensation was not possible as even though a GTO lag was able to produce the required slope, it was not able to maintain stability for higher gain and lag terms. This was likely due to an additional lag appearing in the open loop as was shown in section IV to occur even when NMS dynamics were idealized.

Mixed equalization was achieved with a surprisingly low value of visual lead shown in Equation 16, combined with a small force feedback lag shown in Equation 17

$$H_v = K_p(1 + j\omega\tau_{L_{vis}}); K_p = 3.34,\ \tau_{L_{vis}} = 0.5\ s, \tau = 0.23\ s \tag{14}$$

$$H_{gto} = \frac{K_{gto}}{1 + j\omega\tau_{I_{gto}}}\ e^{-j\omega\ \tau_d}; K_{gto} = 3,\ \tau_{I_{gto}} = 0.3s\ \tau_d = \ 0.025s \tag{15}$$

This came with the drawback of increased phase lags in the low frequency region. A slightly smaller visual delay is also noted to achieve similar phase margins, however can be justified by the significantly lower lead time. Although phase lags measured experimentally in the low frequency region tend to have large error margins, McRuer in his study comparing pilot dynamics with various manipulators [15], observed increased phase lags when moving from free moving to pressure manipulators, referred to as "shifting the phase umbrella to the right".

As MS lag did not inherently destabilize the model, a mixed feedback of visual lead and MS lag was also attempted.

$$H_v = K_p(1 + j\omega\tau_{L_{vis}}); K_p = 3.34,\ \tau_{L_{vis}} = 0.5\ s, \tau = 0.23\ s \tag{16}$$

$$H_{ms} = \frac{K_{ms}(1 + j\omega\tau_{L_{ms}})}{1 + j\omega\tau_{I_{ms}}}\ e^{-j\omega\ \tau_d}; K_{ms} = 20,\ \tau_{I_{ms}} = 0.5\ s, \tau_{L_{ms}} = 0.3s\ \tau_d = \ 0.025s \tag{17}$$

Although seemingly just as effective in achieving integrator dynamics near crossover, there was a significant instability in the dominant NMS poles due to the large MS gain.

VIII. Effect of changing Feel System Dynamics on Equalization

This section explores the influence of various feel system dynamics on the process of equalization, focusing on their compatibility with known crossover characteristics and the physiological plausibility of achieving these dynamics. Multiple studies have been conducted, comparing pilot dynamics and performance when different stick dynamics are considered. Generally, this includes a free moving manipulator, one that has no spring restraints and only an inertia, hence exhibiting double integrator dynamics from force input to stick displacement, a spring restrained manipulator which includes a spring constraint and exhibits second order dynamics, and finally a pressure manipulator which uses a strain gauge on a manipulator fixed/clamped in place to measure the force applied on it, used directly as the input to the controlled element. Considering varying manipulator characteristics is important as changes in manipulator characteristics directly affects the availability of the proprioceptive feedback.

This suggests that when force feedback is unavailable or weak in the case of a free manipulator or one with a weak spring, experimental results showing a deterioration in equalization and performance would indicate force feedback being used for the same. On the other hand when displacement feedback is unavailable in the case of stiff or pressure

manipulators, changes in equalization characteristics would indicate how position feedback is being used by the pilot. A similar approach was used by Bachelder and Aponso, who conducted their own experiment with and without the spring being present in a joystick during a control task [23]. They conducted an analysis of both the equalization characteristics as well as the power spectral density of the stick displacement characteristics, and concluded that force feedback when available contributed to equalization. They further went on to propose a parameter estimation method for the generalized model shown in **??** by optimization of a cost function that includes both optimizing the crossover characteristics, as well as minimizing high frequency response characteristics [12]. Although promising, due to the poor quality of the experiment, the model cannot be verified as such. Although a proprioceptive equalization model was also fitted to more thorough experimental results by Gordon-Smith [16], this model also included a full mechanical model of the neuromuscular system.

A similar approach, inspired by Bachelder and Aponso's results, is used here. Results from studies by McRuer and Magdaleno [15] [13], and a study by Gordon-Smith [16], provide a thorough analysis of the effects of manipulator dynamics on the pilot response function. For each controlled element dynamic, trends observed in prior empirical studies are examined and, based on properties of the neuromuscular system (NMS) model discussed in section VI and section VII, hypotheses regarding possible mechanisms involving proprioceptive equalization are proposed. Due to the absence of clearly defined trends and the risk of overfitting from a large number of free parameters, qualitative fitting was only pursued in the case of integrator control.

For a detailed report on the experimental results used from literature, see Appendix E.

A. Integral Control

For integrator control tasks, the objectives for proprioceptive parameter selection are generally consistent, irrespective of whether proprioceptive pathways are utilized directly for equalization.

An initial attempt at fitting was performed manually by adjusting model parameters to optimize the pilot's open-loop frequency response. The goal was to improve response characteristics near the crossover region while minimizing high-frequency neuromuscular peaking, without altering the crossover frequency or visual lag.

Table 3 Pilot adjustment parameters for various manipulators and Integral control dynamics ($Y_c = K_c/s$) **(Figure 15**

Parameters	Free Manipulator	Spring Manipulator			Pressure Manipulator
	$k_F = 0$	$k_F = k_1$	$k_F = 5k_1$	$k_F = 25k_1$	$k_F = 73k_1;\ K_c = 16.4\ cm/Nm$
$k_{GTO}[Nm]^{-1}$	0	1	-1	4	4
$T_{GTO}[s]$	0	0	0	0	0
$k_{MS}[rad]^{-1}$	5	4	1	1	0
$T_{L_{MS}}[s]$	0.5	0.5	0.7	1	0
$K_p\ [s^{-1}]$	3.85	3.63	4.81	55.98	2.11

$T_{L_{GTO}} = 0,\ T_{I_{GTO}} = 0,\ T_{I_{MS}} = 0,\ \tau = 0.19s$ for all cases

1. Attempting Qualitative Fitting

To assess the model's consistency with experimental trends, manual tuning of H_{GTO} and H_{MS} parameters was performed to emulate integrator-like behavior near the crossover region while minimizing neuromuscular system limitations. The visual loop time delay τ was fixed at 0.19 seconds to ensure that the manipulator with $k_F/k_1 = 1$ achieved a crossover frequency and phase margin consistent with McRuer's verbal adjustment guidelines [2]. The proportional gain K_p was kept constant across all manipulator configurations to facilitate comparison. The fitting reflects expected feedback availability: GTO feedback is easily available in stiff spring scenarios, while MS feedback is more suitable for free and weak spring manipulators. These preferences are found to be inherently enforced by the model structure, as the use of opposite pathways is not mathematically.

The resulting Bode plots, when attempting manual parametrization of the model in Figure 4 to different spring characteristics, optimized for crossover characteristics, while minimizing high frequency peaking, are shown in Figure 15.

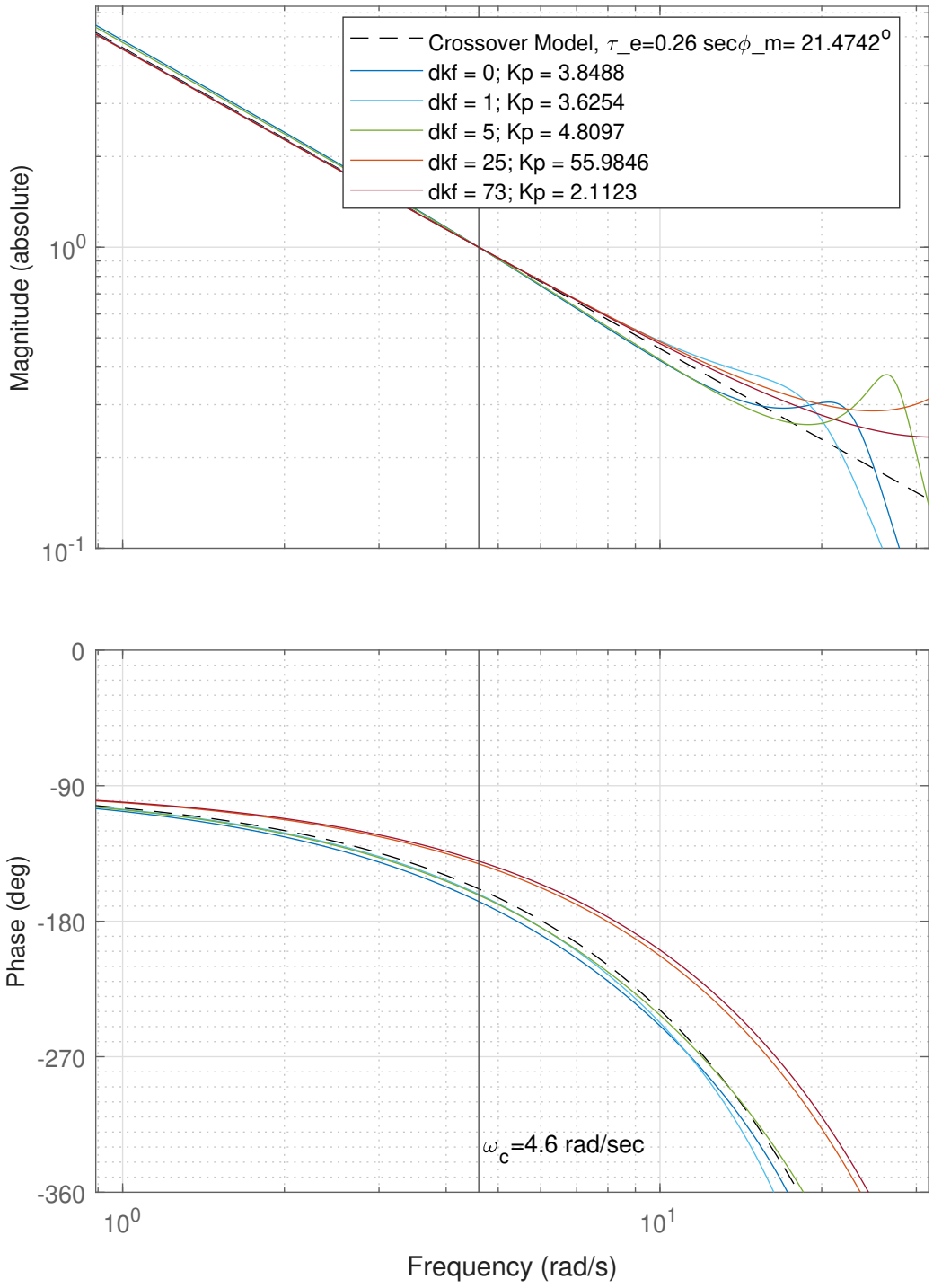

Fig. 15 Pilot Open Loop FRF from e to y_c for Integrator control task and parameters in Table 3

The parameters used for these characteristics are in Table 3.

2. Experimental Trends

After attempting optimal parameters for this model, the resulting response functions are compared to experimental trends. Key trends from Gordon-Smith (1970) [16] and McRuer and Magdaleno (1966) [15] include:

- Spring manipulators produced reduced phase lag and elevated crossover frequencies
- Pressure manipulators exhibited greater phase lag than free manipulators, particularly at low and mid frequencies, although variability was high

Gordon-Smith's findings revealed that pressure manipulators yielded greater phase margin, higher crossover frequencies, and increased natural frequency and damping in dominant NMS poles. These effects were more noticeable with wider forcing function bandwidths. Model results suggest that such phase lag trends can be explained purely through the mechanical open-loop neuromuscular response (Figure 6a), without necessitating proprioceptive feedback.

Additionally, high-frequency data from Gordon-Smith suggest that pressure manipulators result in increased damping, contrary to the model fitting shown in Figure 15, which exhibited reduced damping in free manipulators. This discrepancy likely stems from parameter overuse—particularly increased PEC stiffness due to presumed co-contraction and elevated GTO gains for stiffer manipulators—leading to overfitting.

Although positive GTO gain might reduce phase lag in stiff manipulator scenarios, **it remains uncertain whether this mechanism significantly contributes to observed experimental trends, or if the mechanical system properties alone are responsible.**

While the model qualitatively shows similar trends to that shown by experimental results, due to the lack of equalization terms necessary for an integral control strategy, no comments can be made on proprioceptive equalization.

B. Proportional Control

This section reviews experimental observations from Magdaleno and McRuer (1966) [13], and offers interpretations through the framework of proprioceptive equalization.

Their experiments found that increases in spring stiffness had minimal impact on relative RMS error, while both free and pressure manipulators exhibited higher RMS errors compared to spring manipulators. The highest crossover frequency was observed for $k_F = k_1$ (6 rad/s), while free-moving and pressure manipulators exhibited slightly lower values (5 rad/s).

Based on the relatively invariant crossover frequency and phase lag, the authors inferred the presence of a tight position feedback loop. This conclusion was supported by the observation that K_p remained nearly constant across different manipulator configurations.

When control sensitivity was reduced in proportion to increases in spring stiffness, performance declined and control excursions became smaller. This suggested that the absence of effective position feedback was responsible for the deterioration, as the performance remained stable when force demands were proportionally increased while excursion magnitudes remained unchanged.

These trends align with the model's behavior. Specifically, the inclusion of spindle-based position feedback enhances performance by reducing NMS-induced disturbances and marginally improving the slope of the crossover region. However, it is clear from the simulations that the contribution of spindle feedback is limited—it cannot fully replace the visual feedback loop required for equalization, serving instead as a supplementary mechanism, and a visual lag is necessary to generate equalization characteristics.

C. Double Integrator Control

Experimental results indicate that increasing spring stiffness generally leads to a reduction in effective time delay.

According to Magdaleno and McRuer (1966) [13], crossover frequency remains relatively constant for most spring conditions, with only a slight decrease observed at the highest stiffness level. However, effective time delay was found to decrease as spring stiffness increased, likely due to neuromuscular system (NMS) dynamics shifting to higher frequency ranges.

Optimal performance was achieved using an intermediate control sensitivity combined with a moderately stiff spring. This suggests that both position and force feedback contribute to improved control behavior.

However although performance with a free moving manipulator is worse, the crossover characteristics are still achieved to a similar degree when the frequency response characteristics are studied. Changes in dynamics are not

significant beyond an increase in phase lag that can be easily attributed to lower NMS natural frequency due to the free manipulator. This is despite there being a near absence of force feedback.

While the mechanical model shows that a force feedback lag, if physiologically possible, can be extremely helpful in contributing towards equalization during harder 'acceleration control tasks', rather than completely relying on a visual lead, this experimental evidence is unable to confirm it, as changes in the pilot's dynamics are not significant in the absence of force feedback. This shows that visual feedback alone is capable of achieving the necessary crossover characteristics, and though the absence of force feedback leads to greater rms error due to larger phase lags, this can easily be attributed to smaller NMS natural frequency in the case of free moving and weak spring manipulators in these experiments, rather than the absence of force feedback worse equalization.

IX. Results and Discussion

It was shown through simple mathematical analysis that attempting inner loop equalization through proprioceptive feedback has inherent limitations beyond those exerted by the NMS dynamics. Specifically, even in an ideal case, it was not possible to induce the open loop lead in the pilot FRF, necessary for double integrator control, purely through inner loop equalization. Additionally, it was noted that inducing the open loop lag would require a larger lead time constant in the inner loop acting on proprioceptive feedback than the lead time constant on visual feedback.

Introduction of 2nd order NMS dynamics showed that such a simplified model of the NMS was insufficient in analyzing proprioceptive equalization, as the resulting model was physically implausible for proportional control dynamics. However, another limitation in attempting double integrator control was introduced due to the destabilization of the NMS poles when proprioceptive equalization was considered.

Through use of the mechanical model it is clear that although a lead on the spindle feedback, for proportional CE dynamics, could induce a small lag in the pilot FRF, it was not enough for equalization. However the effectiveness of MS lead in improving NMS characteristics is significant and also confirmed through the experimental observations by Magdaleno and McRuer [13]. This confirmed the experimental observations for proportional control without considering proprioceptive equalization. It can however be noted that this model used muscle stretch x_m as the feedback signal from the spindles. Hess and Bachelder's models however have used the stick position δ, attributed to muscle spindles. Since the mechanical model's transfer function, from q_m to δ, was shown to be approximately equal to the standard second order approximation with a small NMS lag term, the same conditions as obtained in section IV would hold. I.e., an assumption that the pilot is able to directly process and utilize stick position to induce a lead would imply that the NMS second order dynamics can be easily countered through this feedback loop. This also shows how the structural and dual loop models could be validated using experimental data in the region of crossover.

Neither GTO nor MS lead were able to introduce equalization while keeping the model stable.

A GTO lag showed promising results in contributing towards equalization for second order dynamics while also slightly improving NMS dynamics. Additionally, considering the root locus plot, it is possible to show that for an intermediate value of GTO gain based on this model, it would be possible for a skilled pilot to reduce visual compensation effort significantly. When considering such an approach, it would be possible to consider an approximate model as in Equation 3. This could possibly be even further approximated such that the open loop response function of the pilot becomes:

$$H_p = K_p(1 + j\omega\tau_{L_{vis}})e^{-j\omega\tau}\ [(1 + j\omega\tau_{PF})G_{NMS}] \tag{18}$$

Such a format suggests that a combined lead from visual and force feedback is utilized by the pilot for equalization, with G_{NMS} consisting of a standard second order NMS formulation with a lag. A similar expression for equalization with two lead terms has been found to fit better the pilot dynamics observed during control of the pitch dynamics of a jet aircraft [26].

Equalization through a GTO lag, however, cannot be easily verified through experimental data, especially as it would involve separate measurements of command signals from visual (q_v) and proprioceptive (q_{PF}) pathways, which is not possible.

A. Limitations

There is a lack of consideration for disturbance or remnant, which have relevance especially due to disturbance reduction being a major component of the pilot's optimization goals when considering response at higher frequency. Although all analysis was limited to studying the response to the forcing function, which is uncorrelated to the remnant

input by definition, minimization of white noise is likely to be a major goal in adaptation and parameter selection, which was not considered. Only minimization of the NMS characteristics was considered.

Due to a large number of parameters, variability in most could not be considered. Especially different proprioceptive feedback time delays, for which Gordon-Smith [16] identified force feedback time delay to be half of position feedback and Hess identified to be a significant factor in performance in his structural model [27].

This model may not accurately represent the actual proprioceptive feedback sensed by the organs, which may or may not be used for equalization. The model has not been validate to confirm that F_{gto} in the model accurately reflects the actual forces sensed by the Golgi tendons. Similarly, it is unknown whether x_m in the model accurately represents the feedback that could be potentially used for equalization, or if stick position would be more relevant for equalization. This is especially relevant as muscular co-contraction significantly alters the proprioceptively sensed and acted upon forces, whereas mechanical model used here abstracts the individual muscle groups into a single spring damper system with effects of co-contraction only assumed through changes in stiffness.

X. Conclusions

This study investigated the effect of manipulator dynamics on pilot control behavior under different control structures, with a focus on the role of proprioceptive equalization through muscle spindle and Golgi tendon organ (GTO) pathways.

For proportional control, experimental results and modeling suggest that while muscle spindle feedback contributes to improved tracking and reduced neuromuscular disturbance, it **cannot fully replace visual feedback mechanisms**. Although in ideal cases a lead applied to the manipulator position feedback should provide the necessary open loop lag, such feedback shows unrealistic effects when second order NMS dynamics are used. When muscle stretch and velocity feedback theorized to be sensed by muscle spindles, rather than manipulator deflection feedback, are used, the model shows that even though this feedback is extremely useful in reducing the effects of the NMS dynamics and compensating for undesirable feel system dynamics, this is not enough for equalization.

In experimental studies comparing dynamics with different manipulator characteristics, the relatively invariant crossover frequency and phase lag across different manipulators in experimental data support the presence of an **underlying position feedback loop** that compensates for the neuromuscular dynamics, the mechanical model implemented is in agreement with these observations; however it shows that the influence of position feedback appears limited to improving the neuromuscular system characteristics (when changing feel system dynamics makes them worse) and cannot significantly affect crossover equalization.

In **double integrator control**, mathematical analysis showed that an inner loop lag will always be limited in producing the lead term required in the open loop due to an additional lag term being introduced. This effect was observed both with second order NMS dynamics and with the full mechanical model, showing that **purely proprioceptive equalization is impossible**. However, attempting mixed equalization showed that utilizing force feedback lag from the GTOs can significantly reduce pilot effort as a much smaller visual lead time is necessary to achieve equalization. A secondary limitation caused by the neuromuscular system dynamics introduces an upper limit to the force feedback gain and consequently GTO feedback that can be introduced, with larger K_{gto} and therefore more compensation being possible when stiffer manipulators are present, as shown by the root locus plots. The model also suggests that a second order approximation of the neuromuscular system, as in Equation 3, can provide an excellent approximation to study the force being applied on the manipulator during manual control.

Experimental results indicate that increased spring stiffness was associated with reduced effective time delay, likely due to NMS dynamics shifting to higher frequencies. An intermediate spring stiffness combined with appropriate control sensitivity yielded the best performance, implying a complementary role for both GTO and spindle feedback. While GTO feedback can assist in reducing the visual effort required for equalization, it also introduces the risk of instability due to second-order amplification. A GTO pathway with physiological lag, if realizable, may offer significant benefits for tasks requiring acceleration-based control. However this **cannot be confirmed with the current experimental evidence**, and further experimental data, especially in the higher frequency region, might yield better results.

Overall, while proprioceptive pathways enhance performance and contribute to neuromuscular stabilization, they **cannot independently achieve full equalization**. Their primary role appears to be in modulating pilot effort and partially shaping the open-loop dynamics, particularly in more demanding control scenarios. This suggests that while purely proprioceptive equalization is incompatible with current best known models, a mixed equalization method is likely to be utilized if physiologically possible, especially with gain and lag on force feedback being responsible for changes in dynamics near the region of crossover.

References

[1] Van Paassen, M. M., Van Der Vaart, J. C., and Mulder, J. A., "Model of the neuromuscular dynamics of the human pilot's arm," *Journal of aircraft*, Vol. 41, No. 6, 2004, p. 1482–1490.

[2] McRuer, D. T., and Jex, H. R., "A review of quasi-linear pilot models," *IEEE transactions on human factors in electronics*, , No. 3, 1967, pp. 231–249.

[3] Hess, R. A., "Unified theory for aircraft handling qualities and adverse aircraft-pilot coupling," *Journal of Guidance, Control, and Dynamics*, Vol. 20, No. 6, 1997, pp. 1141–1148.

[4] Hess, R. A., "Analysis of aircraft attitude control systems prone to pilot-induced oscillations," *Journal of Guidance, Control, and Dynamics*, Vol. 7, No. 1, 1984, pp. 106–112.

[5] Hess, R. A., "Analyzing manipulator and feel system effects in aircraft flight control," *IEEE Transactions on Systems, Man, and Cybernetics*, Vol. 20, No. 4, 1990, pp. 923–931.

[6] Hess, R. A., "A rationale for human operator pulsive control behavior," *Journal of Guidance and Control*, Vol. 2, No. 3, 1979, pp. 221–227.

[7] Bachelder, E. N., Hess, R. A., Godfroy-Cooper, M., and Aponso, B. L., "Modeling Pilot Pulse Control," *European Rotorcraft Forum*, 2017.

[8] Xu, S., Tan, W., Efremov, A. V., Sun, L., and Qu, X., "Review of control models for human pilot behavior," *Annual Reviews in Control*, Vol. 44, 2017, pp. 274–291.

[9] Hess, R. A., "A unifying approach to human pilot modelling," *IFAC Proceedings Volumes*, Vol. 17, No. 2, 1984, pp. 2609–2613.

[10] Fu, W., van Paassen, M. M., and Mulder, M., "The influence of discrimination strategy on the jnd in human haptic perception of manipulator stiffness," *AIAA Modeling and Simulation Technologies Conference*, 2017, p. 3668.

[11] Boogaard, M., "Proprioceptive Qualities in Manual Control," Master's thesis, Technische Universiteit Delft, 2021. URL `https://resolver.tudelft.nl/uuid:8365c5d2-b52c-4b57-8a5e-ba8fc7115807`.

[12] Bachelder, E. N., and Aponso, B. L., "Human pilot control adaptation: A physiological interpretation," *AIAA SCITECH 2022 Forum*, 2022, p. 2446.

[13] Magdaleno, R. E., and McRuer, D. T., *Effects of manipulator restraints on human operator performance*, Vol. 66, Air Force Flight Dynamics Laboratory, Research and Technology Division, Air Force Systems Command, United States Air Force, 1966.

[14] Bachelder, E. N., and Aponso, B. L., "Handling Qualities and Aircraft Pilot Coupling: New Evidence of Neuromuscular Origins," *AIAA SCITECH 2022 Forum*, 2022, p. 0890.

[15] McRuer, D. T., and Magdaleno, R. E., *Human pilot dynamics with various manipulators*, Vol. 66, Air Force Flight Dynamics Laboratory, Research and Technology Division, Tech Report, 1966.

[16] Gordon-Smith, M., "An investigation into certain aspects of the describing function of a human operator controlling a system of one degree of freedom(Analysis of describing function of human operator controlling system of one degree of freedom)," 1970.

[17] Houk, J., and Henneman, E., "Responses of Golgi tendon organs to active contractions of the soleus muscle of the cat." *Journal of neurophysiology*, Vol. 30, No. 3, 1967, pp. 466–481.

[18] McRuer, D. T., "Pilot Dynamics in Compensatory Systems," *Air Force Flight Dynamics Lab. Tech. Report*, 1965.

[19] Smith, R. H., "A unifying theory for pilot opinion rating," *Proceedings of the 12th Annual Conference on Manual Control*, 1976, pp. 542–558.

[20] Hess, R. A., "Dual-loop model of the human controller," *Journal of guidance and control*, Vol. 1, No. 4, 1978, pp. 254–260.

[21] Hess, R. A., "Structural model of the adaptive human pilot," *Journal of guidance and control*, Vol. 3, No. 5, 1980, pp. 416–423.

[22] Bachelder, E. N., and Aponso, B. L., "A Theoretical Framework Unifying Handling Qualities, Workload, Stability, and Control," *Vertical Flight Society 77th Annual Forum & Technology Display, Virtual*, 2021.

[23] Bachelder, E. N., and Aponso, B. L., "The Feel System is an Extension of Both the Vehicle and Neuromuscular Systems," *47th European Rotorcraft Forum*, 2021.

[24] Magdaleno, R. E., and Mc Ruer, D. T., "Experimental validation and analytical elaboration for models of the pilot's neuromuscular subsystem in tracking tasks," Tech. rep., NASA, 1971.

[25] Van Paasen, M., Van Der Vaart, J., and Mulder, J., "Model of the neuromuscular dynamics of the human pilot's arm," *Journal of aircraft*, Vol. 41, No. 6, 2004, pp. 1482–1490.

[26] Pool, D. M., Zaal, P. M. T., Damveld, H. J., van Paassen, M. M., and Mulder, M., "Pilot equalization in manual control of aircraft dynamics," *2009 IEEE International Conference on Systems, Man and Cybernetics*, IEEE, 2009, pp. 2480–2485.

[27] Hess, R. A., "Effects of time delays on systems subject to manual control," *Journal of Guidance, Control, and Dynamics*, Vol. 7, No. 4, 1984, pp. 416–421.

Part III

Research Appendices

A

Mathematical Analysis of Inner Loop Equalization

A preliminary analysis was performed to evaluate the key differences between the simplified precision model, which assumes visual feedback for equalization, and an inner loop equalization model based on the dual loop model model by Hess [6], which uses proprioceptive feedback as the main pathway for equalization. This is to directly address the first research question, analyzing whether equalization is possible with an inner loop feedback method in ideal conditions. A simplified version of the structural model is employed for a compensatory tracking task and its plausibility is evaluated using open loop dynamics.

Visual equalization based on the precision model [15], depicted in figure A.1a, shows the visual equalization structure used to obtain integrator dynamics in the region of crossover. The equalization model structure depends on the controlled element dynamics, i.e. the parameter k, turning into a lag with time constant τ_{vis} for proportional dynamics ($Y_c = K_c, k = 0$), and a lead with time constant τ_{vis} for double integrator dynamics ($Y_c = K_c/s^2, k = 2$). It models the pilot as a linear system with the displayed error signal as the input, and the stick force/deflection as the output. Equalization occurs within this system impacting the pilot response to the error (i.e. the visual open loop) directly.

In Hess' structural model [7] equalization occurs instead in an inner loop through proprioception, and the essential structure, dependent on controlled element dynamics, is shown in A.2a. In this case, the response is inverted, with an inner loop lag being used to compensate for a double integrator control task ($Y_c = K_c/s^2$), and an inner loop lead for a proportional control task ($Y_c = K_c$).

The actuator input provided by the pilot is a combination of a control signal based on the visual input and proprioceptively sensed feedback. Since equalization occurs in the inner loop it does not impact the open loop dynamics directly. The dual loop model by Hess [6] proposed that an internal model of the controlled element dynamics by an experienced pilot was involved, and included in this inner loop. The structural and revised structural model made this implicit and suggested that based on the dynamics of the controlled element estimated by the pilot, an inner loop lead was present to compensate for proportional dynamics, gain for integrator, and lag for double integrator controlled element dynamics. Only this equalization behavior of an inner loop model is analyzed here.

The **methodology** is outlined as follows:

For the purpose of a preliminary theoretical analysis, disturbance signals as well as the dynamics of the neuromuscular system and stick dynamics are ignored, simplifying the model. The only elements present are the gain, equalization, and an effective time delay, which has been shown to capture crossover dynamics successfully in the case of the simplified precision model [20]. While the simplified precision model (Figure A.1b) is quite transparent in how each element would affect the pilot response dynamics, Hess' models behavior is not as apparent by looking at A.2b.

Different controlled system dynamics are considered as they would induce different equalization behavior in the pilot. The following sections analyze the pilot behavior for each case considering the controlled elements to be proportional ($Y_C(s) = K_c$), integral ($Y_C(s) = K_c/s$), and double integral ($Y_C(s) = K_c/s^2$). Note that while the controlled element dynamics can be written as a transfer function in the Laplace domain, the pilot describing function is defined as a quasi-linear model, with this linear approximation only valid

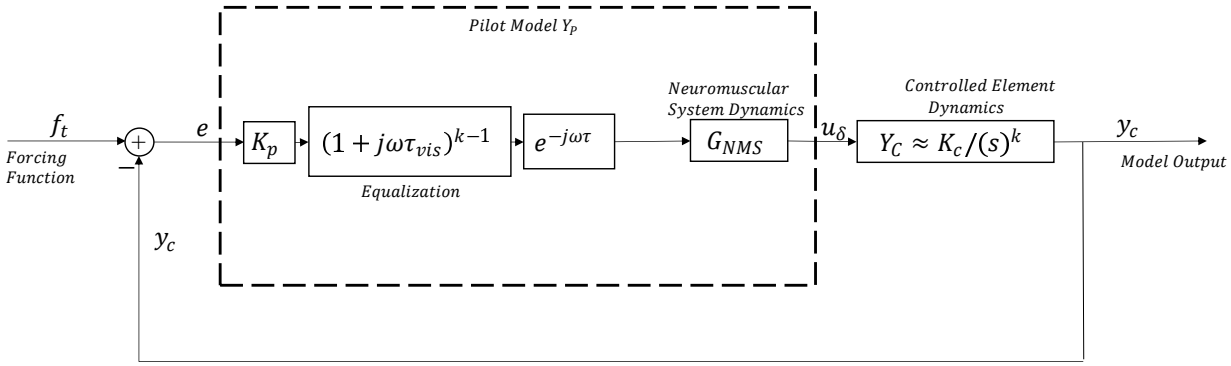

(a) Precision Model of the Human Pilot showing equalization characteristics [15]

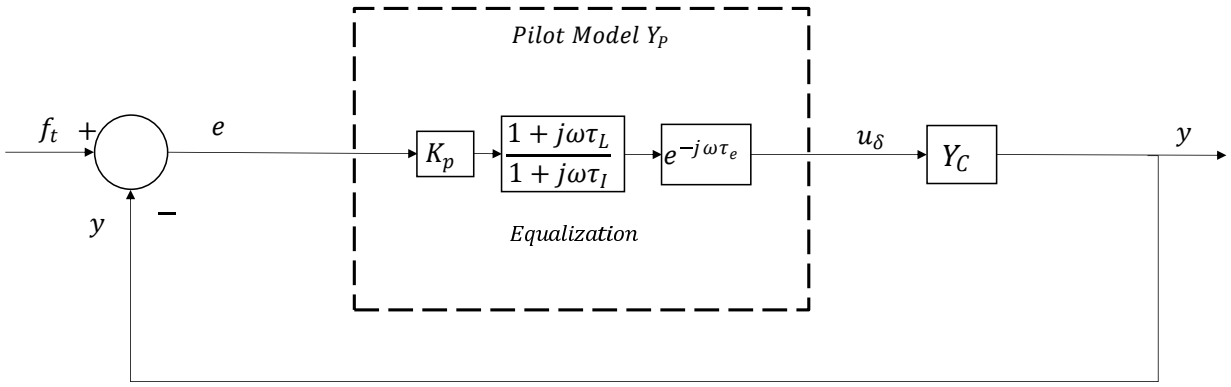

(b) Simplified Precision model without disturbance and NMS dynamics for mathematical analysis

Figure A.1: Simplified Precision Model using visual equalization

when considering frequency response in the steady state. Hence the elements in the pilot's describing function will be written in the frequency rather than Laplace domain.

The open loop dynamics (from e to y_c) of the simplified models are analyzed mathematically in the frequency domain. The impact of each parameter in the open loop dynamics is analyzed with the goal of answering the following questions:

- Does inner loop equalization give the same level of control as the single loop model?
- How does each parameter in the inner loop affect the crossover dynamics?
- Can a physiological interpretation be drawn based on these equalization characteristics?

A.1. Simplified Model - Proportional Control, $Y_c = K_c$

First the controlled element is modeled as a gain, yielding a position control task. It can be observed in real systems where the operator input proportionally relates to position control. In a single axis compensatory task, the pilot can view the position error on the visual display and directly control it through the stick deflection.

For such a control task, Hess's physiological models suggest modeling the pilot central nervous system and the proprioceptive feedback element separately. The dual loop model suggests that the proprioceptive feedback element includes an explicit internal estimated model of the controlled element utilizing the rate estimation of the input signal (force on the stick). Meanwhile the structural model makes this internal model of the controlled element implicit and the proprioceptive feedback element is of the form $H_{PF}(j\omega) = K_{PF}/(1+j\omega\tau_{PF})^{(k-1)}$ where k describes the behavior of the controlled element near the crossover region. For the proportional control task $k = 0$ [48].

This controller can be used in the model described in Figure A.2 to observe the effectiveness of inner loop feedback in equalization.

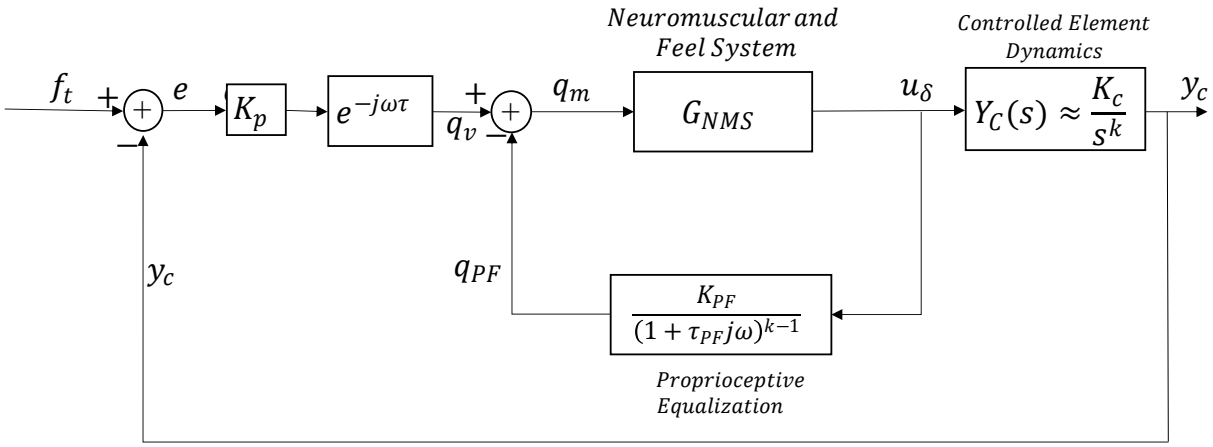

(a) Equalization Characteristics of Hess' Structural Model [8]

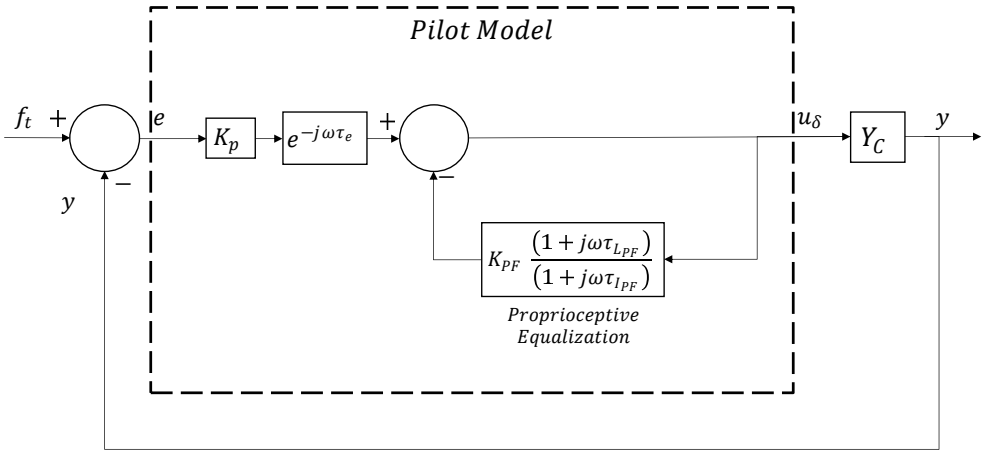

(b) Simplified Inner Loop Model Utilizing Proprioceptive Feedback

Figure A.2: Model diagram of the structural model equalization, along with a simplified model used for mathematical analysis

Table A.1: Describing Functions and Parameter Values for both Simplified Models in a Proportional Control Task, $Y_C = K_C = 1$

Description	Simplified Precision Model	Inner Loop Model
Pilot Model Transfer Function $(U(j\omega)/E(j\omega))$	$H_P(j\omega) = \frac{K_p}{1+j\omega\tau_I}\exp(-j\omega\tau_e)$	$H_P(j\omega) = K_p \exp(-j\omega\tau_e)\frac{1}{1+H_{PF}(j\omega)}$ $H_{PF}(j\omega) = K_{PF}(1+j\omega\tau_{I_{PF}})$
OL Transfer Function $(Y_c(j\omega)/E(j\omega))$	$Y_{OL}(j\omega) = \frac{K_pK_c}{1+j\omega\tau_I}\exp(-j\omega\tau_e)$	$Y_{OL}(j\omega) = \frac{K_pK_c}{K_{PF}+1}\frac{1}{1+j\omega\frac{K_{PF}}{K_{PF}+1}\tau_{L_{PF}}}\exp(-j\omega\tau_e)$
OL Gain	K_pK_c	$\frac{K_pK_c}{K_{PF}+1}$
OL Lag Time (seconds)	τ_I	$\frac{K_{PF}}{K_{PF}+1}\tau_{L_{PF}}$
Theoretical Parameter Values		
Visual Feedback gain	$K_p = 2.3$	$K_p = 6.9$
Proprioception gain	-	$K_{PF} = 2$
Equalization Lead	-	$\tau_{L_{PF}} = 0.6$
Equalization Lag	$\tau_I = 0.4$	-
Model Effective Time Delay	$\tau_e = 0.25$	$\tau_e = 0.25$
Equalization Transfer Function	$\frac{5.75}{2.5+j\omega}e^{-0.25j\omega}$	$\frac{5.75}{2.5+j\omega}e^{-0.25j\omega}$

With proprioceptive feedback absent, the simplified precision model shown by McRuer suggests that the pilot can be modeled as $H_p = K_p/(1+j\omega\tau_I)e^{-j\omega\tau_e}$, having taken into account the effective time delay of the system (τ_e) and a lag (τ_I) which is responsible for equalization in the crossover region [15].

The parameters have been estimated using McRuer's verbal adjustment rules. The same method can be applied to estimate the PF element parameters to obtain best fit in the model. Since there is one too many parameters though, the proprioceptive feedback gain has been fixed to the values that were presented by Hess during validation of the structural model [7]. A comparison of the open loop describing functions for the two equalization strategies is presented in Table A.1. Open loop characteristics are also presented in Figure A.3.

A.1.1. Observations

It noted that in certain conditions (and for the parameter values chosen) the pilot's open loop response transfer functions of both models can be obtained to be exactly identical. The general equivalence condition can be easily observed for both of the models and has also been shown in Table A.1.

- Both models are able to give identical pilot response characteristics that satisfy McRuer's verbal adjustment rules
- Lead in the inner (proprioceptive) loop introduces a lag in the pilot response dynamics
- The lead time necessary in the inner loop is always larger than the desired lag time in the pilot's response. However the difference decreases as proprioceptive feedback gain is increased, which needs to also be compensated by a larger visual gain K_p

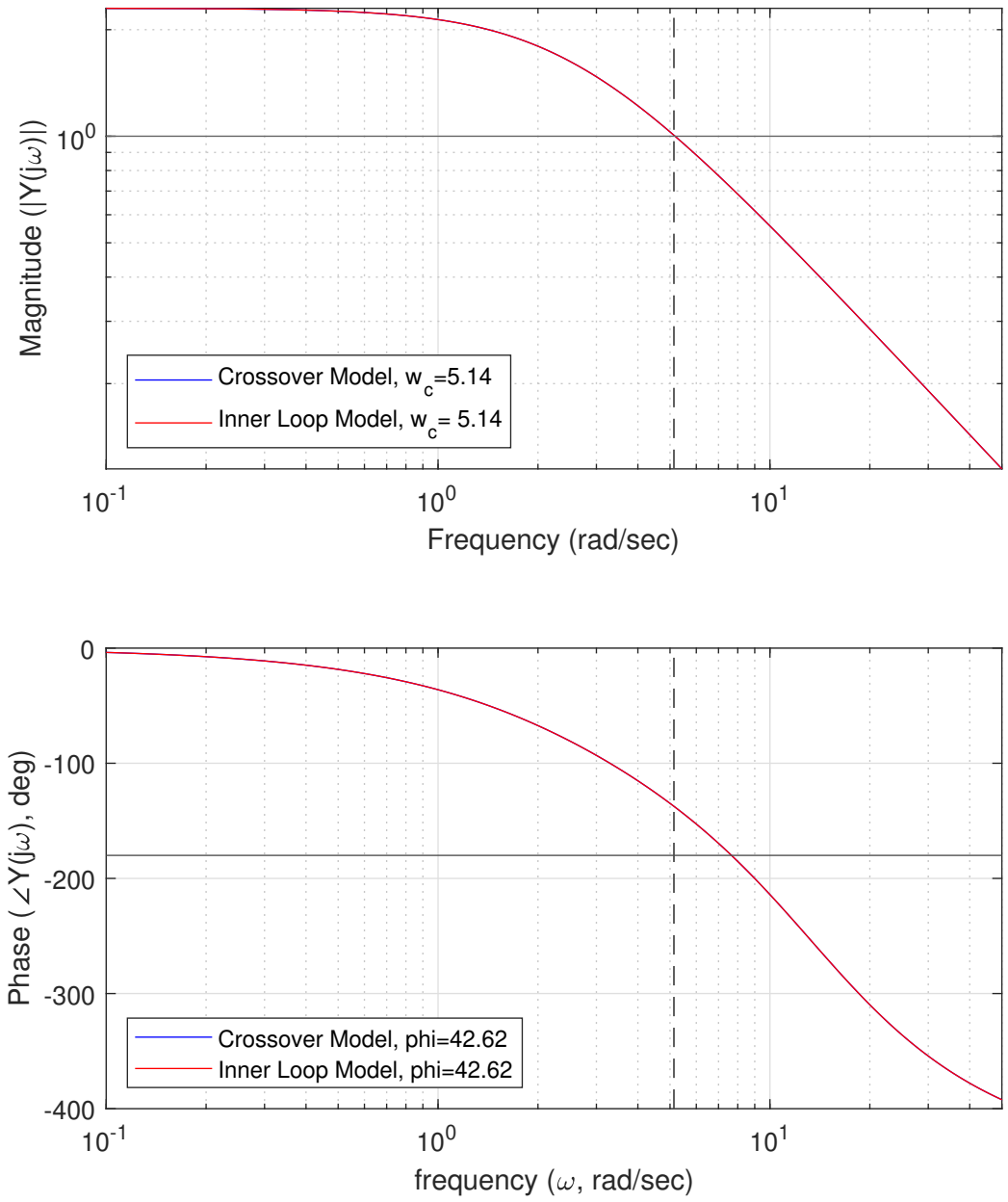

Figure A.3: Open loop Characteristics (from error e to model output y_c) in a **proportional control task** as in Table A.1

Table A.2: Describing Functions and Parameter Values for both Simplified Models during an integral control task, $Y_C(s) = K_C/s$

Description	Simplified Precision Model	Inner Loop Model
Pilot Model Transfer Function $(U(j\omega)/E(j\omega))$	$H_P(j\omega) = K_p \exp(-j\omega\tau_e)$	$H_P(j\omega) = K_p \exp(-j\omega\tau_e)\frac{1}{1+H_{PF}(j\omega)}$ $H_{PF}(j\omega) = K_{PF}$
OL Transfer Function $(Y_c(j\omega)/E(j\omega))$	$Y_{OL}(j\omega) = K_pK_c\frac{1}{j\omega}\exp(-j\omega\tau_e)$	$Y_{OL}(j\omega) = \frac{K_pK_c}{1+K_{PF}}\frac{1}{j\omega}\exp(-j\omega\tau_e)$
OL Gain	K_pK_c	$\frac{K_pK_c}{1+K_{PF}}$
Theoretical Parameter Values		
Visual Feedback gain	$K_p = 4.63$	$K_p = 13.89$
Proprioceptive Feedback gain	-	$K_{PF} = 2$
Model Effective Time Delay	$\tau_e = 0.26$	$\tau_e = 0.26$
OL Transfer Function	$\frac{4.63}{j\omega}e^{-0.26j\omega}$	$\frac{4.63}{j\omega}e^{-0.26j\omega}$

It is clear that both models mathematically satisfy the control requirements to the same degree, in the absence of any other additional elements, such as the neuromuscular system or the remnant.

Realistically speaking, the lag time introduced by a human in a control task cannot be very high, which must be taken into account as a physiological limitation. The values used here align roughly with experimental results reported by McRuer [15].

A.2. Simplified Model - Integrator Control, $Y_c = K_c/s$

In this case, the controlled element is modeled as an integrator, i.e., $Y_c(s) = K_c/s$, corresponding to a velocity control task.

Within the single-loop framework, the pilot perceives an error in velocity on the display and adjusts their input proportionally to minimize this error. The pilot is typically modeled as a gain with a time delay, as the integrative nature of the system naturally introduces the required crossover dynamics. In McRuer's simplified model, the pilot model is simplified to $Y_P(j\omega) = K_p \exp(-j\omega\tau_e)$, since equalization (typically introduced by a lag or lead element) is not necessary for purely integrative systems in the crossover region.

In contrast, considering the simplified PF equalization model, proprioceptive feedback is once again used to form an inner loop that aids in equalization. However, because the plant dynamics already introduce integrator dynamics, a lead or lag term for equalization is not needed. The inner loop is effectively a static gain, $H_{PF}(j\omega) = K_{PF}$, which does not introduce additional dynamics (lag or lead), but rather alters the overall gain distribution in the system. The pilot's visual feedback gain is increased proportionally to offset the attenuation caused by the proprioceptive loop.

In both models, the open loop response (from error e to model output y_c) becomes identical under the condition that the gains are tuned to balance each other. When proposing theoretical values in Table A.2, the PF gain is fixed at $K_{PF} = 2$ corresponding with the value used by Hess [7].

A.2.1. Observations

It noted that in certain conditions (and for the parameter values chosen) the open loop response dynamics of the pilot for both models are exactly identical. The general equivalence condition can be easily observed in Table A.2.

- Both models can give identical pilot response characteristics that satisfy McRuer's verbal adjustment rules
- Since equalization occurs through a pure gain, this represents a trivial case with clear equivalence between the simplified precision model and inner loop model
- A larger proportional gain is applied to the visual feedback in the inner loop model to compensate for the impact of the proprioceptive feedback
- The effective time delay applied for both models is equal

A.3. Simplified Model - Double Integrator Control, $Y_c = K_c/s^2$

In the most challenging control task for the pilot, the controlled element is modeled as a double integrator, i.e., $Y_c(s) = K_c/s^2$. This form corresponds to an acceleration control task, where operator inputs are proportional to system acceleration. The need for equalization becomes critical in this case, as the plant's dynamics inherently introduce two integrators, causing substantial phase delay near the crossover frequency. The pilot must therefore introduce a net lead compensation in the open loop response to achieve stable control with integrator dynamics in the region of crossover.

As shown in Table A.3, while the simplified precision model proposes a visual lead to obtain crossover dynamics, the dual loop and structural models propose an inner loop lag term instead being the method for equalization. In this case a higher PF gain, $K_{PF} = 10$ has been used based on Hess' estimate [7].

A.3.1. Observations

This is the only case where equivalent dynamics could not be obtained in the pilot's open loop response using PF rather than visual equalization.

- There is **an additional lag term** in the open loop induced by the presence of lead equalization in the inner loop.
- To ensure that integrator dynamics at crossover are maintained, the induced lag frequency must be much larger than the crossover frequency, which can only be done by making the proprioceptive feedback gain larger, increased to 10 here based on the parameter value used by Hess [7].

$$\frac{K_{PF}+1}{\tau_{I_{PF}}} >> \omega_c \Rightarrow K_{PF} >> \omega_c \tau_{I_{PF}} \tag{A.1}$$

- To ensure that the phase lags obtained are realistic, the visual time delay had to be reduced significantly. This is likely due to the presence of the additional lag term. Interestingly the effective visual lag used to obtain the dynamics shown in Figure A.5 is even less than the lag used in the integrator control task.
- To counteract the larger PF gain, the visual gain must also be increased. This suggests that a limitation on gains K_{PF} and K_p (limitations in proprioception) corresponds to a limitation in the pilot's ability to produce lead in the simplified precision model.

A.4. Results and Discussion

- The lead time constant in the PF inner loop corresponds exactly to a lag time constant in the visual equalization model (for $Y_c = K_c$).
- When considering a double integrator control task, although a lag term in the proprioceptive feedback block introduces the required lead in the pilot's open loop response characteristics, it also introduces an additional limiting lag term. To reduce the limitation, the proprioceptive gain must be high.
- In general when both lead and lag are produced in the proprioceptive equalization block, a mathematically corresponding equalization term in the simplified precision model would be given as shown.

$$H_{PF}(j\omega) = K_{PF}\frac{1+j\omega\tau_{L_{PF}}}{1+j\omega\tau_{I_{PF}}} \Rightarrow Y_p(j\omega) = \frac{K_p}{K_{PF}+1}\frac{1+j\omega\tau_{I_{PF}}}{1+j\omega\frac{\tau_{I_{PF}}+K_{PF}\tau_{L_{PF}}}{K_{PF}+1}} \tag{A.2}$$

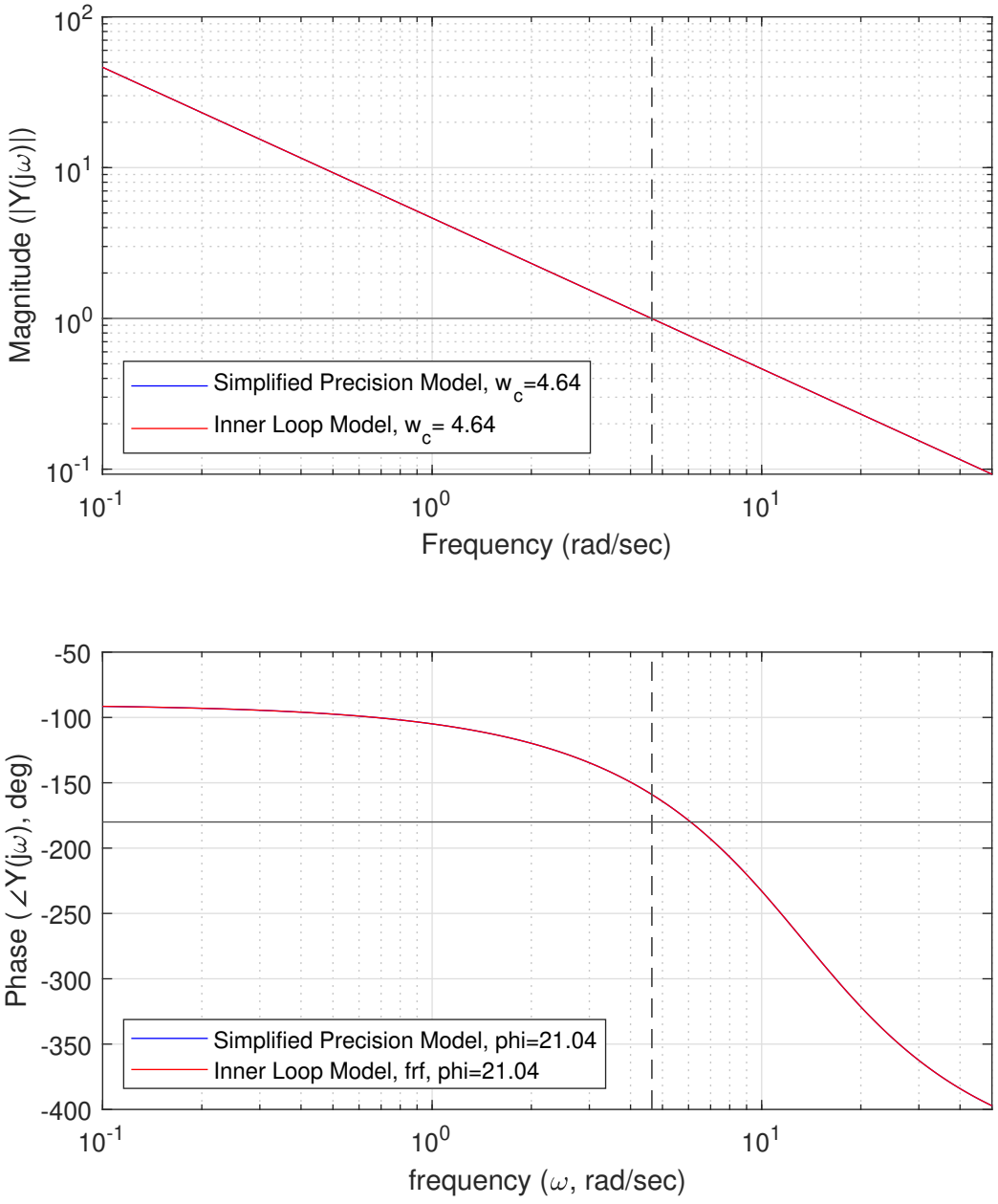

Figure A.4: Open Loop Characteristics (from error e to model output y_c) in a **single integrator control task** as in Table A.2

Table A.3: Describing Functions and Parameter Values for both Simplified Models in an Acceleration Control Task, $Y_C = K_C/s^2 = 1/s^2$

Description	Simplified Precision Model	Inner Loop Model
Pilot Model Transfer Function $(U(j\omega)/E(j\omega))$	$H_P(j\omega) = K_p(1 + j\omega\tau_L)\,\mathsf{exp}(-j\omega\tau_e)$	$H_P(j\omega) = K_p\,\mathsf{exp}(-j\omega\tau_e)\frac{1}{1+H_{PF}(j\omega)}$ $H_{PF}(j\omega) = \frac{K_{PF}}{1+j\omega\tau_{I_{PF}}}$
OL Transfer Function $(Y_c(j\omega)/E(j\omega))$	$Y_{OL}(j\omega) = K_pK_c(\frac{1+j\omega\tau_L}{(j\omega)^2})\ \mathsf{exp}(-j\omega\tau_e)$	$Y_{OL}(j\omega) = \frac{K_pK_c}{K_{PF}+1}\frac{1+j\omega\tau_{I_{PF}}}{\left(1+j\omega\frac{\tau_{I_{PF}}}{K_{PF}+1}\right)(j\omega)^2}\,\mathsf{exp}(-j\omega\tau_e)$
OL Gain	K_PK_C	$\frac{K_pK_c}{K_{PF}+1}$
OL Lag Time (seconds)	-	$\frac{1}{K_{PF}+1}\tau_{I_{PF}}$
OL Lead Time (seconds)	τ_L	$\tau_{I_{PF}}$
Theoretical Parameter Values		
Visual Feedback gain	$K_p = 1.05$	$K_p = 15.225$
Proprioceptive Feedback gain	-	$K_{PF} = 10$
Equalization Lead	$\tau_L = 3s$	$\tau_{L_{PF}} = 0$
Equalization Lag	$\tau_I = 0$	$\tau_{I_{PF}} = 3s$
Model Effective Time Delay	$\tau_e = 0.4$	$\tau_e = 0.17$
OL Transfer Function	$\frac{3.15(0.333 + j\omega)}{(j\omega)^2}e^{-0.4j\omega}$	$\frac{15.225(0.333 + j\omega)}{(j\omega)^2(3.667 + j\omega)}e^{-0.17j\omega}$

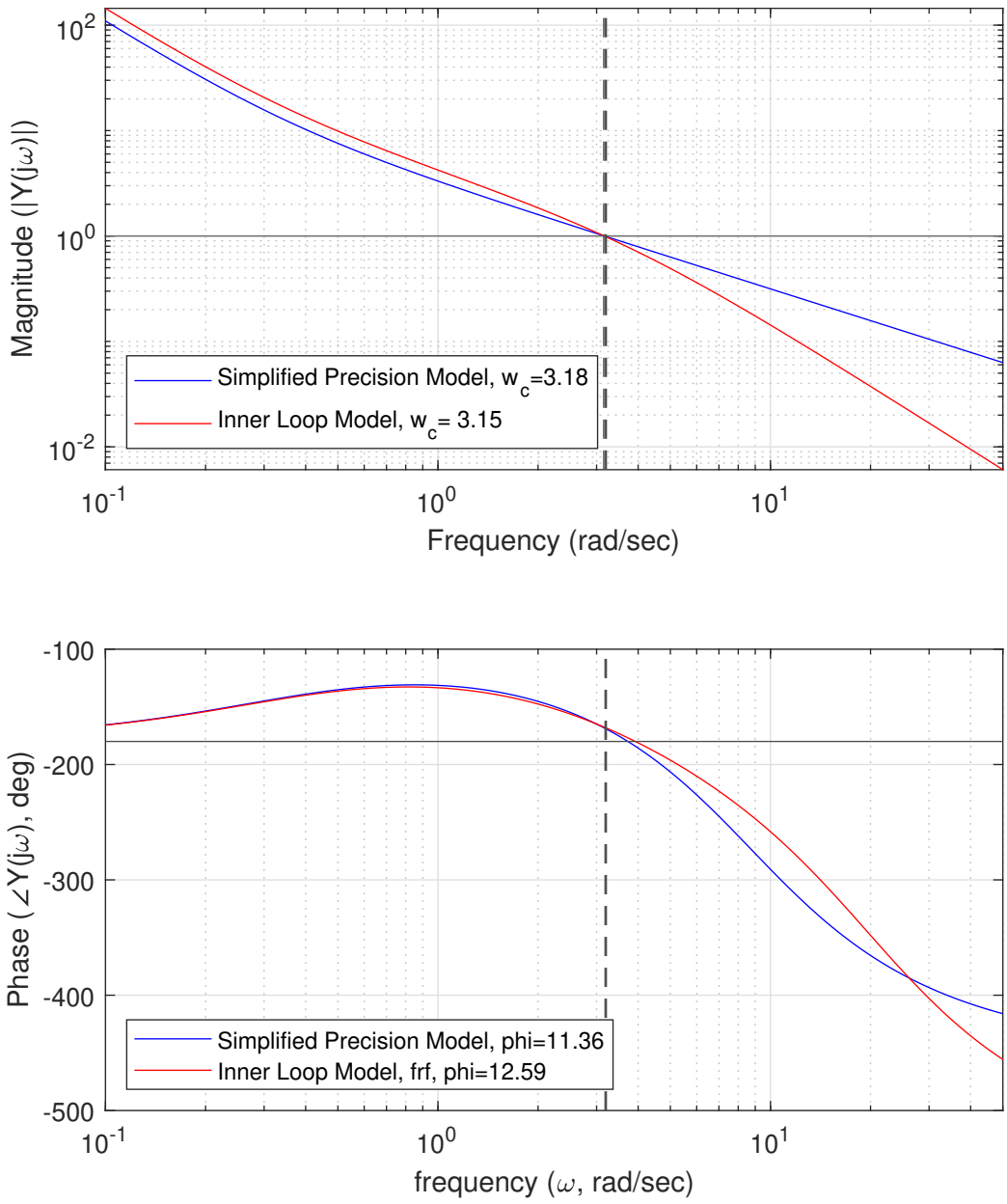

Figure A.5: Open Loop Characteristics (from error e to model output y_c) in a **double integrator control task** as in Table A.3

- If both lead and lag terms are present in the proprioceptive feedback term, a net lag-lead is produced, bounded by human limitations of realistic parameter values.
  - To introduce a net lead in the pilot's response characteristics (for $Y_c = K_c/s^2$), a corresponding lag in the inner loop is necessary. To minimize the resulting phase lag, it would be necessary to have large PF gain as well as no proprioceptive lead.
  - To introduce a net lag in the pilot's response (for $Y_c = K_c/s^2$), a PF lead with a larger time constant is necessary.

It is clear that equalization in the inner loop is mathematically possible to similar effect as the simplified precision model suggests, however with significant limitations, even without the neuromuscular system limitations factoring in.

For proportional control, although inducing an open loop lag is mathematically possible for equalization, it presents a limitation of a greater lag being applied on proprioceptive feedback as compared to what would be necessary on visual feedback.

For double integrator control, inducing an open loop lead term in the pilot's response characteristics will always be limited as **another lag term will be introduced**.

A **mixed equalization** strategy might be possible with a much smaller visual lead making up for this lag (and mathematically canceling out). This would also mean that the visual delay is not reduced to unrealistically low values as the lag in the NMS is countered by a lead acting on visual feedback. The inner loop equalization is not able to produce the effect of pure lead as seen in the simplified precision model, additionally suggesting that purely proprioceptive equalization for a double integrator task is not possible.

This result is also confirmed by the structural model presented by Hess, which compensated for double integrator CE dynamics by **introducing a visual derivative block** (with a non-linear switching behavior rather than a linear addition). This was used by the pilot for equalization, becoming more significant in the case of double integrator control [7]. For an in depth review of the structural model see Chapter 6.

B

Mathematical Analysis with 2nd Order NMS Dynamics

While a purely simplified model is able to establish the possibility of proprioceptive feedback equalization in very ideal conditions, neuromuscular dynamics may create limitations that make it impossible to equalize. To make the system more realistic, a newer simplified model is considered, this time by adding second order NMS dynamics, G_{NMS}. The new model diagrams used for the simplified precision model and the inner loop model respectively can be seen in Figure A.1 and Figure B.4.

$$\text{Case 1: } G_{NMS}(j\omega) = \frac{\omega_n^2}{(j\omega)^2 + (2\zeta_n\omega_n)j\omega + \omega_n^2}; \qquad \omega_n = 10rad/sec; \zeta_n = 0.6; \tag{B.1}$$

$$\text{Case 2: } G_{NMS}(j\omega) = \frac{\omega_n^2}{(1 + j\omega T_{N_1})[(j\omega)^2 + 2\zeta_n\omega_n j\omega + \omega_n^2]}; \qquad T_N = 0.025sec; \tag{B.2}$$

$$\tag{B.3}$$

Additionally, a second case is also considered where an additional lag term is introduced within the NMS. The angular frequency and damping ratio remain the same.

The crossover model, which does not use the 2nd order NMS dynamics and has pure integrator dynamics, is provided for comparison along with the corresponding parameter values. It uses $K_p = \omega_c$, $\tau_e \approx \tau + 2\zeta_n/\omega_n$ and perfect integrator dynamics, corresponding to McRuer's verbal adjustment rules. The goal of the exercise is to check if these crossover dynamics can be matched with the structural model, and how it compares with the precision model. For each case, the parameters in the visual and proprioceptive equalization terms are manually adjusted to obtain the desired crossover dynamics.

The result of the proprioceptive feedback is analyzed through root locus plots and the open loop dynamics (from error e to model output y_c) are plotted along with the precision and crossover model dynamics.

B.1. Proportional Control, $Y_c = K_c$

Case 1: The effective time delay used by the crossover model is $\tau_e = 0.17$, along with a crossover frequency $\omega_c = 5$rad/sec. The parameters used in order to obtain similar crossover dynamics outlined by the verbal adjustment rules, with the precision and the structural models (Figure B.5):

$$\text{Precision Model: } K_p = 2.17,\ \tau = 0.13s; \qquad \text{Equalization: } \tau_I = 0.4s; \tag{B.4}$$

$$\text{Structural Model: } K_p = 7.3,\ \tau = 0.25s; \qquad \text{Equalization: } K_{PF} = 2,\ \tau_{L_{PF}} = 0.6s; \tag{B.5}$$

Case 2: A small lag is introduced in the NMS. The effective time delay for the crossover model the same, and the time delay for the precision model is reduced to $\tau = 0.105sec$ to correct for the change.

For the proprioceptive equalization model however, the delay does not significantly affect the system and all parameters are kept the same, with the resulting FRF plotted in B.5b.

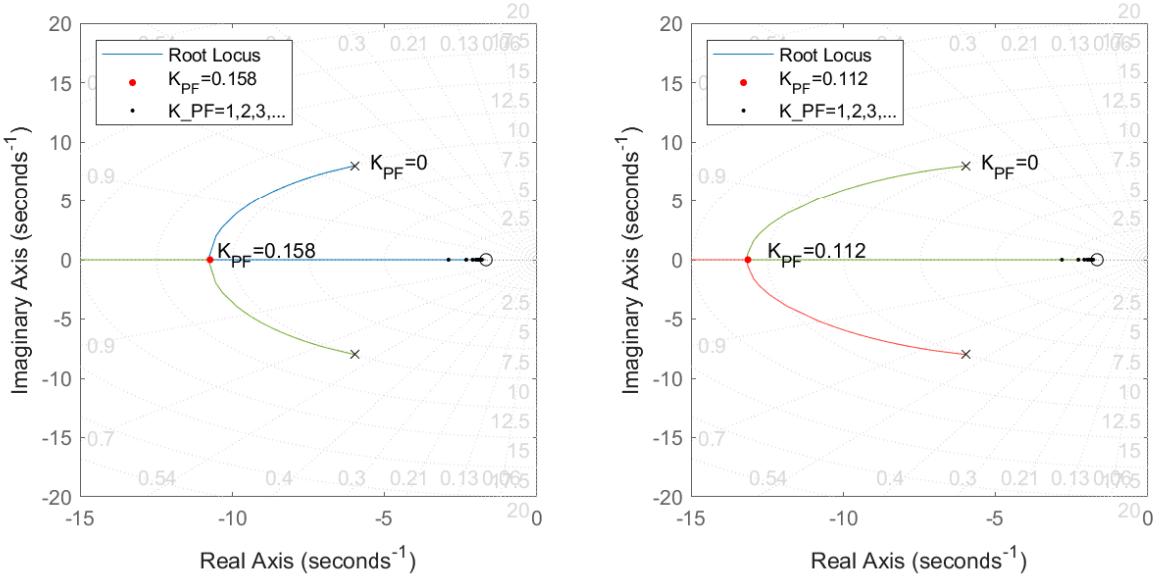

(a) 2nd order NMS with no lag

(b) 2nd order NMS with lag

Figure B.1: Proportional Control Task, effect of closing PF loop on the poles of the **pilot's response characteristics** (response from error e to the pilot's control output u_δ (Figure B.4)

Root Locus plots representing the loop closure of the PF feedback loop are also plotted, with the same PF lead present, $\tau_{L_{PF}} = 0.6s$ (Figure B.1). The FRF for each model, along with the crossover model (no NMS dynamics), is shown in Figure B.5.

B.1.1. Observations

- Inner loop closure with proportional feedback significantly alters the NMS dynamics in the resulting pilot response dynamics.
- A small proprioceptive gain causes the NMS poles to shift significantly in the root locus plot. The effect of the 2nd order dynamics on the response becomes negligible.
- Its effect is also seen in the parameter selection, with the PF equalization model having a much greater visual time delay to achieve the same crossover characteristics since the precision model also has lags introduced due to the NMS dynamics.
- Based on the root locus plots, even a small proprioceptive feedback gain is able to entirely remove the effects of the NMS 2nd order dynamics.
- Introduction of a small lag, T_{N_1}, in the NMS dynamics does not significantly affect the result, with the newly introduced pole also pushed to higher frequencies. This is the opposite of the precision model which is directly affected by the NMS lag term and the visual delay has to be reduced to get the same crossover characteristics.

Although it creates the intended pilot response in the crossover region, the disappearance of visible NMS dynamics makes this control approach physiologically inconsistent. However, rather than discounting proprioceptive feedback as an approach for equalization, this result indicates that the model used might be unrealistic and a better model of the neuromuscular system is necessary. Previous research has already established that spindle lead feedback is present, even if its use for equalization is not expected [27].

B.2. Integrator Control $Y_c = K_c/s$

An identical approach is used for the case of integrator dynamics, however in this case there is no equalization necessary and only the effect of a proprioceptive feedback gain on the neuromuscular dynamics is studied. The crossover model uses $\omega_c \approx 4.64$ rad/sec, and $\tau_e = 0.26s$. To obtain similar characteristics with both models (Figure B.6):

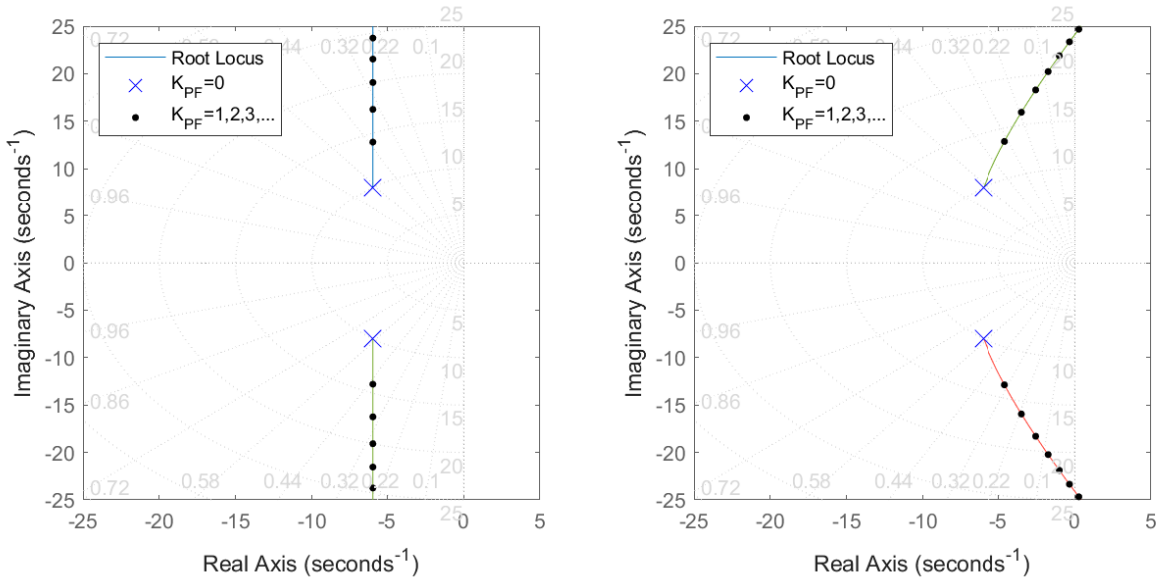

(a) 2nd order NMS with no lag

(b) 2nd order NMS with lag

Figure B.2: Integrator Control, effect of closing PF loop on the poles of the **pilot's response characteristics** (response from error e to the pilot's control output u_δ (Figure B.4)

$$\text{Precision Model: } K_p = 4.45,\ \tau = 0.13s; \tag{B.6}$$

$$\text{Structural Model: } K_p = 13.2,\ \tau = 0.22s; \qquad K_{PF} = 2; \tag{B.7}$$

When a lag in the neuromuscular system of $T_{N_1} = 0.025$ sec is introduced, the delay in the precision model has to be reduced to $\tau = 0.105$ sec in order to maintain the same response characteristics near crossover. Changes in the PF equalization model caused by the NMS lag term are less significant, and the parameter values remain unchanged. The effect of loop closure without and with the presence of the lag term are also presented in the root locus plots in Figure B.2. The FRF for each model, along with the crossover model (no NMS dynamics), is shown in Figure B.6.

B.2.1. Observations

- Loop closure with a pure gain shifts the NMS natural frequency outward, improving open-loop behavior, however this effect is much less significant than in the case of proportional control.
- Damping of the neuromuscular characteristics is slightly reduced, and even more so if a lag is present in the loop.
- The effects of the introduction of the high frequency lag can also be observed in the frequency response functions, with the reduction in damping as well as increase in phase lag. The increase in lag is however still much less than the actual lag term introduced, which had to be compensated through a decrease in the visual time delay in the case of the precision model.
- Proprioceptive feedback gain stabilizes the high frequency control behavior and reduces the effective time delay near the crossover frequency, which has been compensated by a larger visual time delay to maintain the expected crossover dynamics.

The significantly higher visual delay, caused by the PF element significantly increasing the natural frequency of the NMS dynamics, once again suggests that such a model does not work.

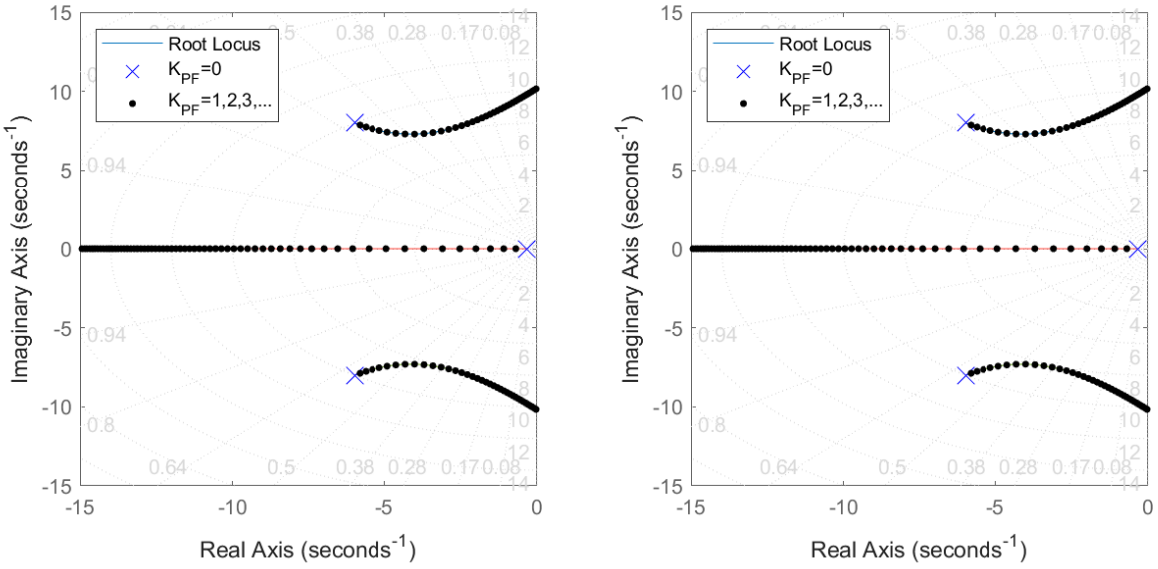

(a) 2nd order NMS with no lag

(b) 2nd order NMS with lag

Figure B.3: Double Integrator Control, effect of closing PF loop on the poles of the **pilot's response characteristics** (response from error e to the pilot's control output u_δ (Figure B.4)

B.3. Double Integrator Control

In the case of double integrator dynamics, a lead in the pilot response (from error e to output y_c) is necessary to compensate for the controlled element dynamics. While a visual lead is used in the precision model, a proprioceptive lag is proposed in the structural model to achieve similar results. The expected crossover characteristics are chosen corresponding with a crossover frequency $\omega_c = 3.2$ rad/sec, along with an effective time delay of $\tau_e = 0.38$ sec.

In the first case when only second order NMS dynamics are introduced with no lag, the parameter values used for both models to achieve crossover characteristics are:

$$\text{Precision Model: } K_p = 1.05,\ \tau = 0.22s; \qquad \text{Equalization: } \tau_L = 3s; \tag{B.8}$$

$$\text{Structural Model: } K_p = 12,\ \tau = 0.08s; \qquad \text{Equalization: } K_{PF} = 10,\ \tau_{I_{PF}} = 3s; \tag{B.9}$$

The value of the proprioceptive gain is once again selected based on Hess' structural model parameters [7], since in order to achieve results as close as possible to crossover dynamics the proprioceptive gain can theoretically be as high as possible, and a proportionally high visual gain to compensate, which is not realistic. Other parameters were adjusted based on the verbal adjustment rules of the crossover model, and the visual delay had to be reduced significantly.

In the second case, when a lag in the NMS is introduced, the time delay in the precision model has to be reduced by the same value to $\tau = 0.195$ sec. In the case of the proprioceptive feedback model as well the visual time delay has to be reduced to $\tau = 0.05$ sec in order to maintain close to expected crossover dynamics.

For both cases, the effect of closing the proprioceptive feedback loop with a lag term is shown in root locus plots in Figure B.3. The FRF for each model, along with the crossover model (no NMS dynamics), is shown in Figure B.7.

B.3.1. Observations

The root locus plot suggests that a similar limitation to what was observed in the case of a simplified model, i.e. an induced lag is present in the pilot's response and limits what an inner loop lead can do for

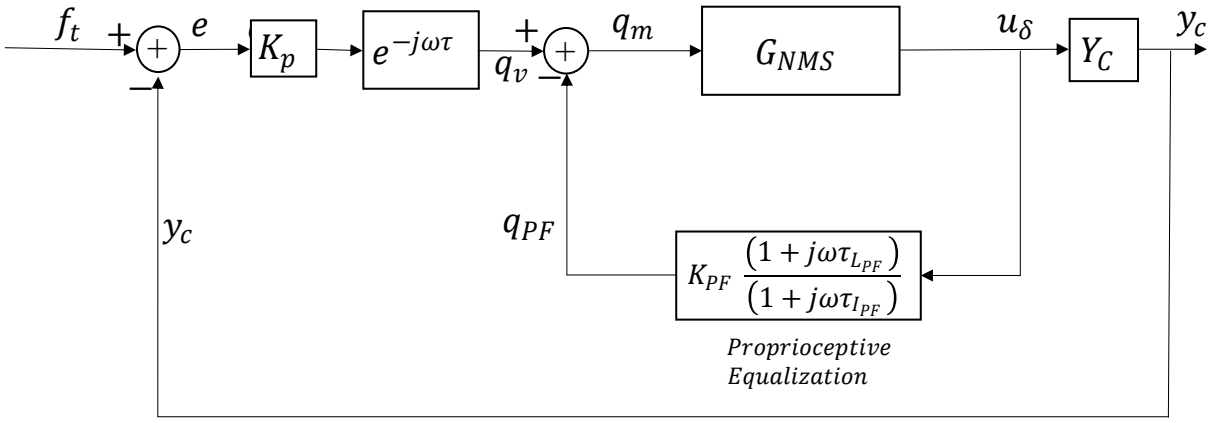

Figure B.4: Simplified inner loop (PF equalization) model with NMS dynamics

equalization, with unrealistically high values of K_{PF} necessary to remove it to any significant degree.

With the addition of second order poles, these are also affected when PF lag is introduced. Loop closure around second-order dynamics with a lag term leads to degraded performance:

- At low gains, a lag term and significant delay are introduced into the open-loop dynamics.
- The second-order poles' natural frequency decreases near the crossover frequency at small gains.
- At higher gains, the natural frequency increases again, but damping becomes very low.

When a delay in the loop is introduced through an NMS lag term, the impact on the proprioceptive feedback equalization is greater than on visual equalization, showing that it makes NMS dynamics even worse and tends towards instability. The visual lead time that is obtained is unrealistically low in both cases, however, suggesting that the system would in fact be unstable and a purely proprioceptive equalization method is not possible if the inner loop is closed around the second order dynamics. Although this does confirm that equalization based on stick displacement feedback in the case of double integrator control is not possible, the same cannot be said about force feedback unless a perfect/isometric manipulator is assumed ($F_c = k_F\delta$, with negligible manipulator mass and damping).

A mixed feedback approach could still be possible, however it might not be the preferred method as it would still make the NMS dynamics worse if the loop is closed around 2nd order dynamics. If a visual lead is also present, it would make the value of the visual delay, τ, become more realistic.

B.4. Conclusions

For proportional control, $Y_c = K_c$, an inner loop lead with such an NMS model being used is unrealistic as it almost completely eliminates the second order dynamics of the NMS. Introducing NMS delay in the form of a lag term does not change this effect significantly.

For double integrator control, $Y_c = K_c/s^2$, an inner loop lag destabilizes the NMS characteristics and might be a poor control strategy for the pilot, even if it helps produce the required lead.

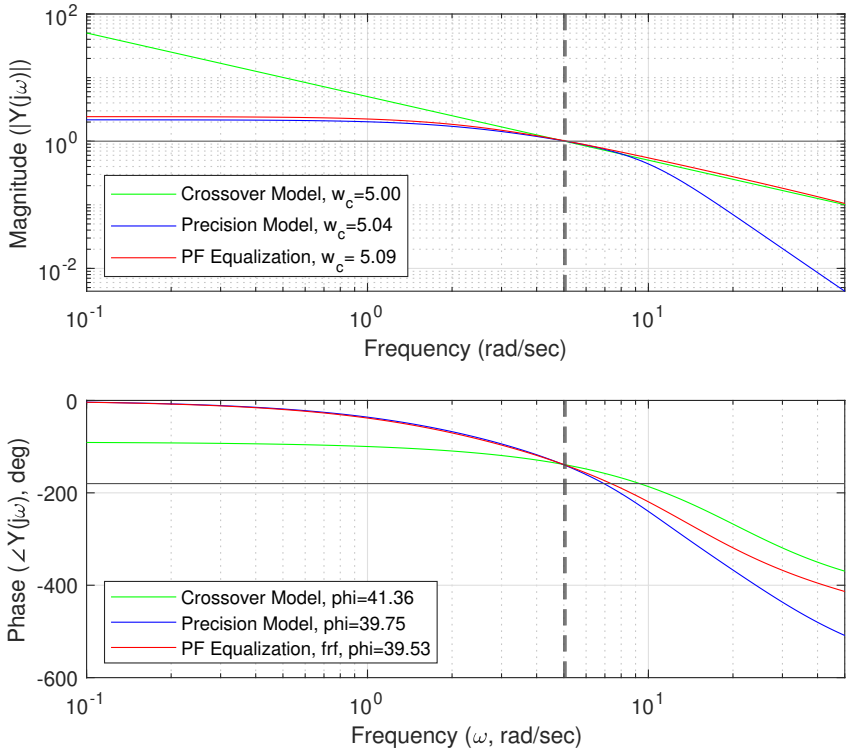

(a) Case 1: NMS 2nd Order dynamics without lag

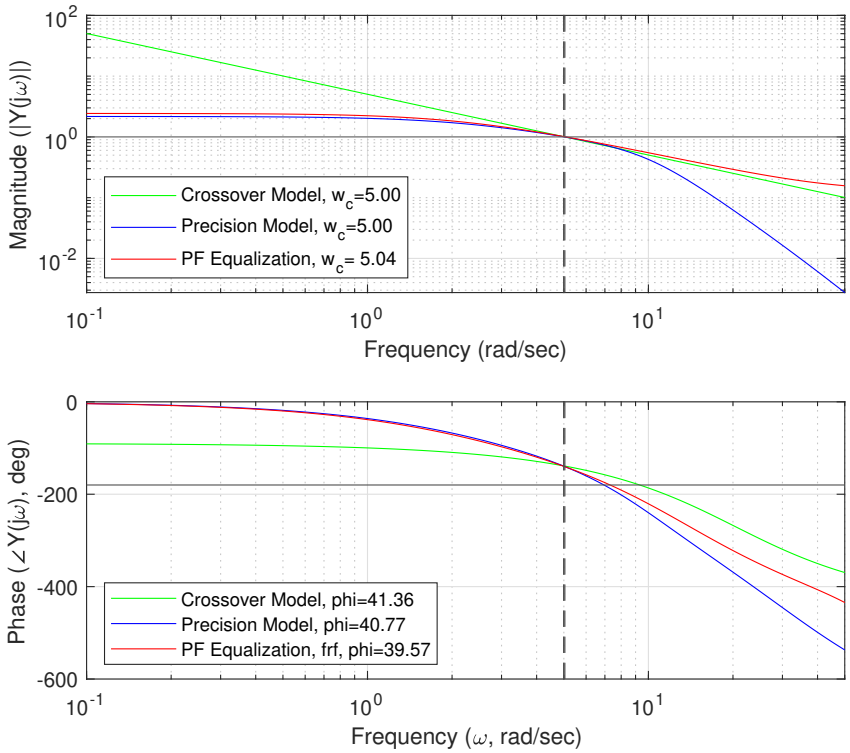

(b) Case 2: NMS 2nd Order dynamics with lag

Figure B.5: FRF from e to y_c showing proportional equalization with different model structures and second order NMS Dynamics

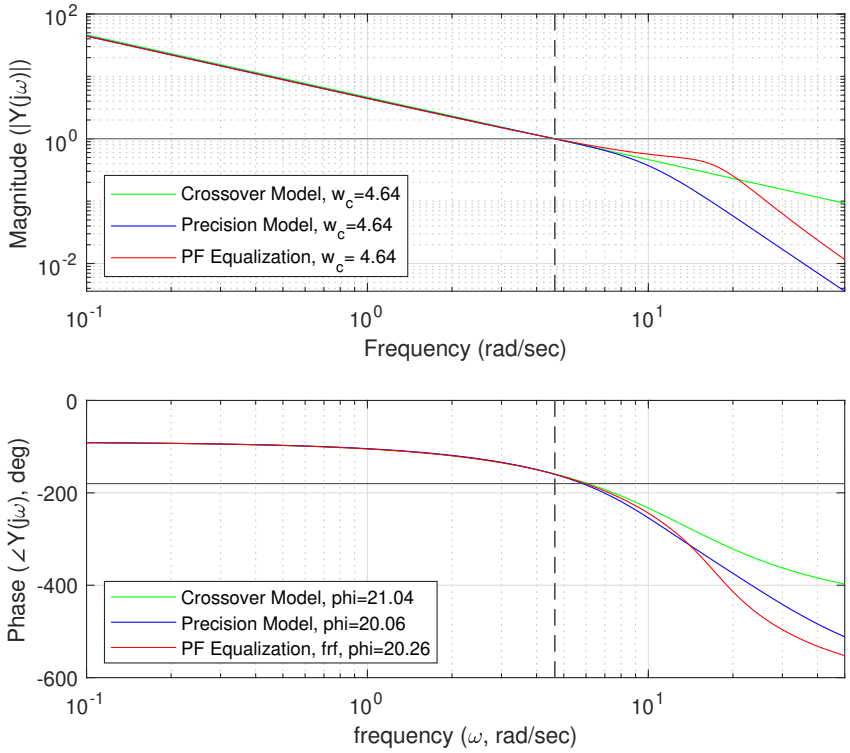

(a) NMS 2nd Order dynamics without lag

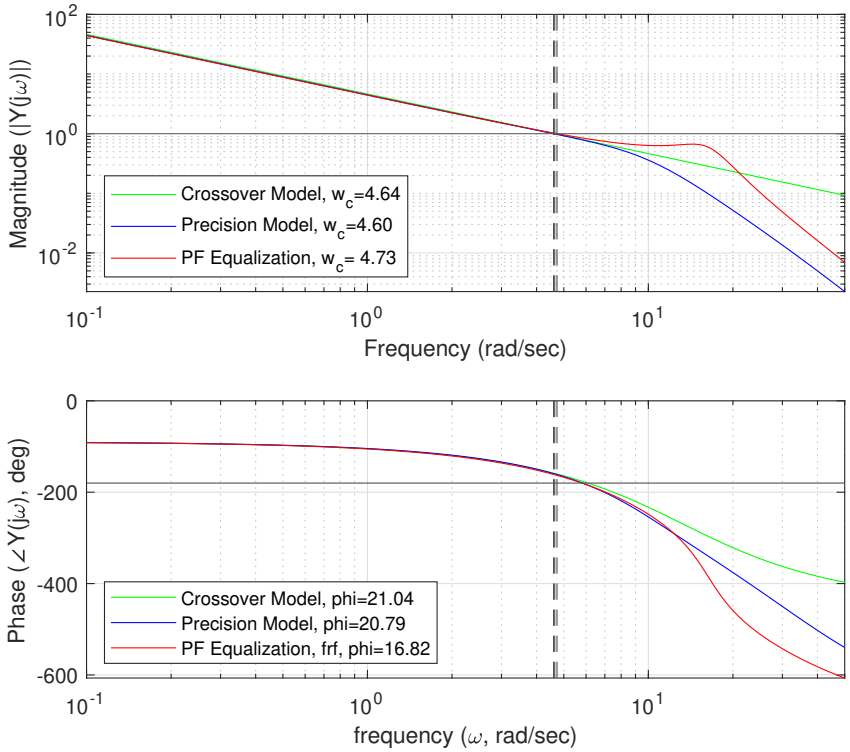

(b) NMS 2nd Order dynamics with lag

Figure B.6: FRF from e to y_c showing integrator equalization with different model structures and second order NMS Dynamics

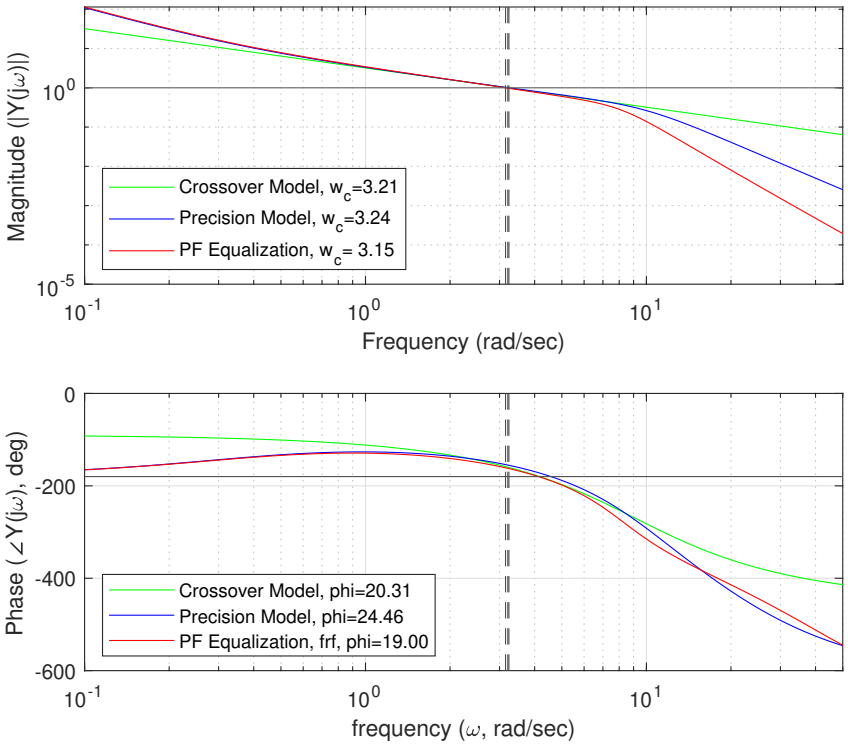

(a) NMS 2nd Order dynamics

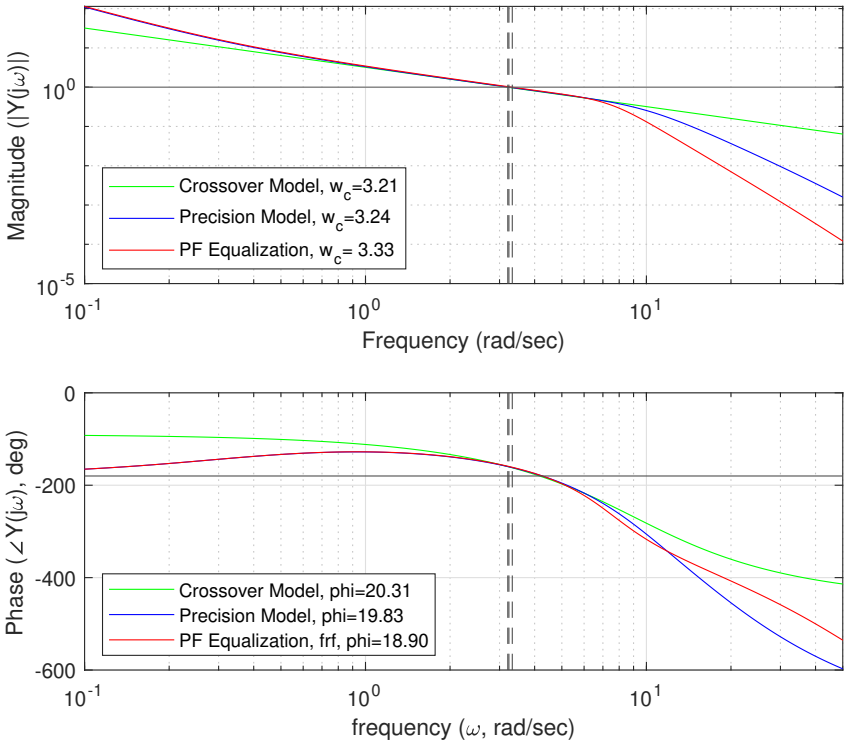

(b) NMS 2nd Order dynamics and Lag

Figure B.7: FRF from e to y_c showing double integrator equalization with different model structures and second order NMS Dynamics

C

Mechanical Model of the Neuromuscular System

C.1. State Space Model

The state-space representation of the neuromuscular system model, as in Fig. 3, is given in standard notation:

$$\dot{x}(t) = Ax(t) + Bu(t) \tag{C.1}$$

$$y(t) = Cx(t) + Du(t) \tag{C.2}$$

The system matrices are defined as:

$$A = \begin{bmatrix} 0 & 1 & 0 & 0 & 0 \\ -(k_F + k_C/R_d)/I_F & -(b_F + b_C/R_d)/I_F & k_C/I_F & b_C/I_F & 0 \\ 0 & 0 & 0 & 1 & 0 \\ (k_C/R_d)/I_L & (b_C/R_d)/I_L & -(k_{SEC} + k_{PEC} + k_C)/I_L & -b_C/I_L & k_{SEC}/I_L \\ 0 & 0 & k_{SEC}/b_m & 0 & -k_{SEC}/b_m \end{bmatrix} \tag{C.3a}$$

$$B = \begin{bmatrix} 0 & 0 & 0 & 0 & \frac{1}{b_m} \end{bmatrix}^T \tag{C.3b}$$

$$C = \begin{bmatrix} 0 & 0 & -k_{SEC} & 0 & k_{SEC} \\ 0 & 0 & 0 & 0 & 1 \\ -(k_C/R_d) & -(b_C/R_d) & k_C & b_C & 0 \\ 1 & 0 & 0 & 0 & 0 \end{bmatrix} \tag{C.3c}$$

$$D = \begin{bmatrix} 0 & 0 & 0 & 0 \end{bmatrix}^T \tag{C.3d}$$

All parameters are as presented in Table II, with R_d=L_{arm}/L_F, which is a correction term to account for different axes of rotation for the limb and the manipulator.

The state vector $x(t)$ is given by:

$$x(t) = \begin{bmatrix} \delta(t) & \dot{\delta}(t) & x_l(t) & \dot{x}_l(t) & x_m(t) \end{bmatrix}^T \tag{C.4}$$

where:

- $\delta(t)$ and $\dot{\delta}(t)$ are the manipulator's angular displacement and velocity
- $x_l(t)$ and $\dot{x}_l(t)$ are the limb/arm's angular displacement and velocity.

- $x_m(t)$ is the angular displacement of the muscle

Note that δ has a different axis of rotation than x_l and x_m.

The only input, $u(t) = q_m(t)$ represents the moment produced by the muscles on the limb in Nm.

The outputs are:

$$y(t) = \begin{bmatrix} F_{gto}(t) & x_m(t) & F_c(t) & \delta(t) \end{bmatrix} \tag{C.5}$$

where:

- $F_{gto}(t)$ is the moment sensed by the GTOs
- $x_m(t)$ is the muscle stretch
- $F_c(t)$ is the contact force in Newtons on the manipulator
- $\delta(t)$ is the angular displacement of the manipulator

The state space model has 5 state variables and 5 eigenvalues.

C.2. Model Dynamics

The same model has been shown in the block diagram Fig. 4, with the blocks defined as:

Muscle Dynamics (from $Q_m(s)$ and $X_l(s)$ to $X_m(s)$)

$$(b_m s + k_{\text{SEC}})X_m(s) - k_{\text{SEC}}X_l(s) = Q_m(s) \tag{C.6}$$

$$G_{\text{muscle}}(s) : X_m(s) = \frac{Q_m(s) + k_{\text{SEC}}X_l(s)}{b_m s + k_{\text{SEC}}} \tag{C.7}$$

Limb Dynamics (from $X_m(s)$ and $F_c(s)$ to $X_l(s)$)

$$(m_L s^2 + k_{\text{SEC}} + k_{\text{PEC}})X_l(s) - k_{\text{SEC}}X_m(s) = F_c(s) \tag{C.8}$$

$$G_{\text{limb}}(s) : X_l(s) = \frac{k_{\text{SEC}}X_m(s) + F_c(s)}{m_L s^2 + k_{\text{SEC}} + k_{\text{PEC}}} \tag{C.9}$$

Grip Dynamics (from $X_l(s)$ and $\Delta(s)$ to $F_c(s)$)

$$G_{\text{grip}}(s) : F_c(s) = (b_c s + k_c)\left(\frac{L_F}{L_{\text{arm}}}\Delta(s) - X_l(s)\right) \tag{C.10}$$

Manipulator Dynamics (from $F_c(s)$ to $\Delta(s)$)

$$F_c(s) = (b_F s + k_F)\Delta(s) \tag{C.11}$$

$$G_{\text{FS}}(s) : \Delta(s) = \frac{F_c(s)}{I_F s^2 + b_F s + k_F} \tag{C.12}$$

For verification of the state space model, this block diagram was also reconstructed in MATLAB using the 'connect' function, to ensure that identical results were obtained.

C.3. Approximate Transfer Functions

For the parameter values shown in Table II (with $k_F = k_1$), the resulting system from q_m to δ written in Transfer function form consists only of two dominant poles and three high frequency poles all on the real

axis (Equation C.13). This can be easily approximated as a system with second order dynamics and a phase lag.

$$\begin{aligned}\frac{\delta(j\omega)}{q_m(j\omega)} &= \frac{1.4421\times10^6(j\omega+42.8)}{(j\omega+419.7)(j\omega+54.02)(j\omega+41.62)((j\omega)^2+9.589j\omega+265.7)}\\ &\approx \frac{0.2461}{(1+0.0216j\omega)\left[\frac{(j\omega)^2}{16.3^2}+2\frac{(0.294)}{16.3}j\omega+1\right]}\end{aligned} \tag{C.13}$$

Other transfer function approximations are also presented for reference.

$$\frac{F_{gto}(j\omega)}{q_m(j\omega)} \approx \frac{\left(\frac{(j\omega)^2}{14.9^2}+2\frac{(0.185)}{14.9}j\omega+1\right)}{(1+0.0216j\omega)\left(\frac{(j\omega)^2}{16.3^2}+2\frac{(0.294)}{16.3}j\omega+1\right)} \tag{C.14}$$

$$\frac{x_m(j\omega)}{q_m(j\omega)} \approx \frac{(0.1029)\left(\frac{(j\omega)^2}{26.1^2}+2\frac{(0.0129)}{26.1}j\omega+1\right)}{(1+0.022j\omega)\left(\frac{(j\omega)^2}{16.3^2}+2\frac{(0.294)}{16.3}j\omega+1\right)} \tag{C.15}$$

$$\frac{F_c(j\omega)}{q_m(j\omega)} \approx \frac{(0.3642)\left(\frac{(j\omega)^2}{15.1^2}+2\frac{(0.0510)}{15.1}j\omega+1\right)}{(1+0.0216j\omega)\left(\frac{(j\omega)^2}{16.3^2}+2\frac{(0.294)}{16.3}j\omega+1\right)} \tag{C.16}$$

$$G_{FS}(j\omega) = \frac{\delta(j\omega)}{F_c(j\omega)} \approx \frac{0.6757}{\left(\frac{(j\omega)^2}{15.1^2}+2\frac{(0.0510)}{15.1}j\omega+1\right)} \tag{C.17}$$

$$\tag{C.18}$$

These same dominant poles have been shown in Fig. 6 of the Technical Report. These approximations indicate that approximations for considering proprioceptive feedback are possible, however the 2nd order zeros must also be considered. This means that the generalized model presented by Bachelder [11] (Section 7.3) is flawed for the same reason. A more appropriate approximation, if considering F_c feedback, would use Equation C.19. To use such a mathematical model, the feel system/manipulator characteristics would have to be known for a given control task, and the neuromuscular system has three unknown parameters (same as the precision model) ω_n, ζ_n and T_N.

$$G_{NMS}(j\omega) = \frac{F_c(j\omega)}{q_m(j\omega)} = \frac{\omega_n^2}{(1+j\omega T_{N_1})\left((j\omega)^2+2\zeta_n\omega_n\ j\omega+1\right)}\frac{1}{G_{FS}(j\omega)} \tag{C.19}$$

D

Proprioceptive Feedback Analysis

A complete set of plots covering the results in Section VI are presented here. Proportional and Double Integrator Equalization is considered, with an inner loop (PF) lead assumed for the former, and a lag for the latter. Three different manipulator characteristics are also considered, with the assumption that stiffer manipulators would provide greater force feedback information to the pilot. The three different manipulators considered, $k_F = k_1, 5k_1, 25k_1$, are the same as used by Magdaleno [13]. $k_F = k_1$ corresponds with a manipulator natural frequency ($\sqrt{k_F/I_F}$) of 15 rad/sec.

This inner loop closure incorporates a neuromuscular activation lag of 0.01 second (in the block G_{act}) and a proprioceptive compensation delay of 0.025 seconds.

$$G_{act}(j\omega) = K_{act}/(1 + j\omega T_{act}); K_{act} = 0.3\ Nm, T_{act} = 0.01\ s \tag{D.1}$$

$$H_{gto} = K_{gto}\ \frac{1 + j\omega T_{L_{gto}}}{1 + j\omega T_{I_{gto}}} e^{-j\omega\ \tau_d}; \tau_d = 0.025\ s \tag{D.2}$$

$$H_{ms} = K_{ms}\ \frac{1 + j\omega T_{L_{ms}}}{1 + j\omega T_{L_{ms}}} e^{-j\omega\ \tau_d}; \tau_d = 0.025\ s \tag{D.3}$$

Integral control with proprioceptive/visual gain only is included in the same plots when the corresponding lead/lag time constant is zero.

For all root locus plots: Thicker markers correspond to unit increase in K_{gto} or K_{ms}. The plots on the right show the dominant NMS poles (zoomed in). Only stable configurations are shown, the abrupt cutoff thus shows when any pole moves into the right half plane, and is thus not possible.

For all FRF plots: Only phase plots for stable configurations are visible. An approximate crossover frequency of 5 rad/sec for proportional control and 3 rad/sec for double integrator control were also included in the plots.

D.1. Proportional Control Task: PF lead compensation

Figure D.1 shows root locus plots corresponding to the inner loop closure, tracing the locus of poles of the transfer function from q_v to δ when a GTO or MS lead is introduced. Figure D.2 and Figure D.3 show the same plots for stiffer manipulator configurations.

Figures D.7, D.8, and D.9 show the frequency response functions from q_v to δ when a GTO lead is introduced, with different lead time constant values, $T_{L_{gto}}$.

Figures D.10, D.11, and D.12 show the frequency response function from q_v to δ when a MS lead is introduced, with different lead time constant values, $T_{L_{ms}}$.

D.1.1. Observations

The root locus plots for GTO lead show that the immediate effect of introducing the lead is a reduction in damping and the dominant NMS poles becoming unstable.

Introduction of a lead through MS feedback appears to increase the natural frequency of the NMS dynamics, however also reducing the damping of the dominant poles slightly. Overall, however, the Bode

plots suggest that the effect of a smaller lead time has a positive effect on phase lags by pushing the NMS response to higher frequencies, however for larger lead times the system becomes unstable, with non-dominant poles moving into the right half plane.

This suggests that MS feedback lead is beneficial for suppressing NMS dynamics slightly, however cannot be used for equalization.

D.2. Double Integrator Control Task: PF lag compensation

Figure D.4 shows root locus plots corresponding to the inner loop closure, tracing the locus of poles of the transfer function from q_v to δ when a GTO or MS lag is introduced. Figure D.5 and Figure D.6 show the same plots for stiffer manipulator configurations.

Figures D.13, D.14, and D.15 show the frequency response functions from q_v to δ when a GTO lag is introduced, with different lag time constant values, $T_{I_{gto}}$.

Figures D.16, D.17, and D.18 show the frequency response function from q_v to δ when a MS lag is introduced, with different lag time constant values, $T_{I_{ms}}$.

D.2.1. Observations

Based on root locus plots, an introduction of a GTO lag stabilizes the neuromuscular dynamics by increasing damping for smaller values of PF gain. However further increase leads to damping reducing once again. With a pure gain however, the damping consistently decreases. This also has the effect of reducing phase lag as K_{gto} is increased.

A lag on GTO force feedback is thus able to produce the necessary lead in the pilot's response characteristics, while also reducing phase lag. Beyond a certain gain however, the dynamics become worse again, reducing the damping.

A small lag through MS feedback, however, appears to reduce the damping of the NMS dominant poles, which is also shown in the root locus plots with the dominant poles moving to the right. In the region of crossover, the change in slope is much less pronounced when compared with the GTO feedback. This suggests that a lag on the muscle stretch is not a significant contributor towards equalization, however may be beneficial for smaller adjustments in the region of crossover such as adapting to changing manipulator characteristics. This is in line with observations made by Magdaleno, that with sufficient position feedback availability, changes in the manipulator characteristics have a less significant effect on the pilot's response [13].

D.3. Integrator Control Task

Even with an integrator control task when no equalization is necessary, a small lead on MS feedback can result in better suppression of NMS dynamics and better crossover characteristics. Based on the frequency response plots, increasing GTO gain can reduce phase lag in the region of crossover, however also slightly reducing the damping of the NMS poles.

Based on root locus plots, a pure gain causes NMS 2nd order characteristics to become more unstable without improving crossover characteristics. A negative gain appears to be able to induce a lead in the pilot's response characteristics, however at the expense of greater phase lag as well as much worse and potentially unstable NMS characteristics.

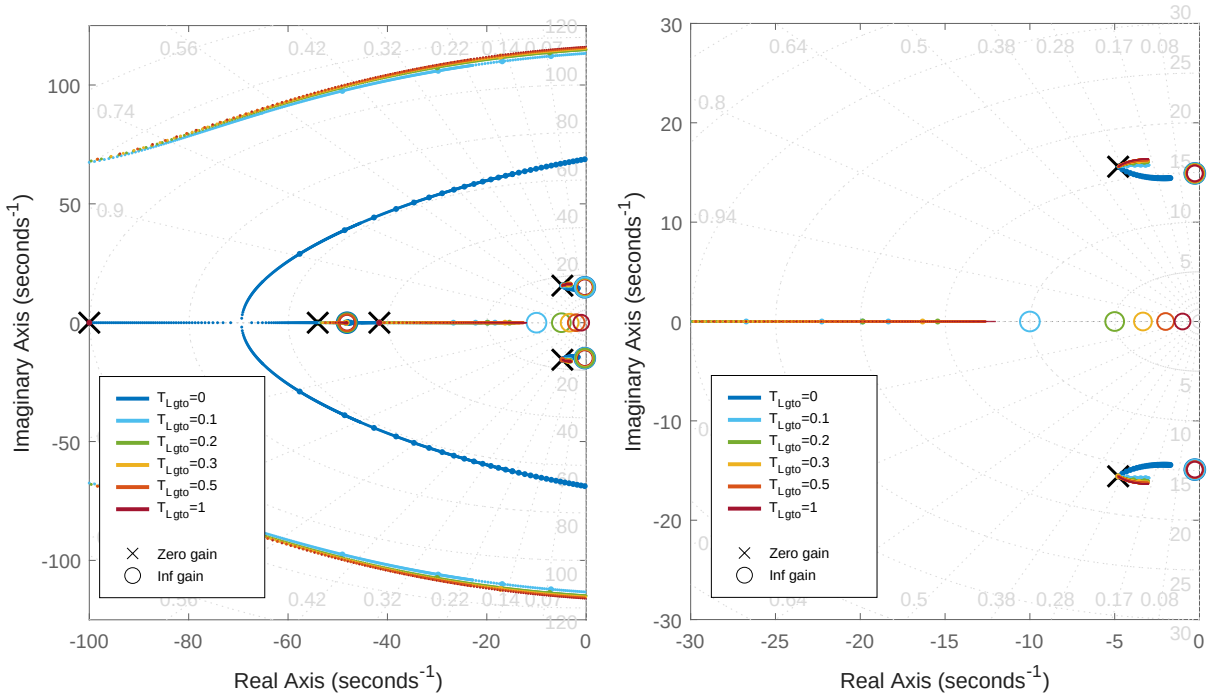

(a) GTO Lead, $k_F/k_1 = 1$

(b) GTO Lead, $k_F/k_1 = 1$, Dominant Poles (zoomed in)

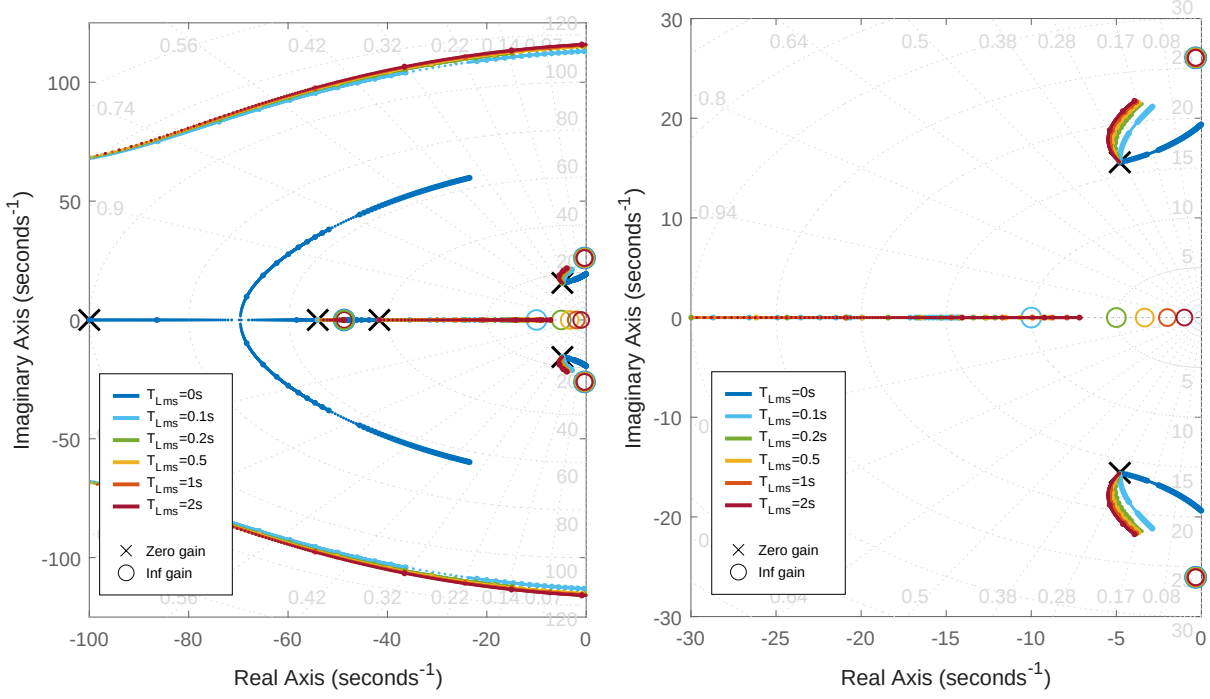

(c) MS Lead, $k_F/k_1 = 1$

(d) MS Lead, $k_F/k_1 = 1$, Dominant Poles (zoomed in)

Figure D.1: Root Locus for PF inner loop closure, showing poles of the response from q_v to δ, when GTO or MS based lead is introduced (for $Y_c(s) = K_c$ CE dynamics), $k_F = k_1$

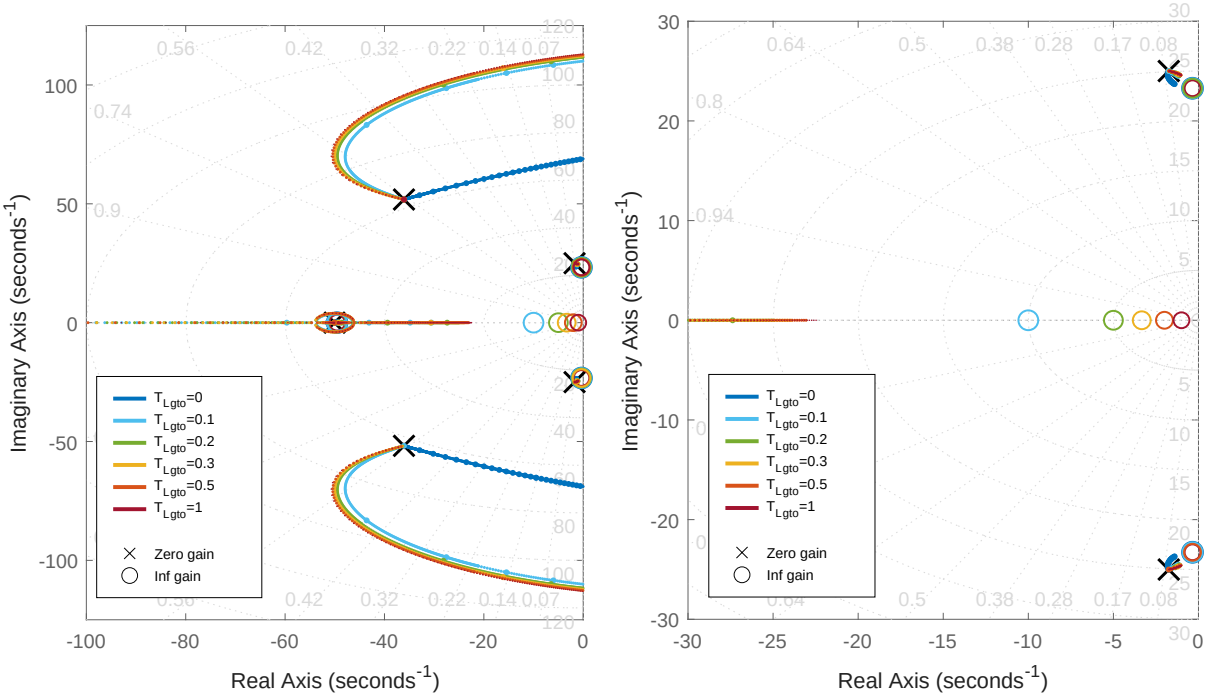

(a) GTO Lead, $k_F/k_1 = 5$

(b) GTO Lead, $k_F/k_1 = 5$, Dominant Poles (zoomed in)

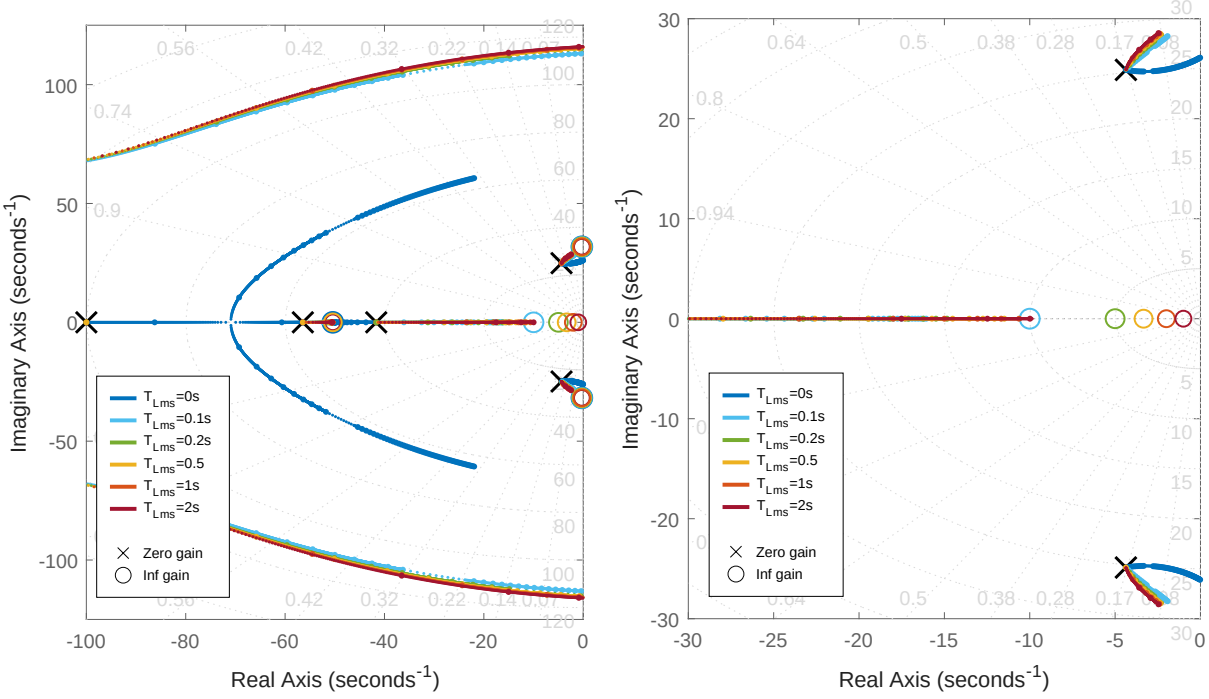

(c) MS Lead, $k_F/k_1 = 5$

(d) MS Lead, $k_F/k_1 = 5$, Dominant Poles (zoomed in)

Figure D.2: Root Locus for PF inner loop closure, showing poles of the response from q_v to δ, when GTO or MS based lead is introduced (for $Y_c(s) = K_c$ CE dynamics), $k_F = 5k_1$

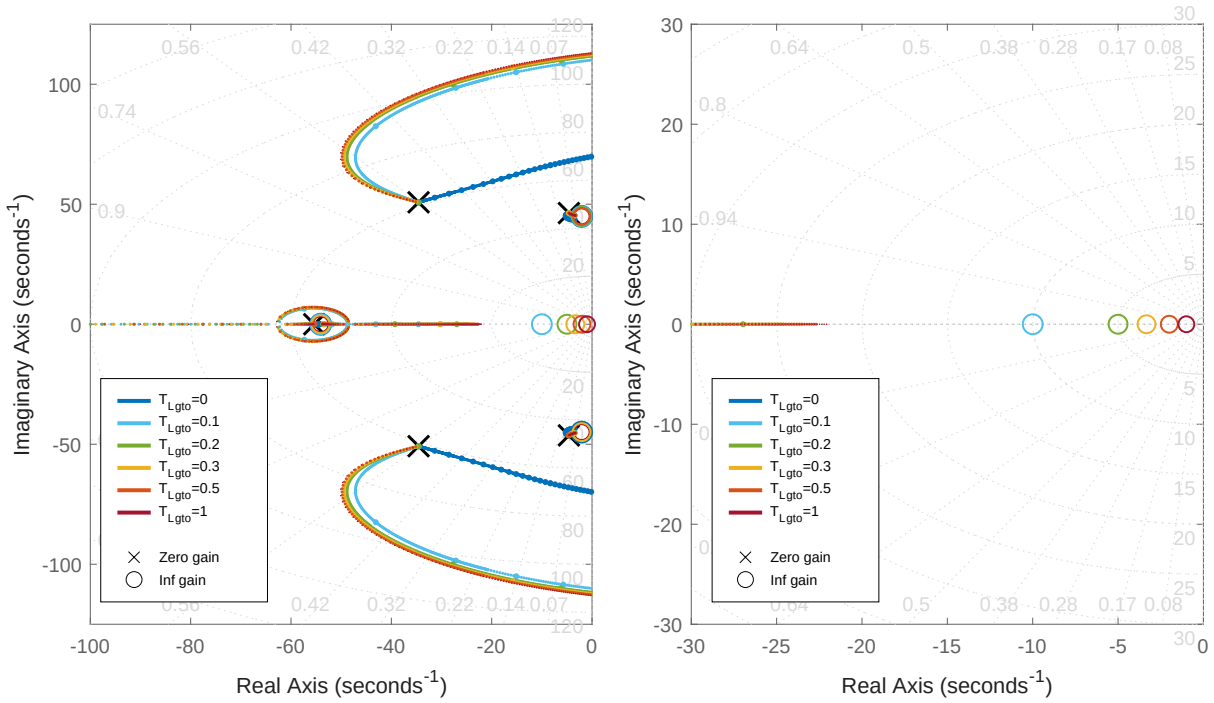

(a) GTO Lead, $k_F/k_1 = 25$

(b) GTO Lead, $k_F/k_1 = 25$, Dominant Poles (zoomed in)

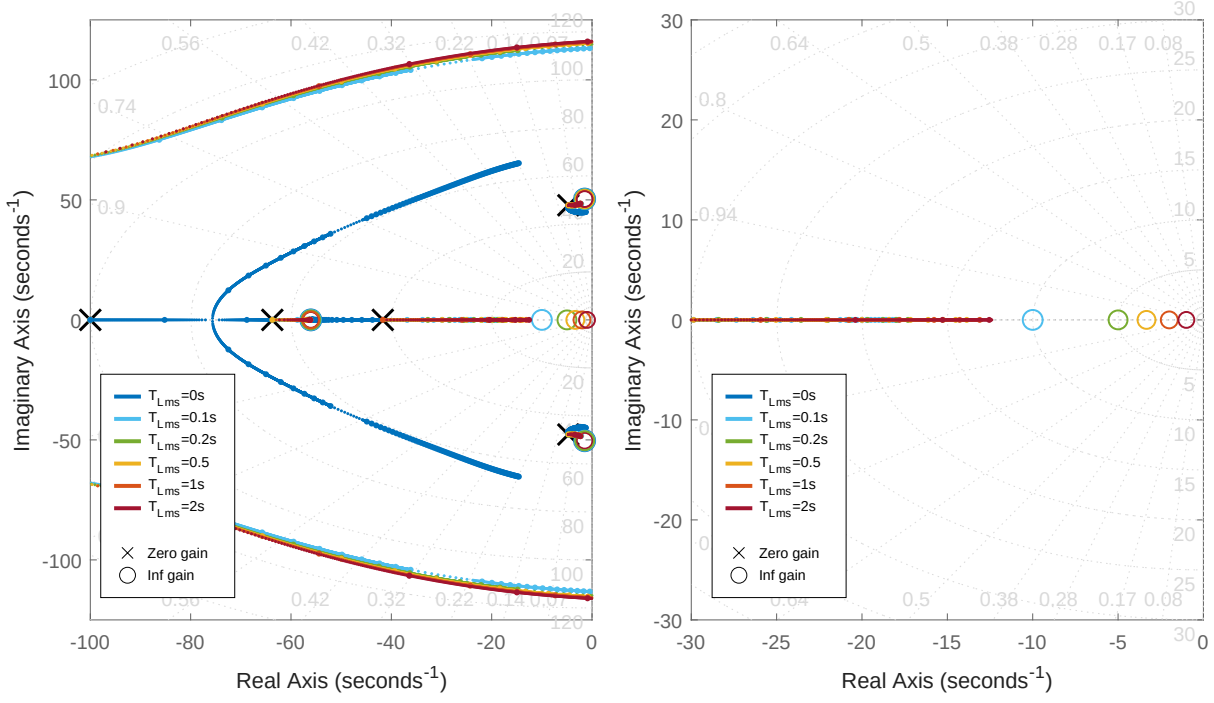

(c) MS Lead, $k_F/k_1 = 25$

(d) MS Lead, $k_F/k_1 = 25$, Dominant Poles (zoomed in)

Figure D.3: Root Locus for PF inner loop closure, showing poles of the response from q_v to δ, when GTO or MS based lead is introduced (for $Y_c(s) = K_c$ CE dynamics), $k_F = 25k_1$

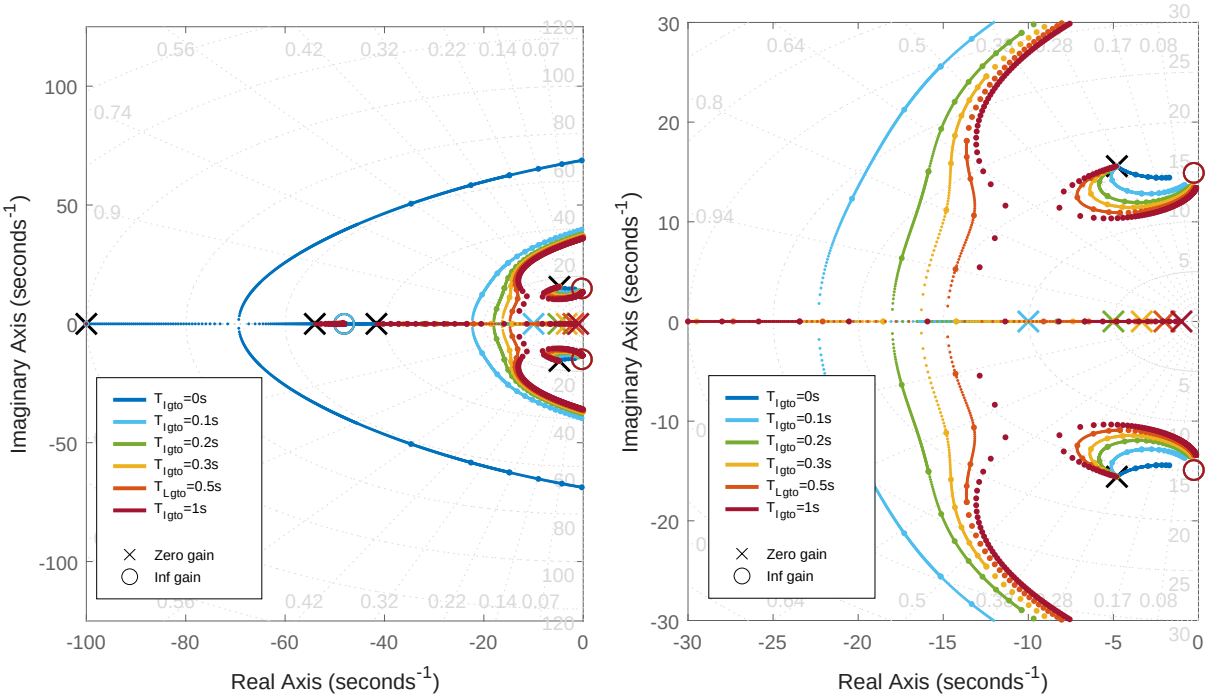

(a) GTO Lag, $k_F/k_1 = 1$

(b) GTO Lag, $k_F/k_1 = 1$, Dominant Poles (zoomed in)

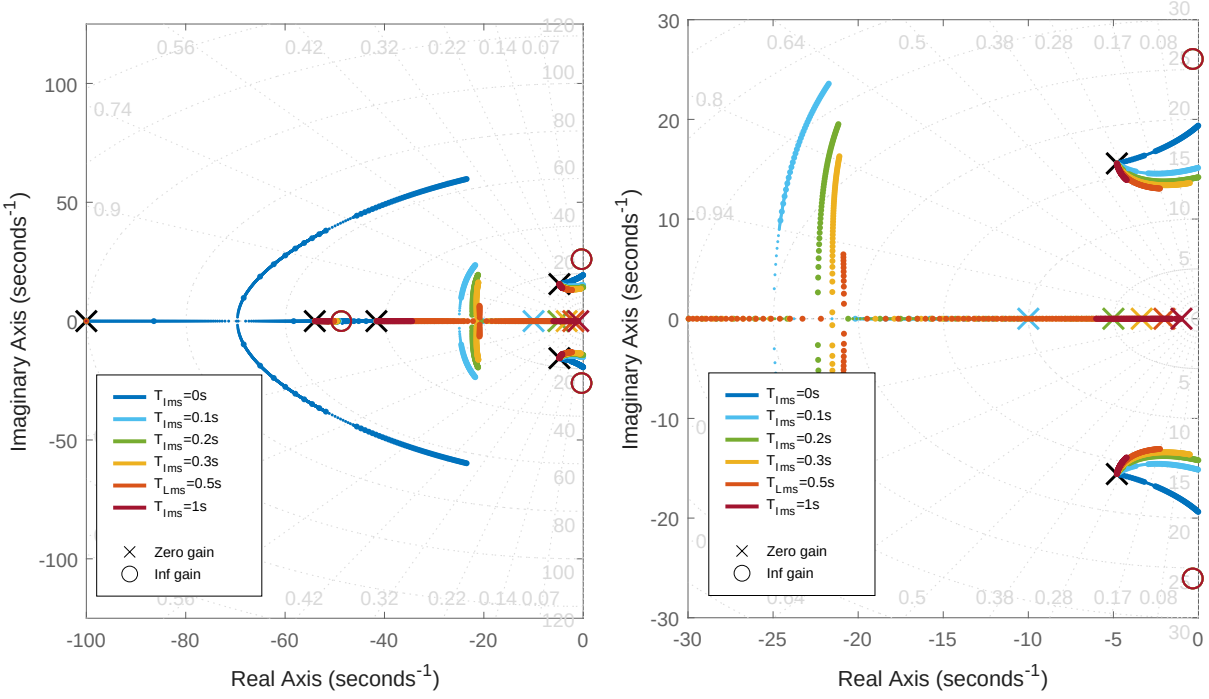

(c) MS Lag, $k_F/k_1 = 1$

(d) MS Lag, $k_F/k_1 = 1$, Dominant Poles (zoomed in)

Figure D.4: Root Locus for PF inner loop closure, showing poles of the response from q_v to δ, when GTO or MS based lag is introduced (for $Y_c(s) = K_c/s^2$ CE dynamics), $k_F = k_1$

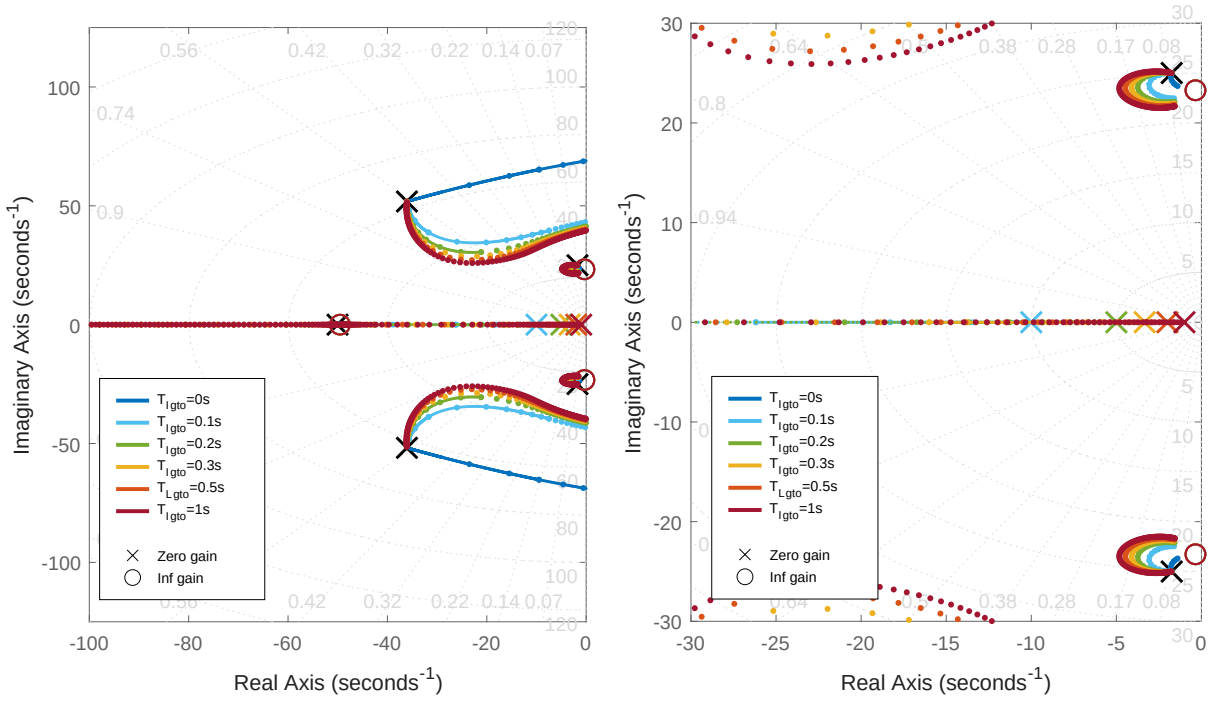

(a) GTO Lag, $k_F/k_1 = 5$

(b) GTO Lag, $k_F/k_1 = 5$, Dominant Poles (zoomed in)

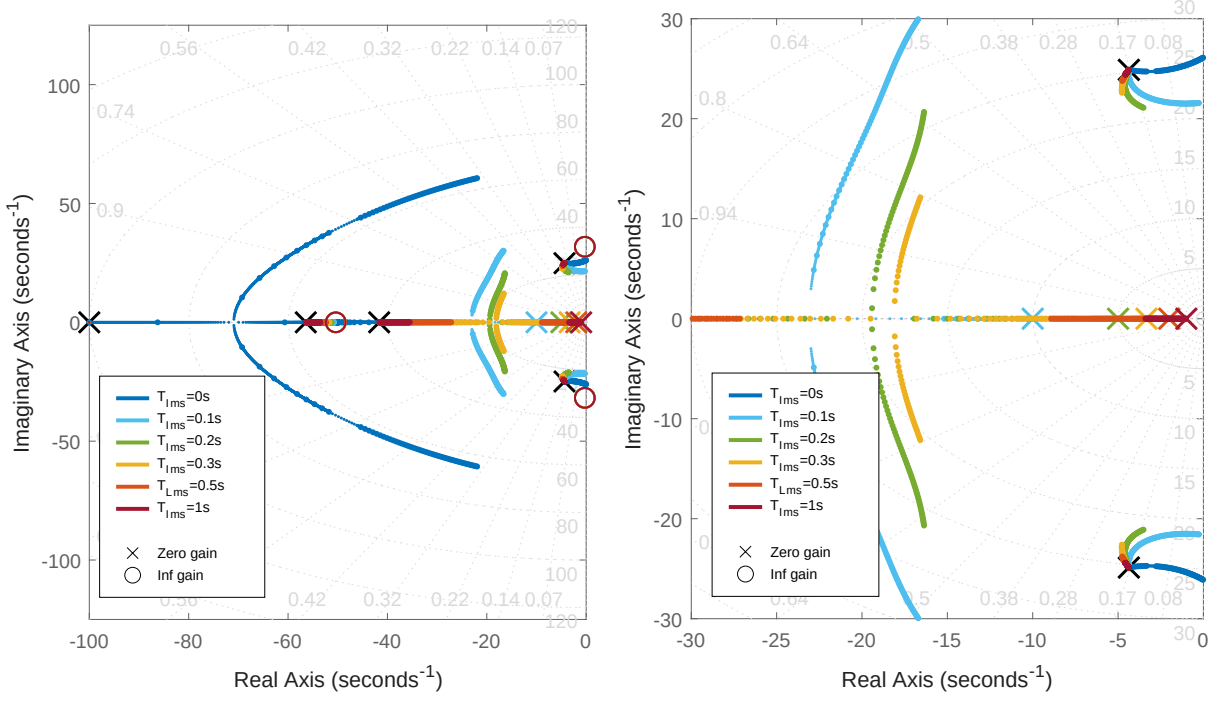

(c) MS Lag, $k_F/k_1 = 5$

(d) MS Lag, $k_F/k_1 = 5$, Dominant Poles (zoomed in)

Figure D.5: Root Locus for PF inner loop closure, showing poles of the response from q_v to δ, when GTO or MS based lag is introduced (for $Y_c(s) = K_c/s^2$ CE dynamics), $k_F = 5k_1$

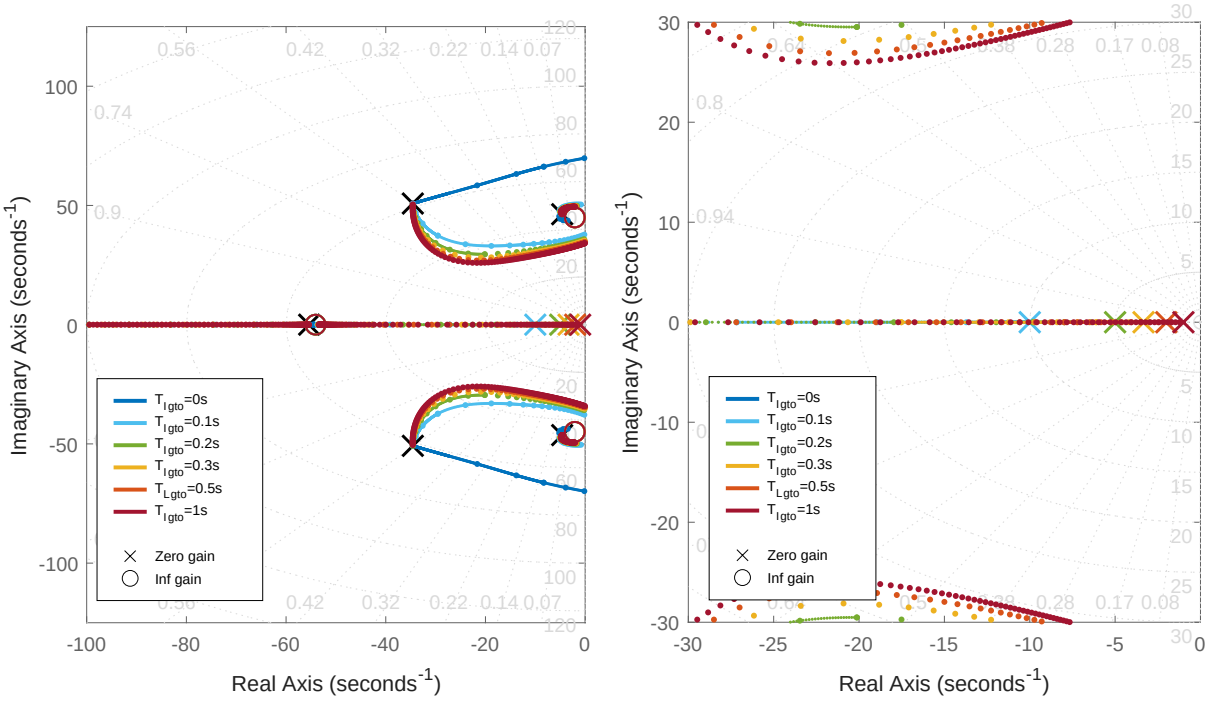

(a) GTO Lag, $k_F/k_1 = 25$

(b) GTO Lag, $k_F/k_1 = 25$, Dominant Poles (zoomed in)

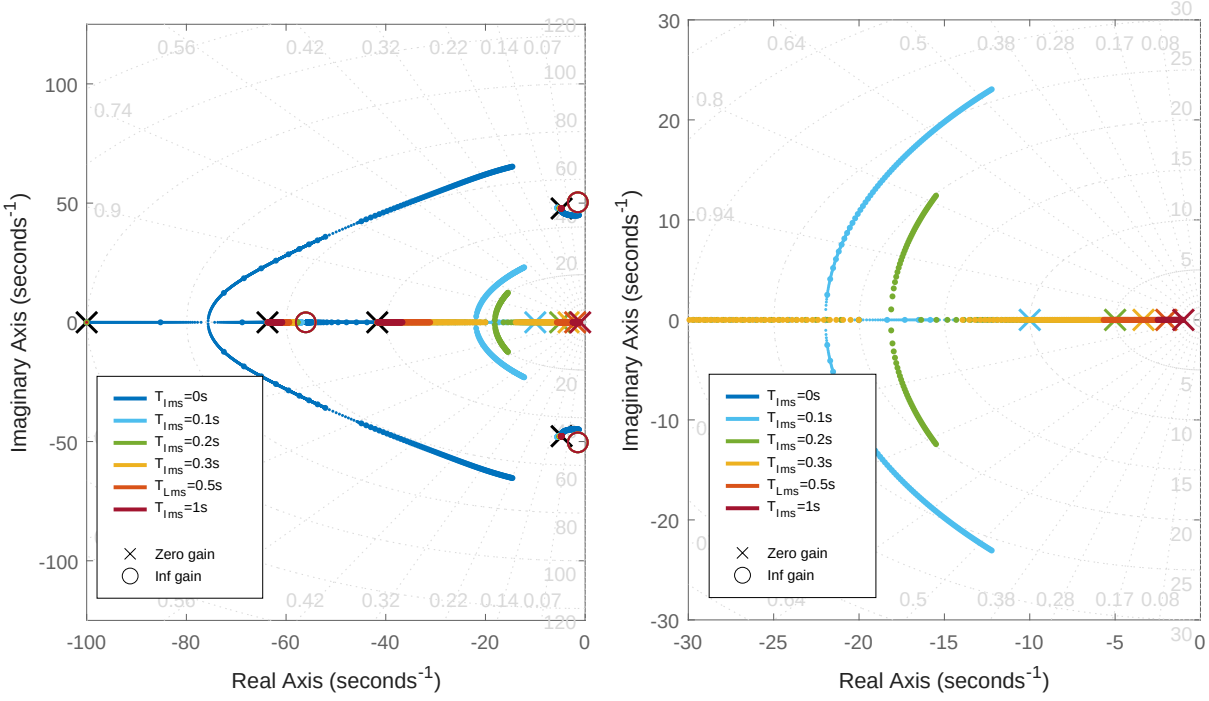

(c) MS Lag, $k_F/k_1 = 25$

(d) MS Lag, $k_F/k_1 = 25$, Dominant Poles (zoomed in)

Figure D.6: Root Locus for PF inner loop closure, showing poles of the response from q_v to δ, when GTO or MS based lag is introduced (for $Y_c(s) = K_c/s^2$ CE dynamics), $k_F = 25k_1$

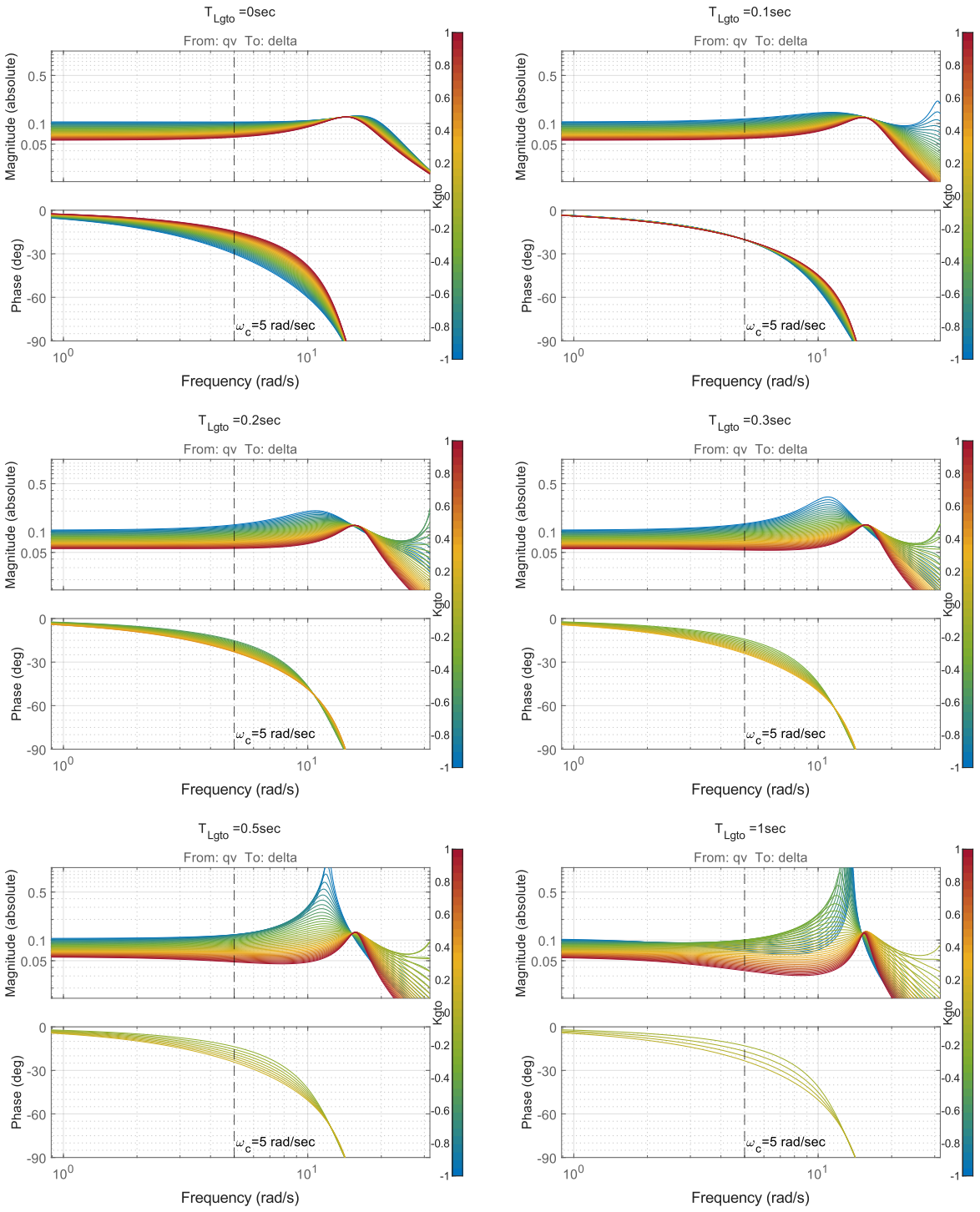

Figure D.7: FRF from q_v to δ, showing the effect of inner loop closure with a GTO lead ($Y_c(s) = K_c$ CE dynamics), $k_F = k_1$

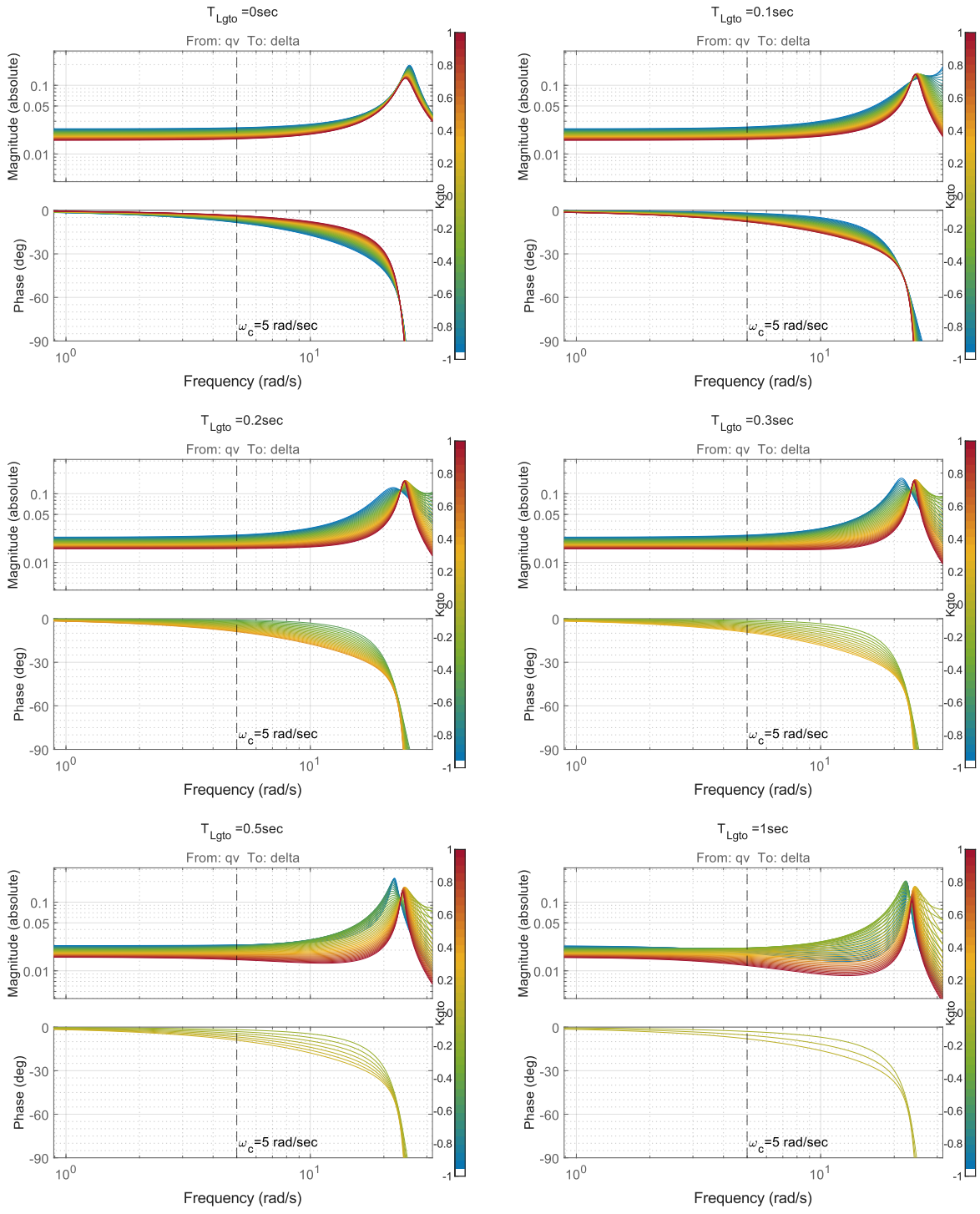

Figure D.8: FRF from q_v to δ, showing the effect of inner loop closure with a GTO lead ($Y_c(s) = K_c$ CE dynamics), $k_F = 5k_1$

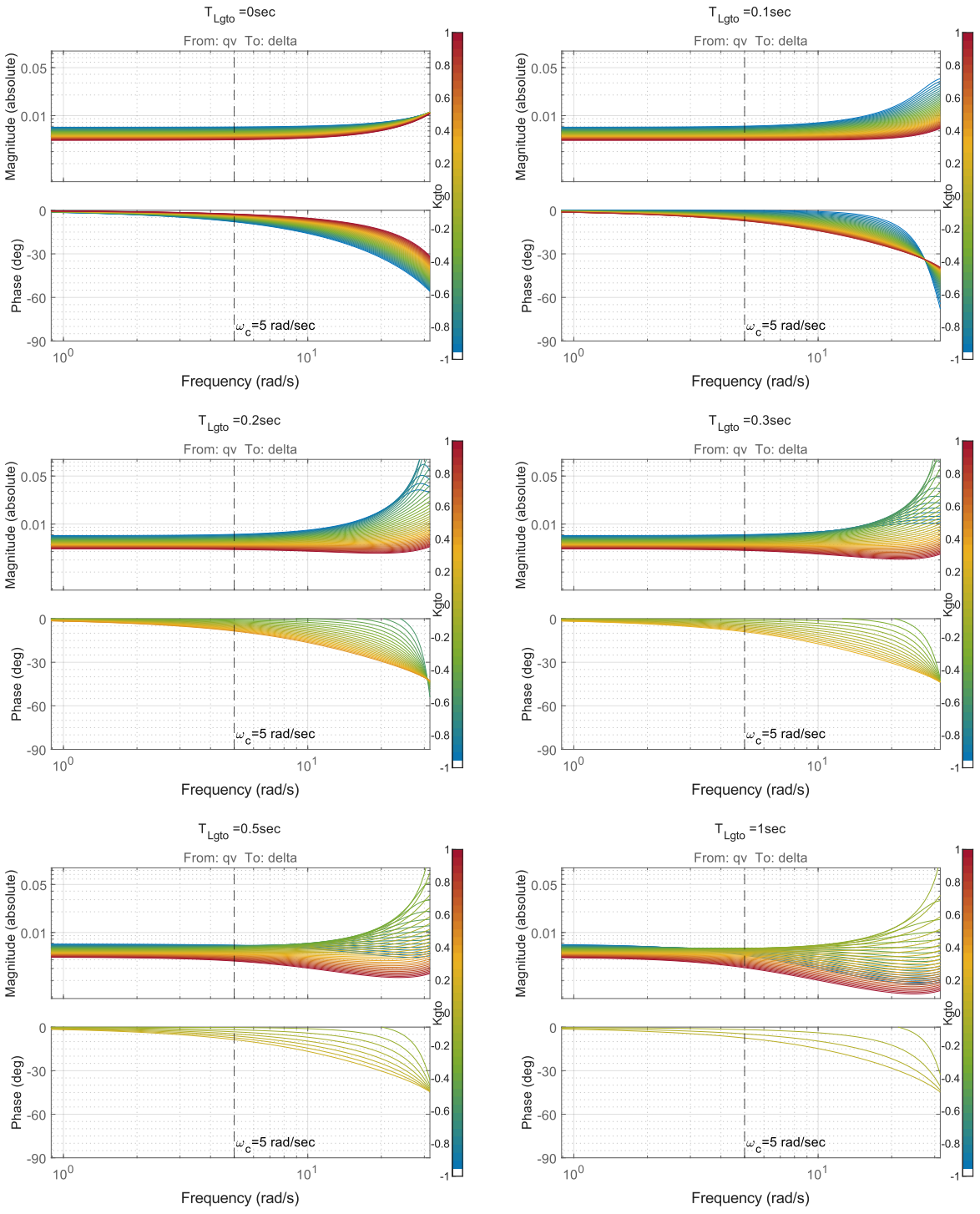

Figure D.9: FRF from q_v to δ, showing the effect of inner loop closure with a GTO lead ($Y_c(s) = K_c$ CE dynamics), $k_F = 25k_1$

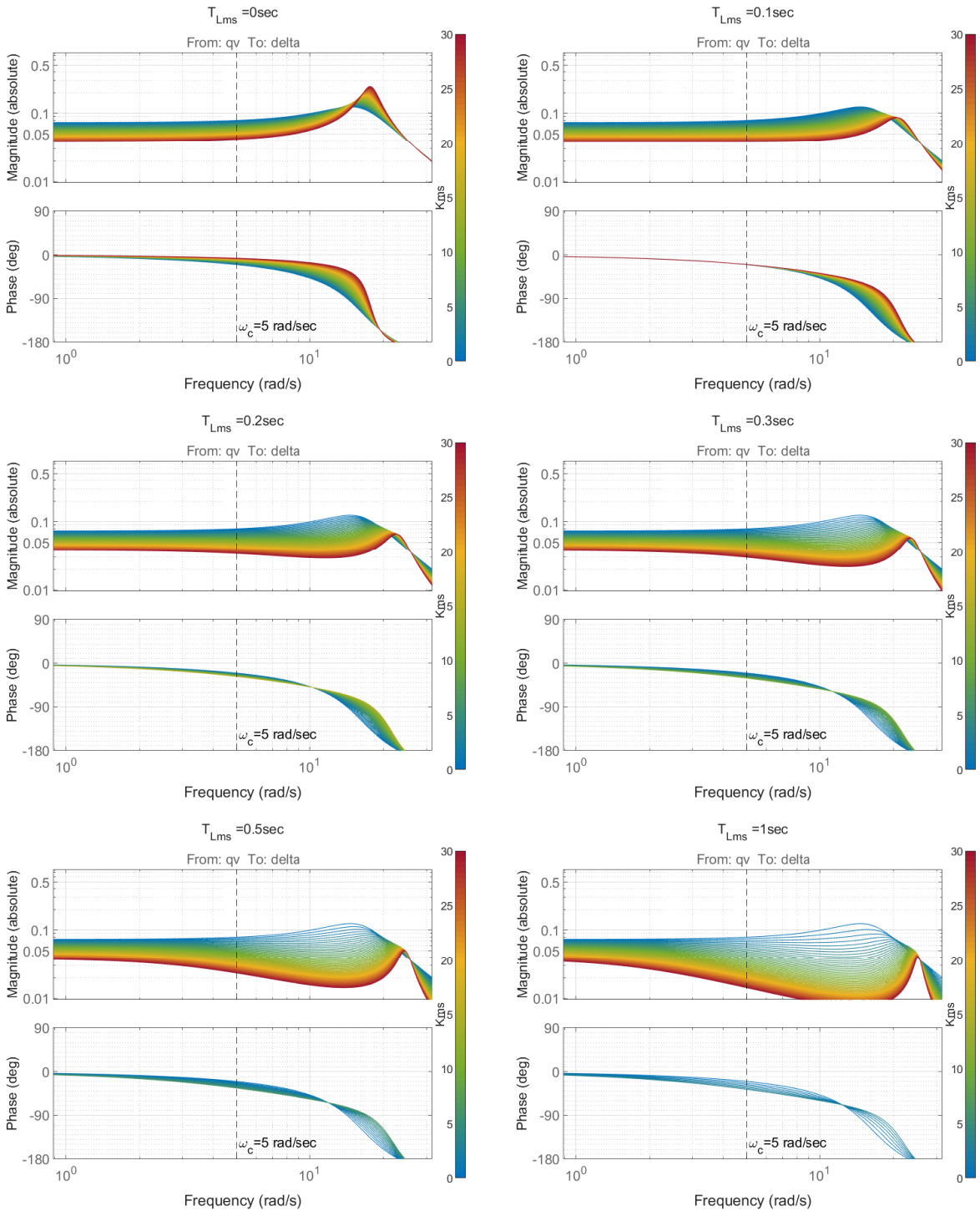

Figure D.10: FRF from q_v to δ, showing the effect of inner loop closure with a MS lead ($Y_c(s) = K_c$ CE dynamics), $k_F = k_1$

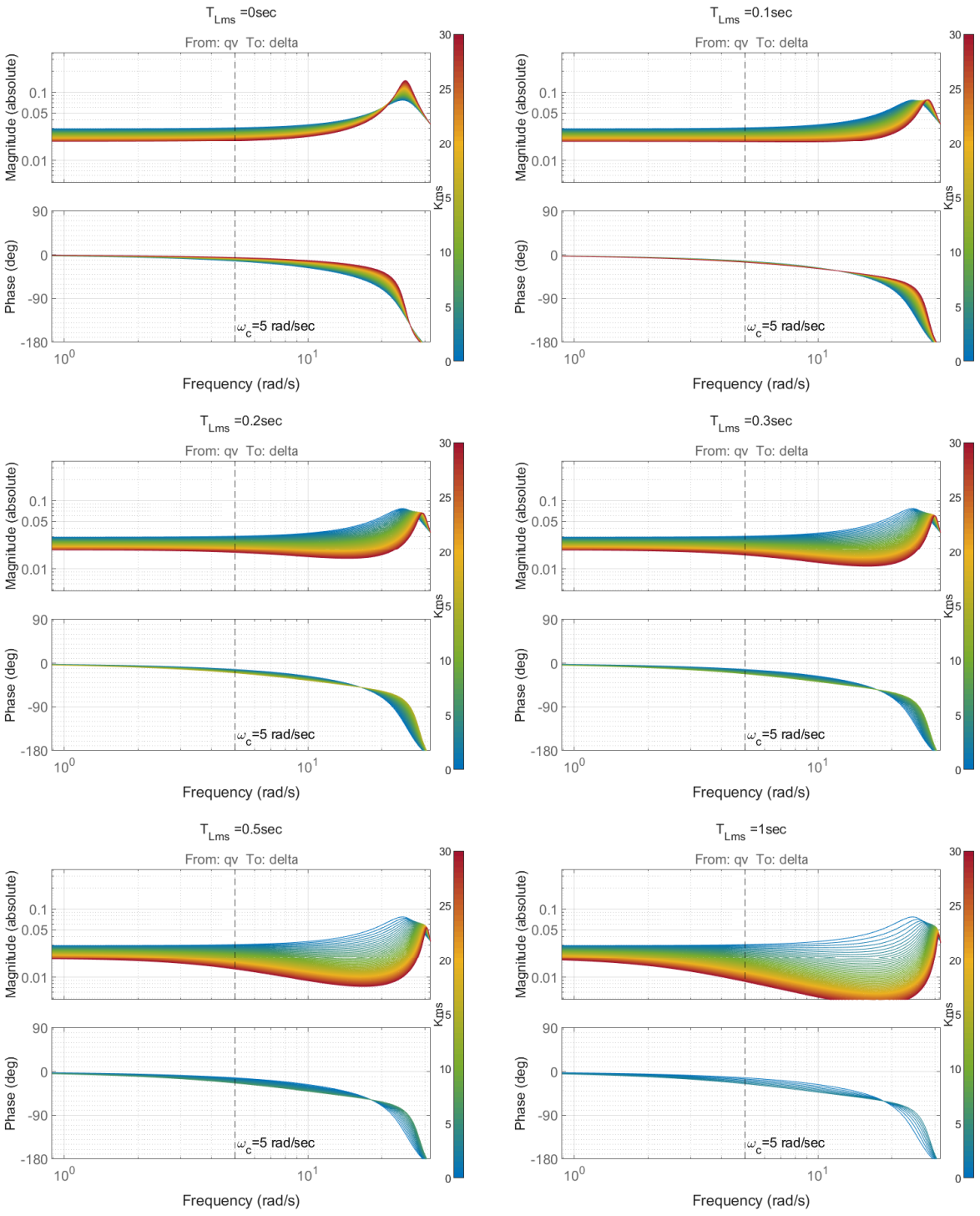

Figure D.11: FRF from q_v to δ, showing the effect of inner loop closure with a MS lead ($Y_c(s) = K_c$ CE dynamics), $k_F = 5k_1$

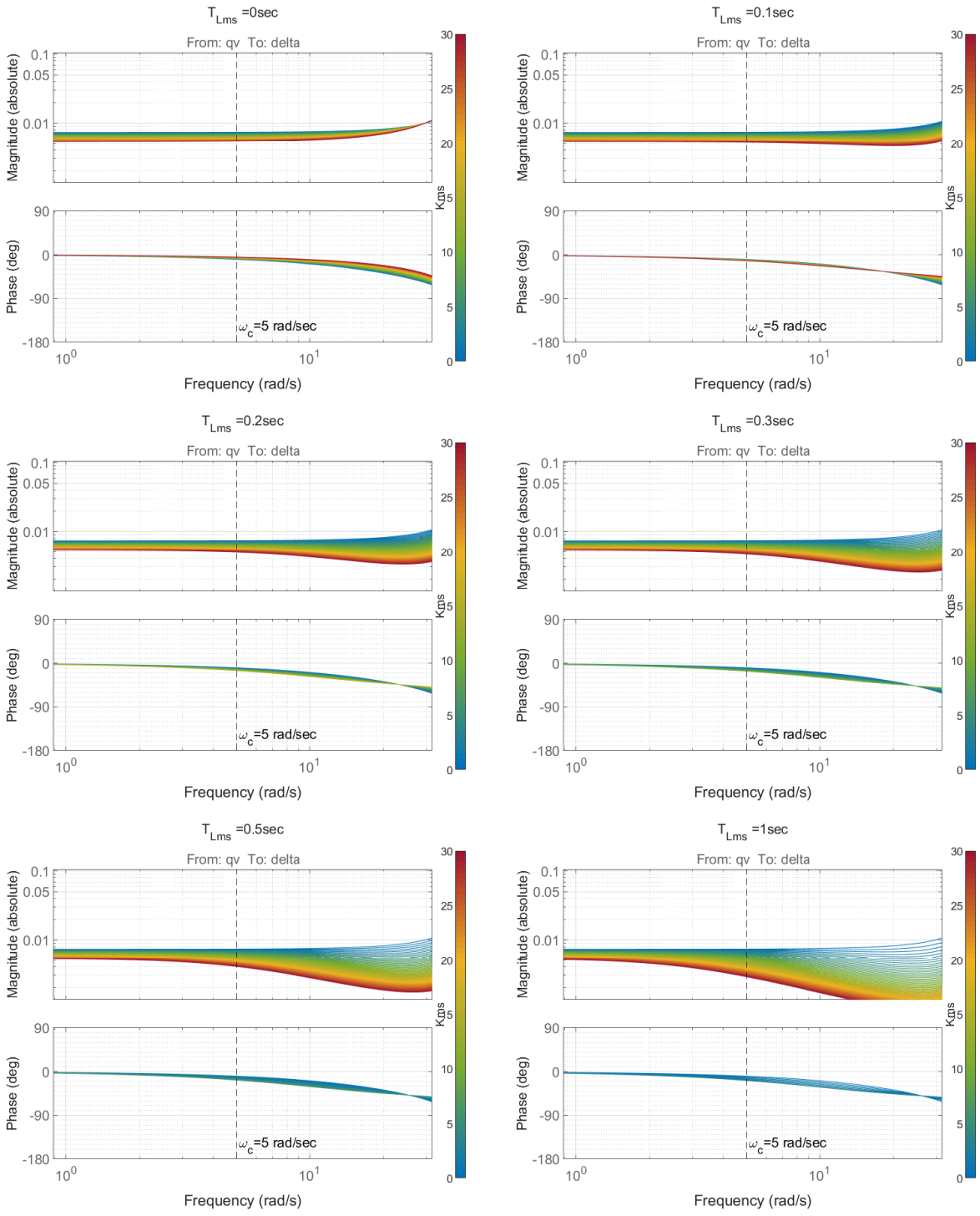

Figure D.12: FRF from q_v to δ, showing the effect of inner loop closure with a MS lead ($Y_c(s) = K_c$ CE dynamics), $k_F = 25k_1$

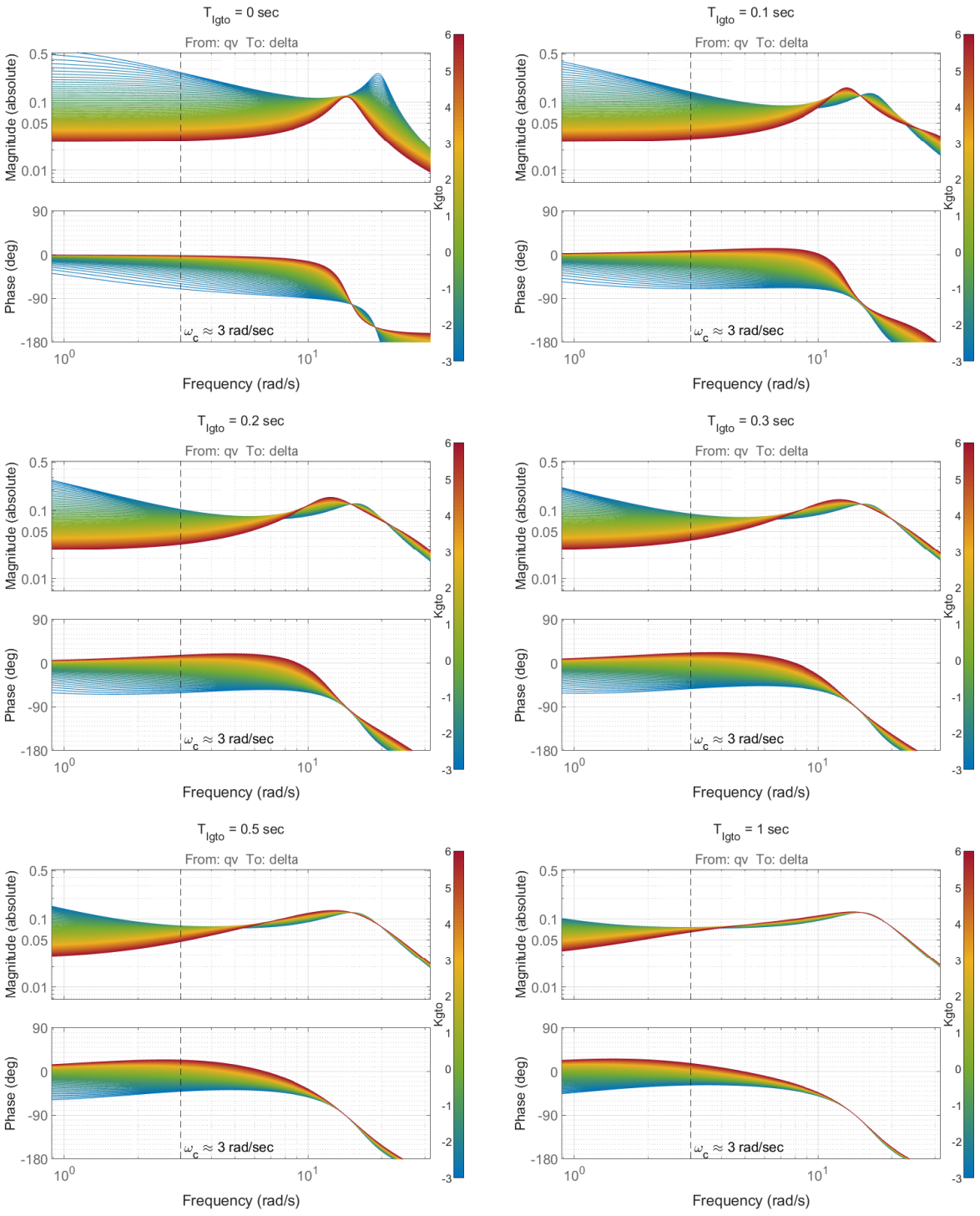

Figure D.13: FRF from q_v to δ, showing the effect of inner loop closure with a GTO lag ($Y_c(s) = K_c/s^2$ CE dynamics), $k_F = k_1$

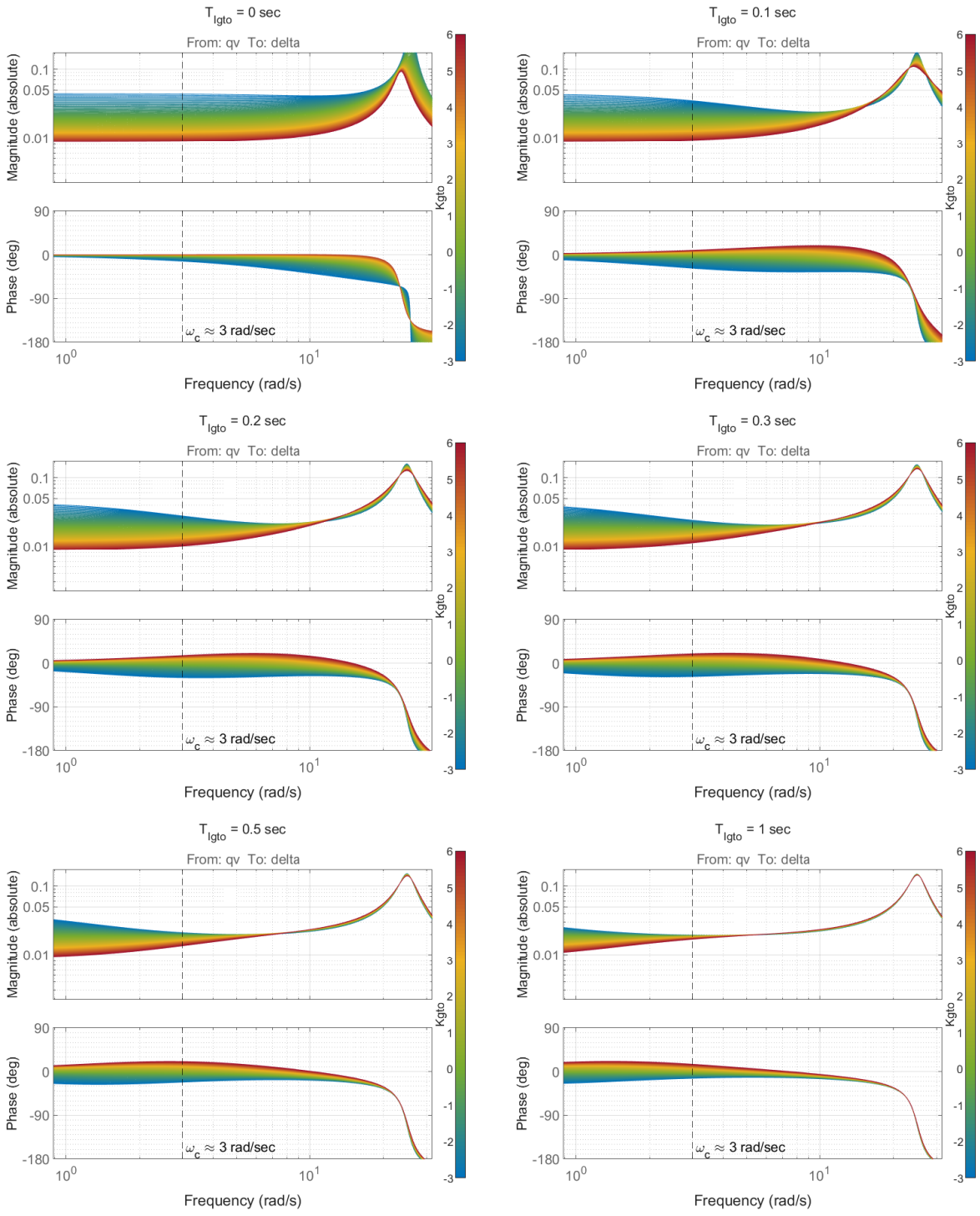

Figure D.14: FRF from q_v to δ, showing the effect of inner loop closure with a GTO lag ($Y_c(s) = K_c/s^2$ CE dynamics), $k_F = 5k_1$

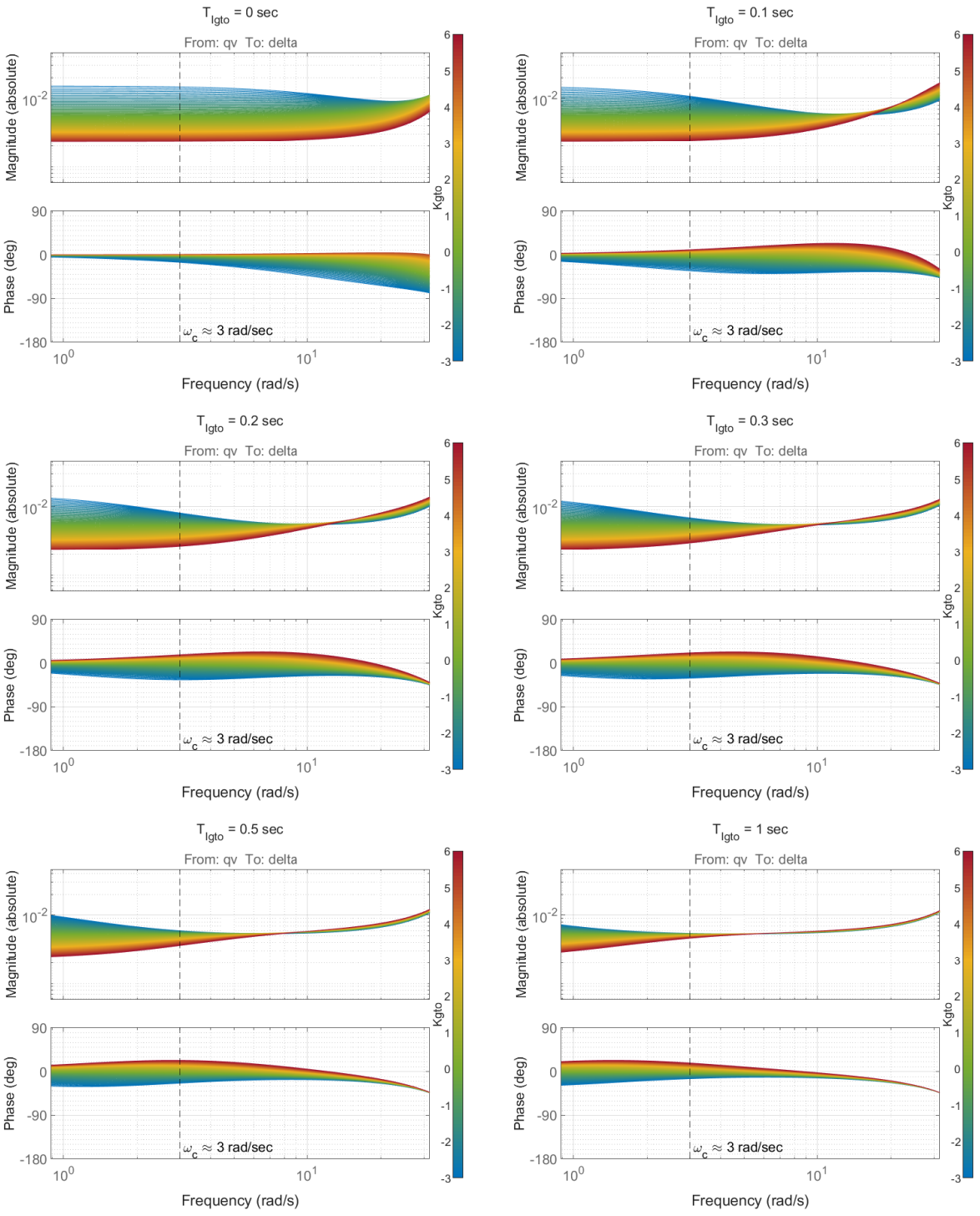

Figure D.15: FRF from q_v to δ, showing the effect of inner loop closure with a GTO lag ($Y_c(s) = K_c/s^2$ CE dynamics), $k_F = 25k_1$

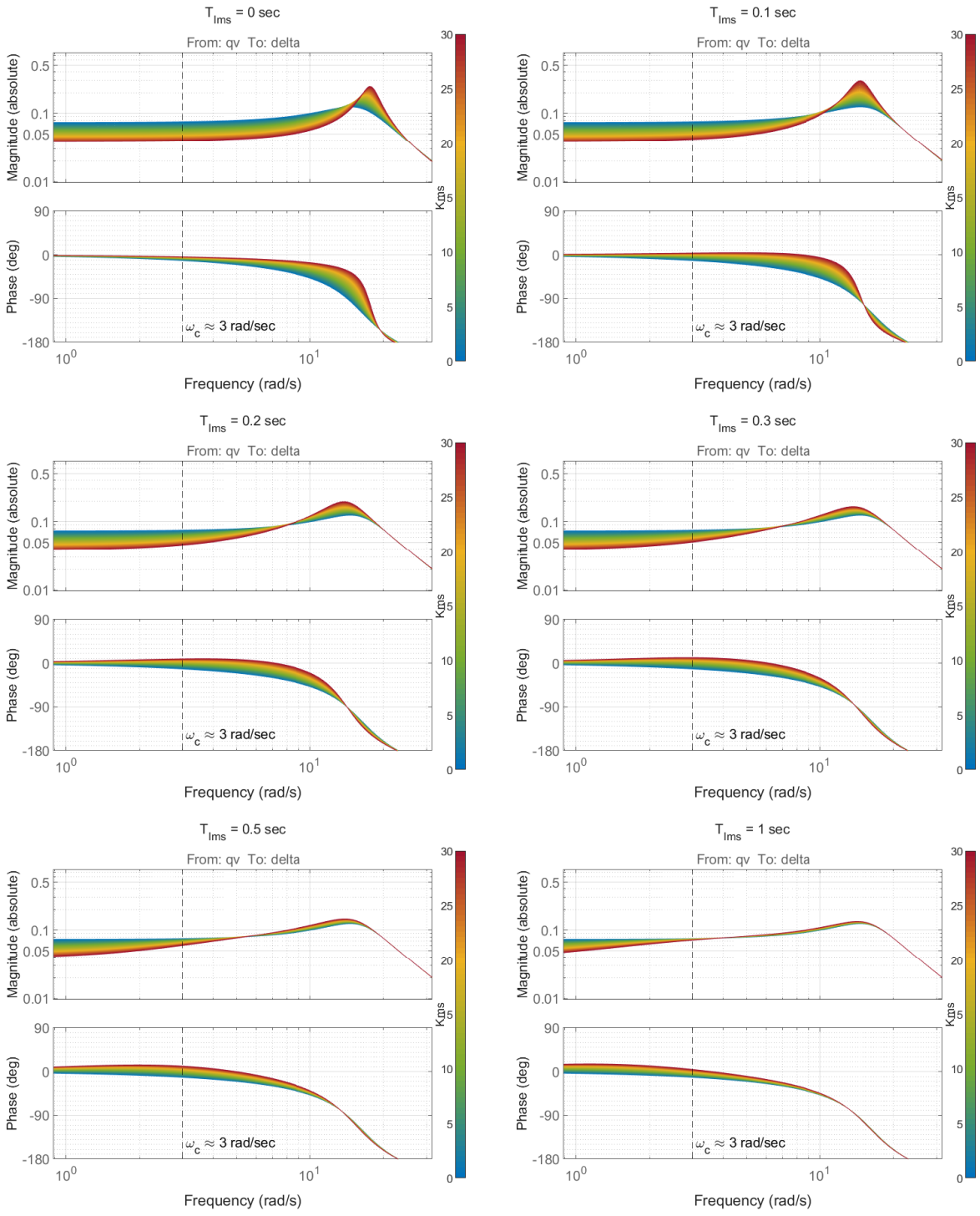

Figure D.16: FRF from q_v to δ, showing the effect of inner loop closure with a MS lag ($Y_c(s) = K_c/s^2$ CE dynamics), $k_F = k_1$

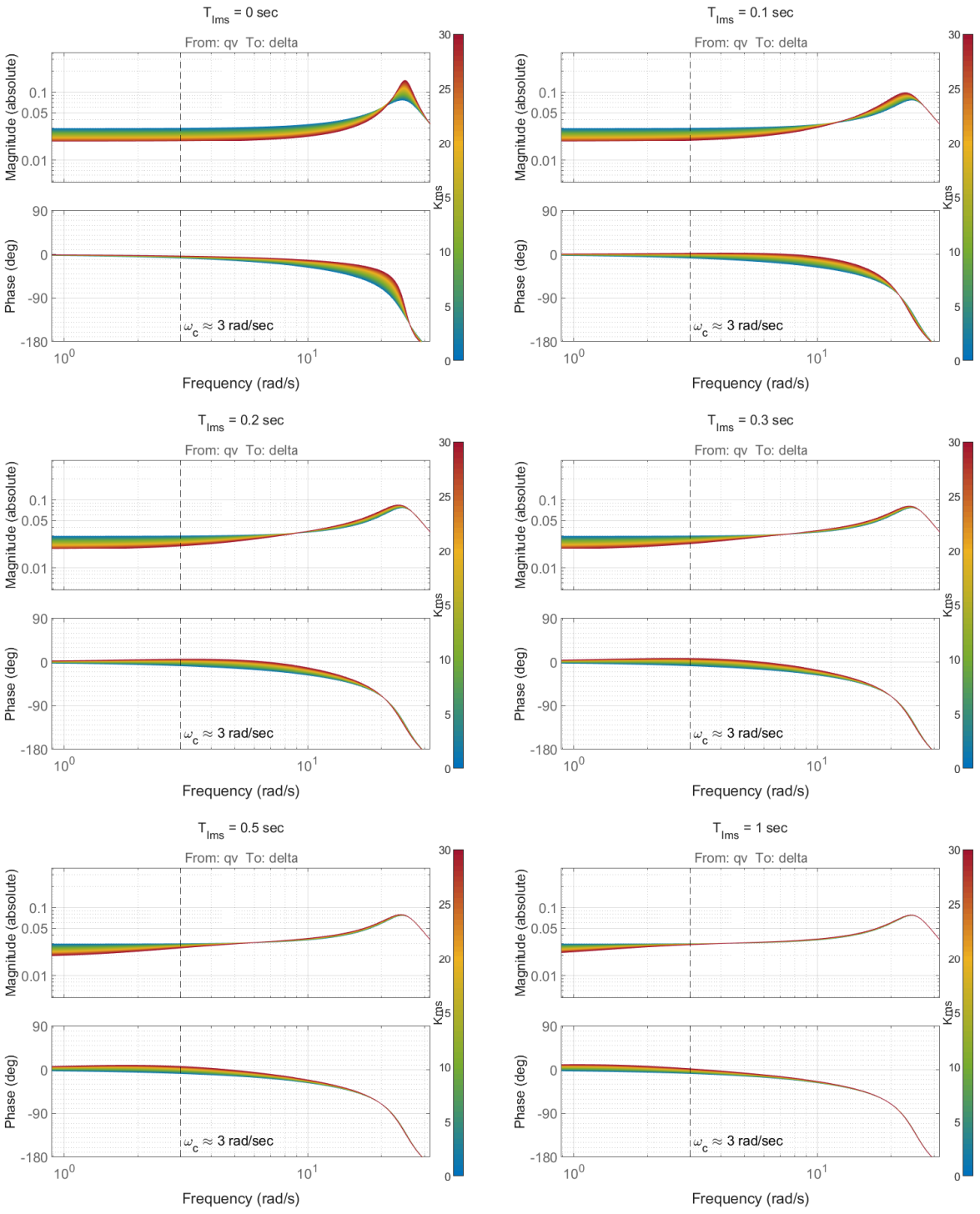

Figure D.17: FRF from q_v to δ, showing the effect of inner loop closure with a MS lag ($Y_c(s) = K_c/s^2$ CE dynamics), $k_F = 5k_1$

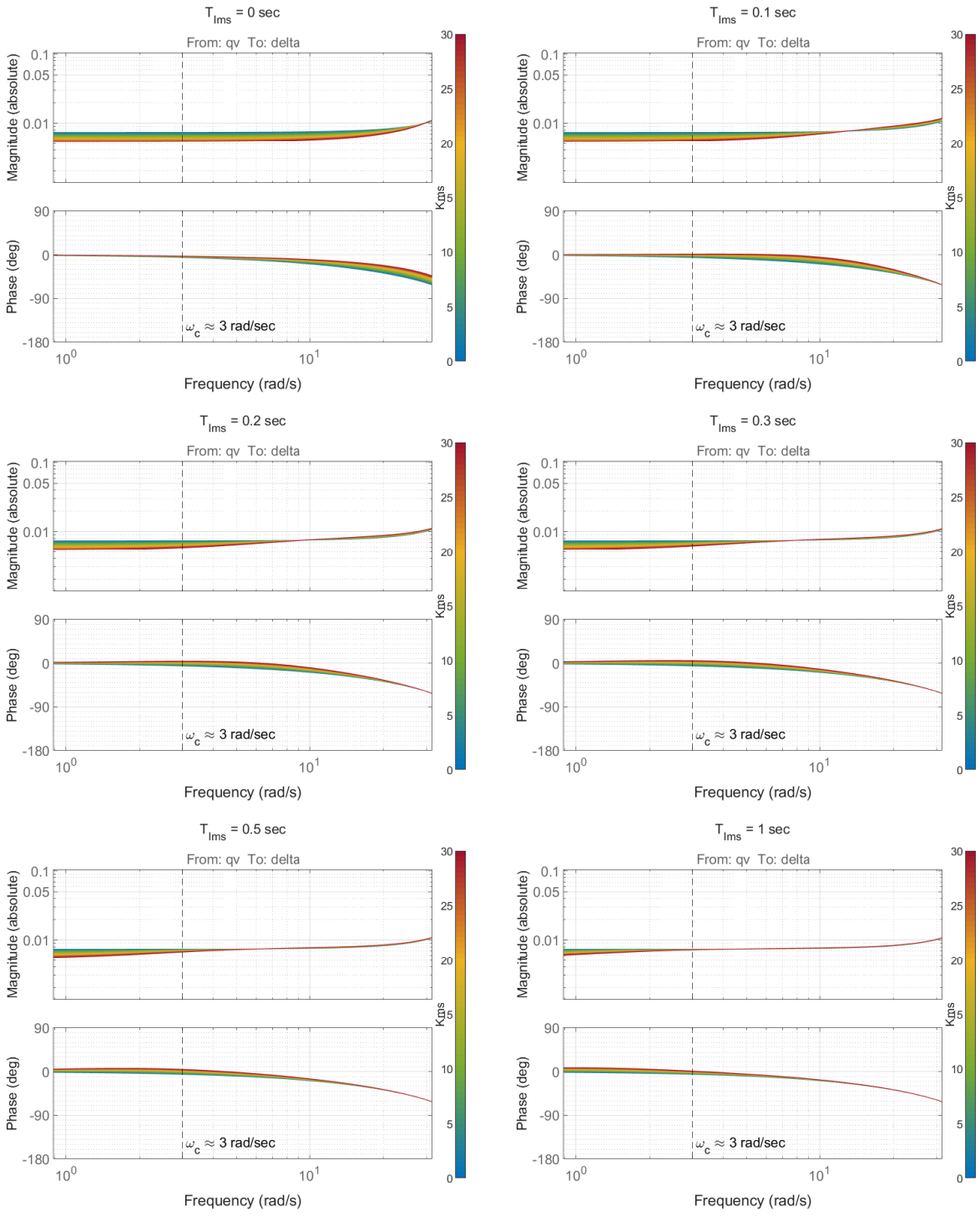

Figure D.18: FRF from q_v to δ, showing the effect of inner loop closure with a MS lag ($Y_c(s) = K_c/s^2$ CE dynamics), $k_F = 25k_1$

E

Experimental Data Trends

The experimental data used in Section VIII is presented here along with the main trends utilized for qualitative comparison with the model.

E.1. Integrator Control

Figure E.1 shows the results obtained by Gordon-Smith [10] comparing the pilot response in an integrator control task with a free moving an pressure manipulator at two different bandwidth values for the forcing function. While only a single controlled element (integral) was used, the experiment had 8 subjects and the results were recorded for three different forcing function bandwidths ($\omega_i = 1.5rad/sec, 2.5rad/sec, 4rad/sec$). The changes in the neuromuscular system natural frequency were more significant as bandwidth increased, with a very large decrease in natural frequency as well as damping observed for the largest forcing function bandwidth. The differences in phase lag in the high frequency region remained consistent throughout, however there was also a noticeable change in the low frequency region for the higher bandwidth of 4 rad/sec, corresponding to McRuer and Magdaleno's observations of the 'phase umbrella' [12].

Additionally, Gordon-Smith also observed a change in the high frequency neuromuscular peak characteristics. The dominant poles of the neuromuscular system characteristics were pushed to higher frequencies and also showed a larger damping constant.

Figure E.2 shows the results obtained by McRuer and Magdaleno comparing the pilot response in a integrator control task with a free moving, a spring centering and a pressure manipulator, at two different forcing function bandwidths. B5 in their experiment corresponds with an input bandwidth of approximately 2 radians per second, while R2.2 approximately 4 radians per second. A single trained pilot with experience in similar tracking tasks was involved in the experiment, due to limitations on the number of runs that could be recorded. Their previous publication extensively studying pilot dynamics in compensatory systems ([20]) was cited to have established this pilot as representative of a population of pilots, and he was also the single subject in another study on compensatory and pursuit displays due to the same limitations [46].

They also observed lower RMS error and high frequency phase lags when using spring restrained and pressure manipulators. Additionally, they also observed an increase in phase lag at low frequencies. With a simplified extended crossover model, this meant an increase in the parameter 'α' representing low frequency dynamics in the precision model (Equation 3.5), and in general it was indicated that the phase curve 'umbrella' as a whole shifted to the right.

As low frequency data has high error rates and larger non-linear tendencies, while also being less relevant, this information is largely ignored in Section VIII in favor of high frequency data which gives clearer indication of what is happening in the neuromuscular system.

The figure also shows the crossover frequency increases with spring restrained and pressure manipulators.

E.2. Proportional Control

Two parallel publications by McRuer and Magdaleno were used for the data in this scenario. Figure E.3 shows data from the same study by McRuer as discussed in the case of Integrator control. Frequency

response functions in the case of a proportional task for two different input bandwidths are presented. The same results are observed, with the change from free moving to spring centring manipulator being less significant in this case. Low frequency changes are only observed in the case of the high bandwidth forcing function.

Figure E.4 shows the results from a parallel study by Magdaleno and McRuer [13]. Manipulators with varying spring sensitivities are compared along with free and pressure manipulators. In the first case, the spring stiffness is increased without any changes in the controlled element sensitivity, meaning that the excursions on the manipulator would remain the same to achieve stable control. In this case it is observed that neither the RMS errors, nor the phase lags change significantly. In the second case, the controlled element sensitivity is increased proportional to the spring stiffness so that the force exerted remains approximately the same to maintain control, while stick excursions become smaller. In this case it is observed that the manipulator with the moderate spring stiffness performs the best, with the highest crossover frequency and static gain, suggesting that position feedback was the primary control pathway for proportional control, with the authors concluding that a tight position feedback loop is present, enabling the pilot to act as a 'position output device'.

E.3. Double Integrator Control

Data from the same two publications have been used. Figure E.5 shows data from the study by McRuer and Magdaleno [12] comparing the same three manipulators in a double integrator control task, for two different input bandwidths. There is a significant improvement in rms error and crossover frequency when using the pressure and spring manipulator, and the phase lag reduces. The low frequency shift is not as significant in this control scenario.

Figure E.6 shows data from the study by Magdaleno and McRuer [13], where manipulators with different spring constants are compared similarly. In the first case, the spring restraint is increased without any change in control sensitivity, so the same excursions with larger force are necessary to achieve similar input. In this case, the error is least for an intermediate spring rate ($k_F = k5k_1$), only slightly less than the pressure controller. Although the pressure controller has smaller low frequency gain, it has a significantly lower phase lag near the crossover frequency. This is attributed by the authors to lower effective time delays as the neuromuscular dynamics are pushed to higher frequencies due to the spring characteristics.

In the second case, when controlled element sensitivity is increased in proportion to the spring constant, an intermediate value results in lower error and slightly higher crossover frequency. The author concluded that larger spring rates help in increasing natural frequency of the NMS and improving phase lag, while larger control sensitivity allows the pilot to use smaller stick motions for control. The pressure controller with the highest sensitivity however appears to show significantly lower crossover frequency and larger errors.

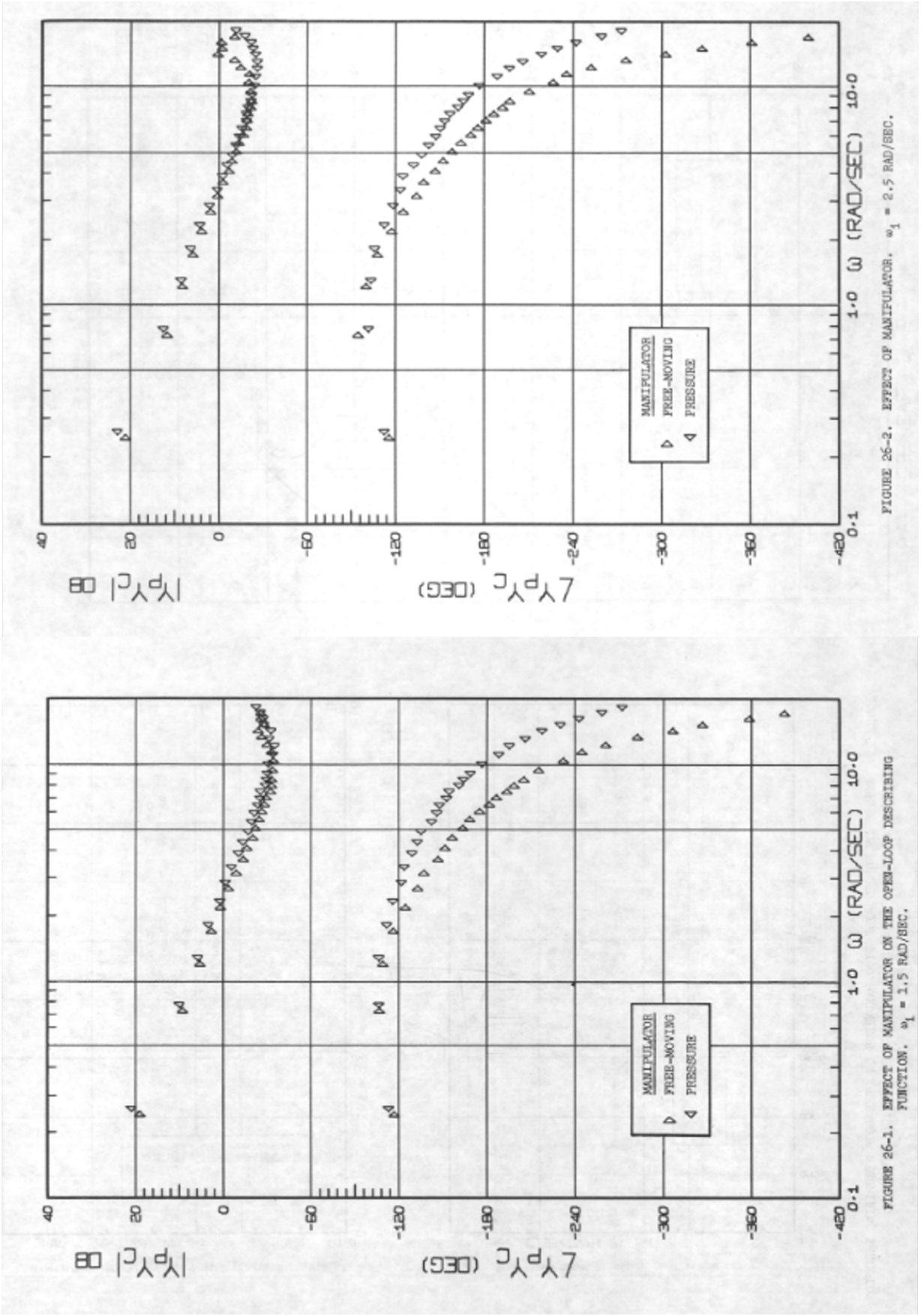

Figure E.1: *Integrator Controlled element Dynamics Pressure and Free Moving Manipulator, Gordon-Smith 1970, Fig. 26-1 and 26-2 [10]*

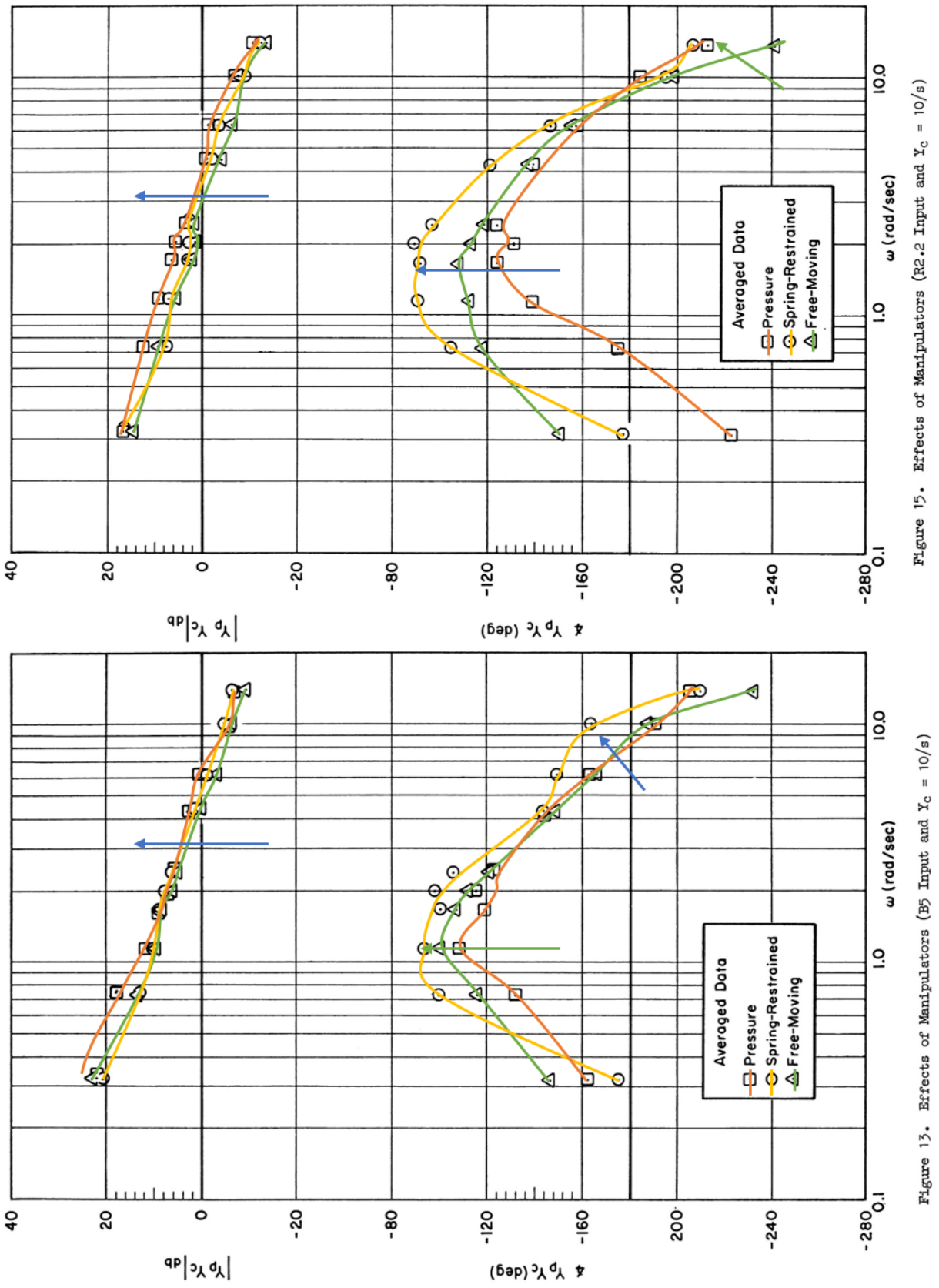

Figure E.2: *Integrator Controlled element Dynamics Pressure, spring restrained and Free Moving Manipulator, McRuer and Magdaleno 1966, Fig. 13 and 15 [12]*

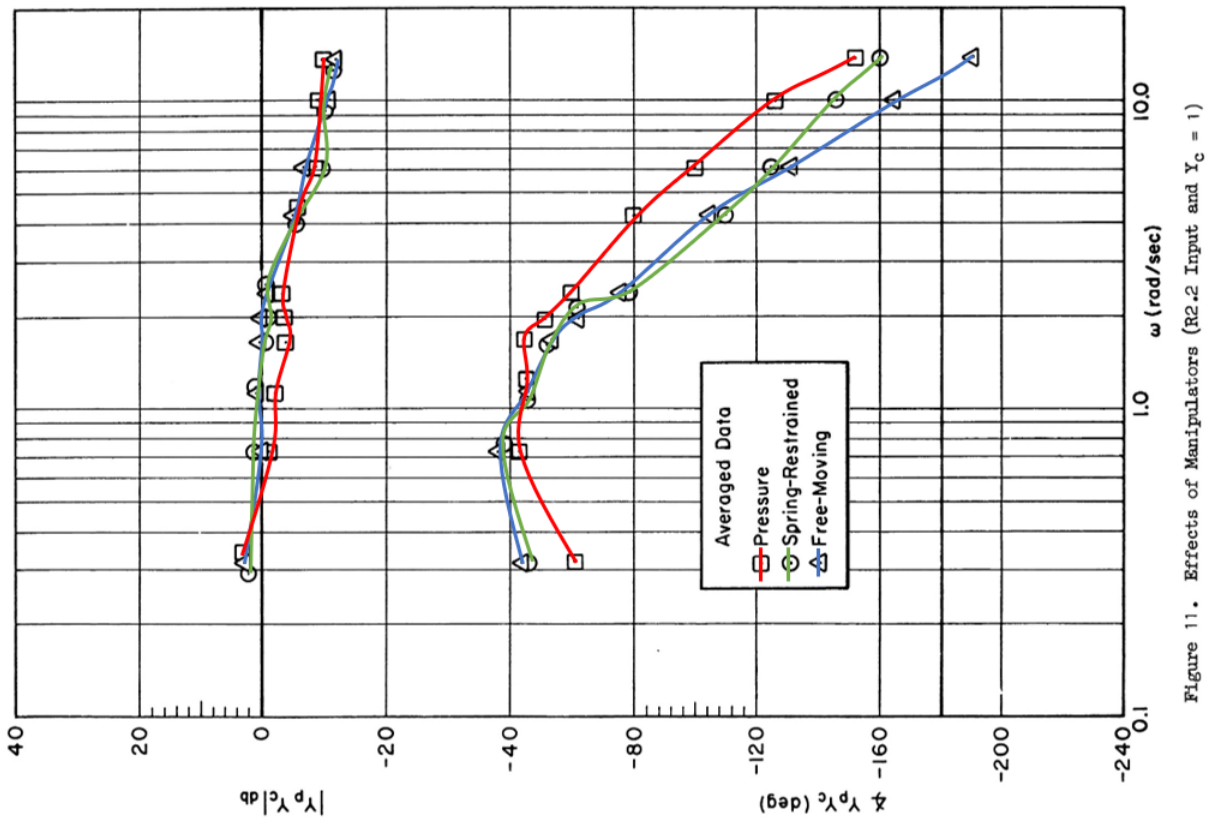

Figure 11. Effects of Manipulators (R2.2 Input and $Y_c = 1$)

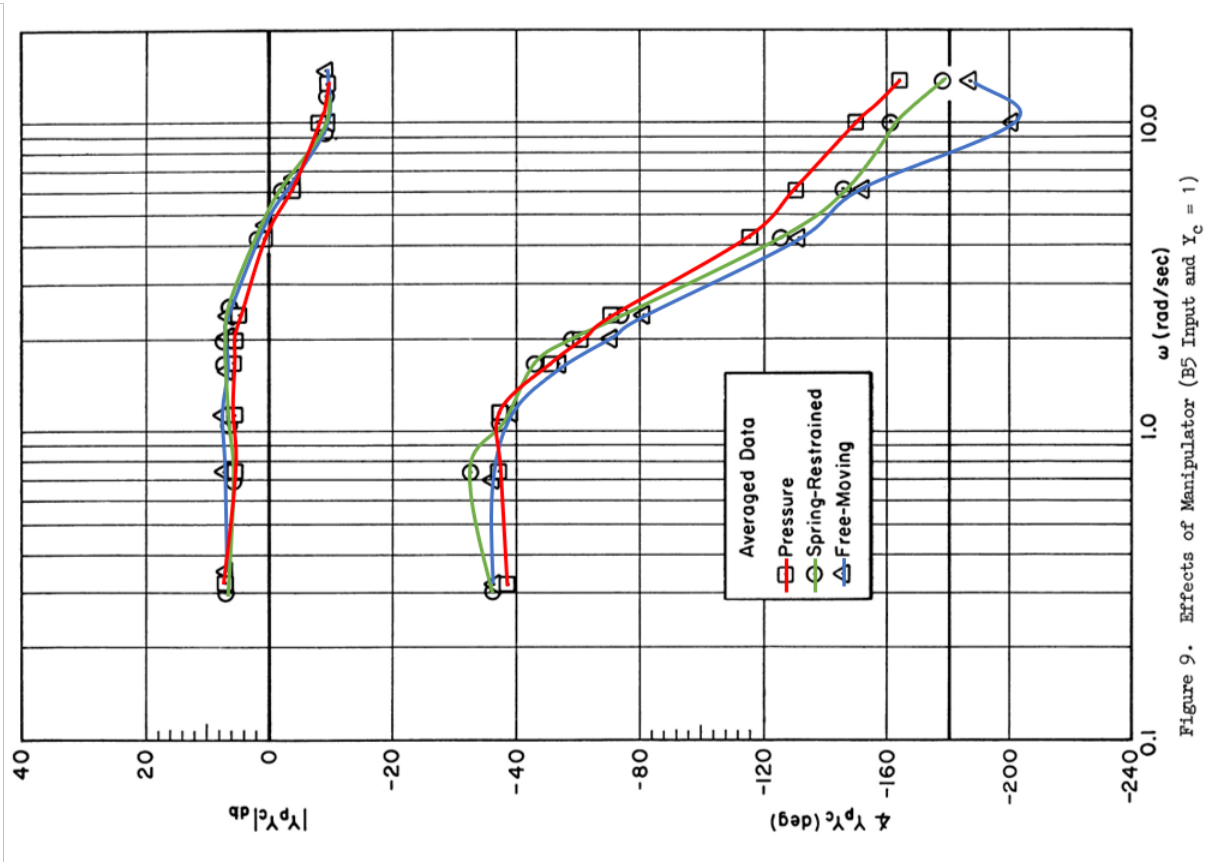

Figure 9. Effects of Manipulator (B5 Input and $Y_c = 1$)

Figure E.3: *Proportional Control with manipulators at two different input bandwidths, McRuer and Magdaleno 1966, Fig. 9 and 11 [12]*

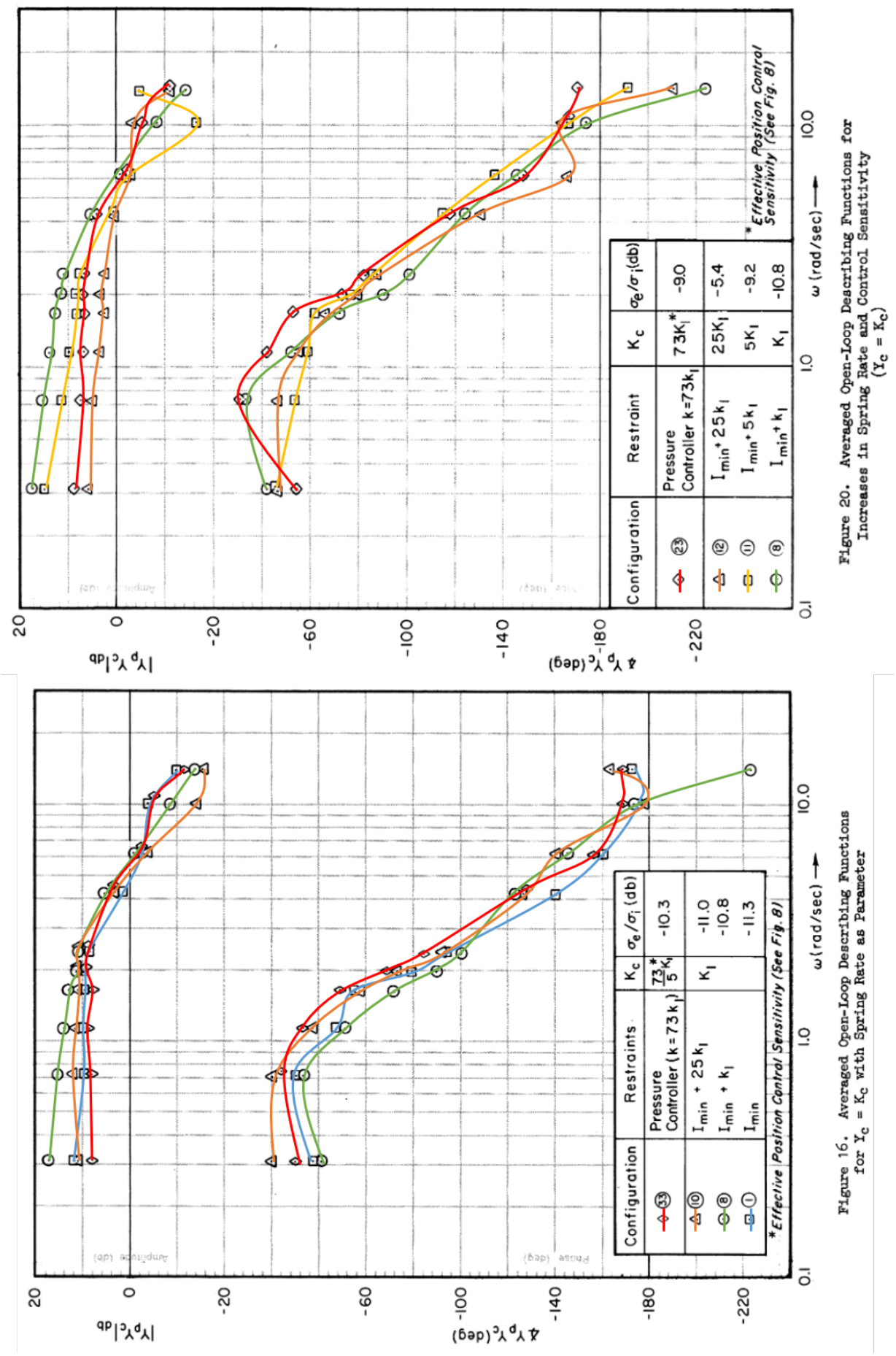

Figure E.4: *Proportional Control with different manipulators without and with control sensitivity changes, Magdaleno and McRuer 1966, Fig. 16 and 20 [13]*

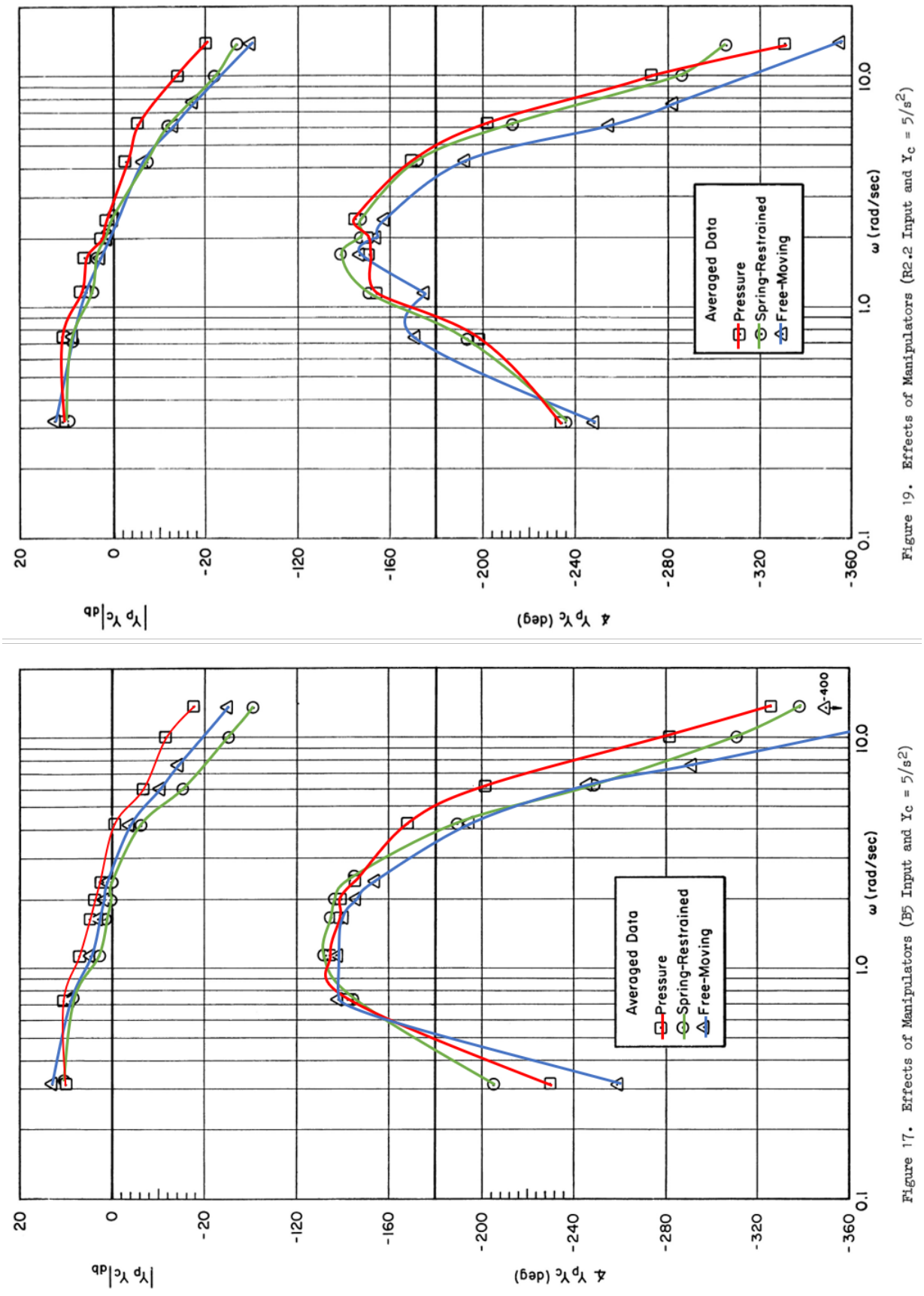

Figure 19. Effects of Manipulators (R2.2 Input and $Y_c = 5/s^2$)

Figure 17. Effects of Manipulators (B5 Input and $Y_c = 5/s^2$)

Figure E.5: *Double Integrator Control with different manipulators for two different input bandwidth, McRuer and Magdaleno 1966, Fig. 17 and 19 [12]*

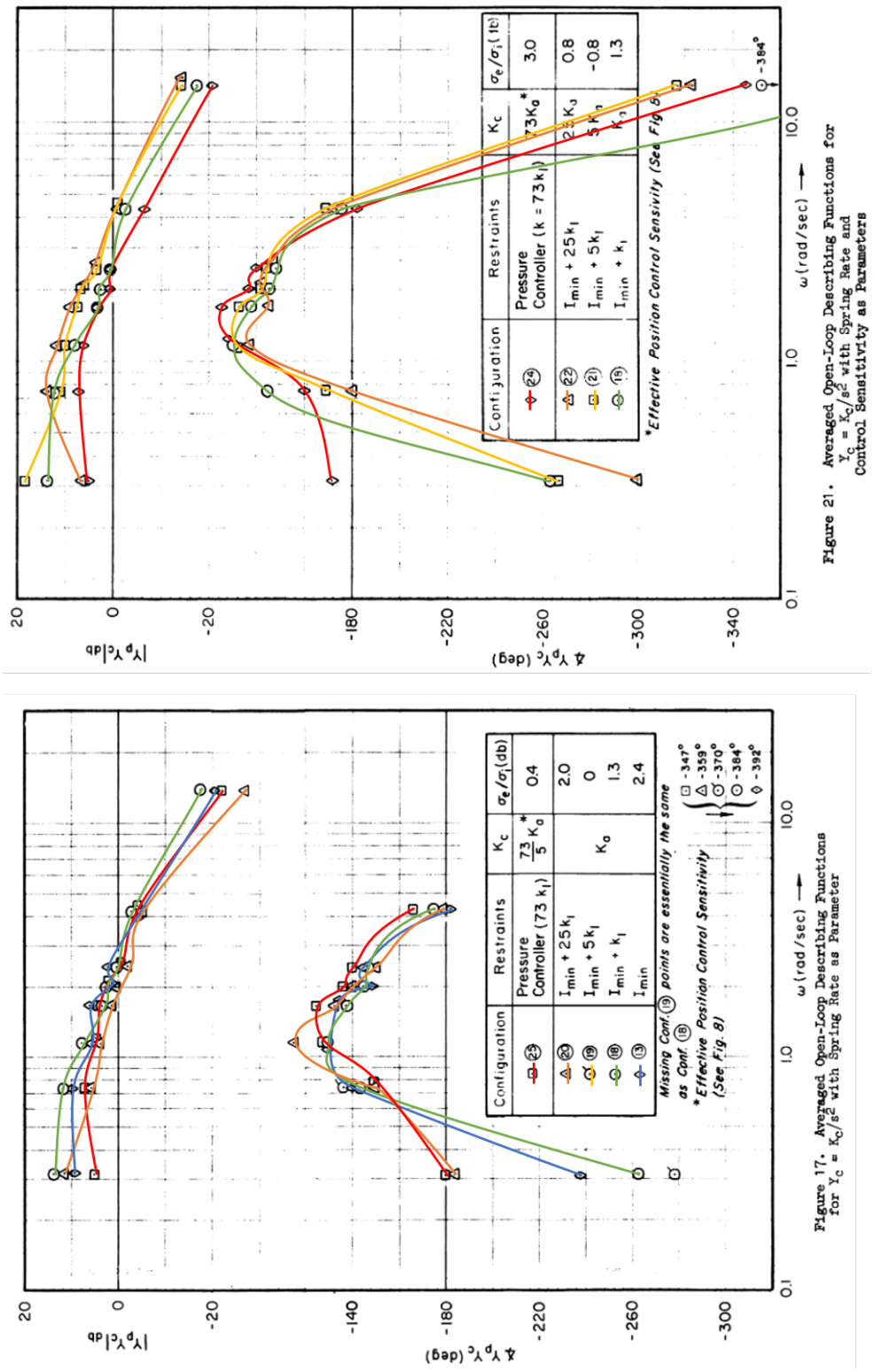

Figure E.6: *Double Integrator Control with different manipulators without and with control sensitivity changes, Magdaleno and McRuer 1966, Fig. 17 and 21 [13]*